R90-916528-80
NASA CR-189044

NASA

HIGH TEMPERATURE STATIC STRAIN GAGE DEVELOPMENT

By
C.O. Hulse, R.S. Bailey, H.P. Grant,
W.L. Anderson and J.S. Przybyszewski

United Technologies Research Center

Prepared for
National Aeronautics and Space Administration

NASA Lewis Research Center
Contract NAS3-23722
August 1991

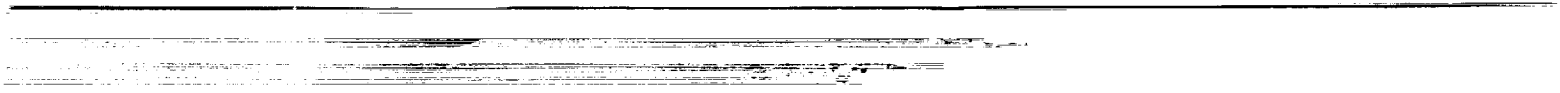

REPORT DOCUMENTATION PAGE

Form Approved
OMB No. 0704-0188

1. AGENCY USE ONLY (Leave blank)	2. REPORT DATE	3. REPORT TYPE AND DATES COVERED
	August 1991	FINAL June 1983 - October 1990

4. TITLE AND SUBTITLE

HIGH TEMPERATURE STATIC STRAIN GAGE DEVELOPMENT

5. FUNDING NUMBERS

C-NAS3-23722
WU-505-62-50

6. AUTHOR(S)

C.O. Hulse, R.S. Bailey, H.P. Grant, W.L. Anderson, J.S. Przybyszewski

7. PERFORMING ORGANIZATION NAME(S) AND ADDRESS(ES)

United Technologies Research Center
Silver Lane
East Hartford, CT 06108

8. PERFORMING ORGANIZATION REPORT NUMBER

R90-916528-80

9. SPONSORING/MONITORING AGENCY NAME(S) AND ADDRESS(ES)

National Aeronautics and Space Administration
Lewis Research Center
21000 Brookpark Road, Cleveland, OH 44135

10. SPONSORING/MONITORING AGENCY REPORT NUMBER

NASA CR-189044

11. SUPPLEMENTARY NOTES

Project Manager, Mary V. Zeller, Instrumentation & Control Technology Division
NASA Lewis Research Center

12a. DISTRIBUTION/AVAILABILITY STATEMENT

Unclassified
Subject Category 05

12b. DISTRIBUTION CODE

13. ABSTRACT *(Maximum 200 words)*

Final results are presented from a program to develop a thin film static strain gage for use on the blades and vanes of running, test stand gas turbine engines with goals of an 3 mm x 3 mm gage area and total errors of less that 10% of ±2,000 microstrain after 50 hours at 1250 K. An earlier report described the results from Tasks 1 and 2 of this contract which identified Pd containing 13 Wt. % Cr as a new strain sensor alloy that appeared to be potentially usable to 1250 K. In subsequent work it was discovered, in contrast with its behavior in bulk, that Pd-13Cr suffered from oxidation attack when prepared as a 4.5 μm thick thin film. Continuing problems with electrical leakage to the substrate and the inability of sputtered alumina overcoats to prevent oxidation led to the discovery that sputtered alumina contains appreciable amounts of entrapped argon. After the argon has been exsolved by heating to elevated temperatures, the alumina films undergo a linear shrinkage of about 2% resulting in the formation of cracks. These problems can be largely overcome by sputtering the alumina with the substrate heated to 870 K. With 2 μm thick hot sputtered alumina insulation and overcoat films, total 50 hr drifts of about 100μstrain (2 tests) and about 500 μstrain (1 test) were observed at 1000K and 1100K, respectively. Results of tests on complete strain gage systems on constant moment bend bars with Pd temperature compensation grids revealed that oxidation of the Pd grid was a major problem even when the grid was overcoated with either a hot or cold sputtered alumina overcoat.

14. SUBJECT TERMS

strain gages
elevated temperatures
static strain
electrical resistance
sputtered

15. NUMBER OF PAGES
122

16. PRICE CODE

17. SECURITY CLASSIFICATION OF REPORT	18. SECURITY CLASSIFICATION OF THIS PAGE	19. SECURITY CLASSIFICATION OF ABSTRACT	20. LIMITATION OF ABSTRACT
Unclassified	Unclassified	Unclassified	SAR

UNITED TECHNOLOGIES RESEARCH CENTER
East Hartford, Connecticut 06108

R90-916528-80

High Temperature Static Strain Gage Development

FINAL REPORT
Contract NAS3-23722

PRINCIPAL INVESTIGATOR Charles O. Hulse
C. O. Hulse

APPROVED BY E. R. Thompson
E. R. Thompson
Assistant Director of Research
for Materials Technology

DATE December 1990

TABLE OF CONTENTS

TABLE OF CONTENTS cont.

LIST OF TABLES

LIST OF FIGURES

LIST OF FIGURES (cont.)

1.0 SUMMARY

The results are given of a program to develop sputtered thin film static strain gages for use on the blades and vanes of gas turbine engines running on test stands. The ultimate goal was a gage 3 mm x 3 mm in area that would operate for at least 50 hours to temperatures of at least 1250 K with an error of less than 10 percent of a full scale range of ±2,000 microstrain. Earlier work on this contract had identified Pd-13Cr as a new strain gage alloy potentially useful to 1250 K. This work confirmed that composition was optimum and that the alloy required the use of a protective overcoat when prepared as a 4.5 μm thick thin film. It was also discovered that conventionally prepared sputtered thin films of alumina were not suitable for use as overcoats to protect this sensor alloy from oxidation or to provide good electrical insulation from the substrate. Alumina thin films prepared by sputtering at 870 K did provide good electrical insulation from the substrate and protection from oxidation attack.

The thermal coefficient of resistance of the Pd-13Cr alloy is approximately 175 μΩ/Ω/K which requires the use of a thermal compensation grid in the adjacent leg of the Wheatstone bridge. During the testing of complete strain gage installations on bend bars, it was discovered that compensation grids of pure Pd were subject to oxidation attack at intermediate temperatures. This was not prevented by the use of either cold or hot sputtered alumina overcoats. This problem should not have arisen if these grids had been made of pure Pt. At the current state of development, it is possible to prepare thin film static strain gages which should perform well up to 1100 K. Additional work will be needed to confirm this conclusion and to extend the range of use to 1250 K.

2.0 INTRODUCTION

The further development of improved gas turbine engines with higher efficiencies and greater thrust is dependent upon the discovery and use of improved materials and better designs. Although materials property data and mathematical modeling can be used to estimate the stresses experienced by rotating parts inside a running turbine engine, accurate experimental measurements of strain are urgently needed to confirm these estimates. This is particularly important in air cooled gas turbine blades and vanes where high temperatures and very high thermal gradients are present which can vary significantly with time and different operating conditions. Accurate estimates of strain are particularly difficult to make because we do not as yet have sensors capable of accurately measuring the temperatures at specific points on these parts.

In recognition of these needs, NASA initiated a series of programs to address this problem. These included an initial program to survey various techniques which might be used for measuring static strain at elevated temperatures (ref. 1). This effort identified the laser speckle technique and resistance strain gages as the two best candidates for further development. It was also determined in this program that the major problem which limited the use of resistive strain gages at higher temperatures was that a metallurgically stable sensor alloy was not existent. A subsequent NASA contract (ref. 2) identified two potential alloys for this use, Fe-10.6Cr-11.9Al and Pd-13Cr, both in weight percent.

Parallel efforts were also initiated by NASA to further develop and demonstrate the usefulness of the laser speckle technique (ref. 3, 4). In this work it was determined during experiments in a jet burner rig at the United Technologies Research Center (UTRC) that in a high pressure environment with air moving at high speeds at high temperatures, turbulence in the air could make it impossible to obtain useful data using this system. This approach to the measurement of strain at high temperatures has been the subject of additional effort at NASA Lewis Research Center (ref. 5) and it has been used successfully to measure the strains in a single rotating disk testing facility in a vacuum at UTRC at temperatures to 950 K (ref. 6).

The general purpose of the present contract was to develop a new resistive strain alloy and a complete strain gage measurement system capable of operating inside a gas turbine engine running on a test stand. The specific program goals were to develop a static strain gage system capable of at least 50 hours of operation at temperatures up to 1250 K on a vane or rotating gas turbine blade. The surface dimensions of the gage were limited to

3 mm x 3 mm. The maximum height above the airfoil were to be less than 0.2 mm for a foil gage and 0.5 mm for a wire gage. The desired maximum strain capability was ±2,000 μstrain (0.2 percent strain) at 1250 K and ±3,000 μstrain at 1100 K with an inaccuracy of no more than ±10 percent of the full scale reading. This program was part of a much larger NASA initiative, the HOST Program, to develop improved Hot Section Technology for gas turbine engines.

The technical effort for this contract was broken down into the following tasks:

Task 1 - Alloy Improvement - Further improvement of the PdCr and FeCrAl alloys developed previously (ref. 2)

Task 2 - Development of Gage Fabrication Techniques - Examinations of sputtering and one other alternative fabrication technique for each of two alloys.

Task 3, 7, 9 and 10 - Reports and Reviews.

Task 4 - Gage System Study and Component Test Plan Formulation.

Task 5 - Gage System Component Fabrication, Testing and Analysis - Flat plate specimens of components evaluated and appropriate modifications implemented.

Task 5A - Gage System Component Fabrication, Testing and Analysis - Oxidation protection investigation.

Task 6 - Gage Design, Fabrication and Test Plan Formulation.

Task 8 - Gage System Fabrication, Testing and Analysis - A total of 16 complete strain gage systems will be prepared with 4 complete systems supplied to NASA.

Tasks 1 and 2 of this contract were concerned with continued modifications to the two alloys mentioned above (ref. 2) to determine the best compositions of each alloy and then to select the best alloy type for use as a resistive sensor element. The results of this work have been published (ref. 7) and are included in a previous contract report (ref. 8). These results are briefly reviewed in Section 3 of this report.

3.0 REVIEW OF PRIOR WORK ON THIS CONTRACT

The primary purpose of previously reported work (ref. 8) on Task 1 and 2 of this contract was to optimize the compositions of the two sensor alloys identified earlier (ref. 2) and then to select the better one for use in preparing complete sputtered strain gage systems. The compositions of the two initial alloys were Fe-10.6Cr-11.9Al and Pd-13Cr, both expressed in weight percent. Arc melted boules of many different alloys were prepared and examined metallographically to satisfy the requirement that the alloying elements were in solid solution and that the alloy was single phase. Drop cast rods of various alloys were then prepared and exposed to oxidation at 1250 K. Measurements of the change in weight of these samples failed to reveal any alloys with improved resistances to oxidation so that the compositions of the optimum alloys remained the same as originally developed.

As shown in Figure 3.1, the change in resistance of the Pd-13Cr alloy is linear with absolute temperature as would be expected for a material in which the only barriers for electron motion are due to their interactions with lattice vibrations in a metallurgically stable alloy. This alloy was designed to be inherently resistant to oxidation because a chromium oxide scale should form which would tend to prevent further attack. Figure 3.2 presents an electron microprobe profile across the surface structure of this alloy after a 40 hour exposure in air at 1250 K. The concentration of chromium as chromium oxide has increased at the surface permitting the concentration of chromium in the underlying alloy to remain essentially constant in the metallic state.

As shown in Figure 3.3, greater concentrations of Cr in Pd result in higher values of resistivity and a decrease in the sensitivity of resistance to temperature, both advantageous for its use as a strain sensor. Although the range of solid solution of Cr in Pd extends to about 22 weight percent, alloys containing concentrations greater than 13 percent were not recommended because their resistance versus temperature behavior was slightly nonlinear. It was felt that this might be due to a small tendency towards solid solution ordering which could result in unwanted changes in resistance as a function of time and temperature.

Several problems became evident when the Pd-13Cr alloy was prepared as a 6.5 μm thick sputtered film. The change in resistance of the sputtered material over a 50 hour period at 1250 K compared with the material in bulk is shown in Figure 3.4. Most of the Cr in the film has apparently been consumed to form the oxide scale. The thermal

coefficient of resistance of the film after this exposure was similar to that for pure Pd. These results indicated that the film requires an overcoat protection film to avoid oxidation attack. A second, less pervasive observation was that the sputtered film also contained occasional much larger nodules of Pd-13Cr than typically present. These were apparently not as well bonded to the substrate as the rest of the film and they showed a tendency to come loose after being exposed to thermal cycling. Examples are shown in Figure 3.5.

A more serious problem which became apparent when sputtered thin films of Pd-13Cr were deposited on 2 μm thick sputtered films of aluminum oxide was that the alumina films did not provide adequate electrical insulation from the substrate. Figure 3.6 shows for example two cycles of resistance versus temperature data for such a Pd-13Cr grid where the data are not linear with temperature and finally shorts to the substrate occur at 1250 K.

4.0 TEST PLANS

In Task 4 of this work, a study was made to identify the most important issues that needed to be addressed for each of the components that make up a complete strain gage system. Overall guidelines and materials properties identified are given in Appendix A. The issues addressed included insulation layer integrity, self-temperature-compensation configurations (multi-element), heat treatment and overcoating of thin films for stability, thin film adhesion, and lead-wire to lead-film connections. Based on these issues, a test plan was developed to examine these possible problem areas as well as others that would be encountered by the separate preparation and testing of individual system components. With the knowledge obtained from component testing, a subsequent test plan was then developed to evaluate the behavior of complete strain gage systems in the last phase of this program.

5.0 EXPERIMENTAL PROCEDURE

5.1 INTRODUCTION

The majority of testing performed during Tasks 5 and 5A was designed to evaluate electrical stability of the gage element at elevated temperatures for various gage preparation procedures. Samples for this evaluation were prepared by fabricating a series of layers on metallic or ceramic substrates. A diagram of the layers constituting a typical sample for elevated temperature testing on a Hastelloy-X substrate is shown in Figure 5.1.1 On metallic substrates the first layer was a grown oxide followed by a sputtered oxide covering the entire top surface of the substrate. These combined oxide layers served to insulate the sensor element from the conductive substrate. On the ceramic substrates these oxide layers were not required as the sensor element could be deposited directly onto the non-conductive substrate. The second thin film component was the Pd-13Cr strain gage element material. This material was deposited in the desired grid pattern using a photoresist mask to define the pattern. Sputtered leadfilms of Pd-13Cr extended from the grid to the far end of the substrate. Since the results of earlier work on this contract showed that the element needed to be protected from oxidation, a protective overcoat layer was deposited over the grid and all but the end of the leadfilms. To improve the effectiveness of the overcoat some samples had an additional protective topcoat layer sputtered on top of the overcoat.

Since these samples were designed to evaluate the sensor under no-load conditions, the sensors were fabricated on rectangular substrates without the need for a tapered section nor the means to grip both ends of the sample during test. Since the testing apparatus provided a mechanical electrical connection to the sensor, these samples also did not need to have leadwires bonded to the sputtered element as part of the fabrication procedure.

Testing of Task 5 and 5A samples consisted of heating the samples at controlled rates while recording changes in sample resistance. Stability of the PdCr element after various fabrication techniques was determined by repeated thermal cycling, as well as recording resistance drift while maintaining the sample at a constant temperature.

In Task 8 complete strain gage systems including welded leadwires were fabricated on superalloy bend bars. Methods used for preparing insulating layers, gage elements, overcoats, and topcoats were similar to those used in Task 5A. These samples incorporated an additional sputtered Pd temperature compensating element and underwent a more complete testing schedule including determination of gage factor at room temperature and elevated temperatures as well as electrical stability over time at elevated temperatures.

5.2 SAMPLE PREPARATION - TASKS 5 AND 5A

5.2.1 Insulating Layers

The Hastelloy-X substrates for resistance measurements at elevated temperatures were 0.188 cm thick and 1.27 cm x 8.25 cm in surface dimensions. An adherent grown alumina insulating layer was formed on the substrates using the following previously established procedures (ref. 9). All substrates were polished to a 0.25 μm finish, coated with 0.13 to 0.18 mm of NiCoCrAlY by electron beam vapor deposition, and repolished to a 0.25 μin finish, removing 0.025 to 0.050 mm of NiCoCrAlY in the process. The grown alumina was formed on this surface by a 4 hour vacuum heat treatment at 1300 K followed by 100 hours in air at the same temperature. This treatment formed an oxide layer approximately 1.5 to 2.0 μm thick.

An additional 1.5 to 2.0 μm thick alumina insulating layer (fillcoat) was deposited on the grown oxide surface by R.F. sputtering in an Ar-20% O atmosphere. This layer was stabilized by heat treating the substrate at 1270 K for 1 hour in air to assure that the alumina was in the stable alpha form. Defects in the insulating fillcoat layer were a continuing source of sample failure during this program. The major source of defects appeared to be particulate contamination which dislodged from sputtering chamber surfaces during pump down or sputtering. Removal of these particles during cleaning operations left holes or thin spots in the insulation film. Cracks were also seen in the fillcoat following the 1270 K stabilization heat treatment. These cracks were at least in part due to the coefficient of linear thermal expansion (CTE) mismatch between the alumina and the Hastelloy-X. The alumina may also shrink and crack when heated due to the loss of argon adsorbed in the film during sputtering (ref. 10). Electron microprobe analysis of alumina sputtered in Ar-20% O on a room temperature substrate has shown that the alumina film is oxygen rich as sputtered. This analysis showed the alumina to contain 51.9 wt% oxygen as opposed to 47.1 wt% for stoichiometric alumina. As these films are heated to elevated temperatures, the alumina loses oxygen and approaches the stoichiometric composition. After a 30 minute heat treatment in air at 1140 K the oxygen content of the alumina had dropped 1.6 wt% to 50.3 wt%. After 10 hours at 1250 K the oxygen content had further dropped to 49.6 wt%. This loss of oxygen as the alumina fillcoat was heated to 1270 K during the stabilization heat treatment may have also resulted in shrinkage and cracking of the fillcoat layer. Pinholes caused by arcing to the substrate during sputtering are also a source of shorts or low resistance between the PdCr film and the substrate resulting in a shunting of the grid resistance. Of a total of 22 samples on Hastelloy-X substrates on which resistance measurements were made during Tasks 5 and 5A, 10 samples exhibited a low resistance to ground which resulted in failure of the gage either before or during testing.

Three changes in the original test plan were implemented to increase the effectiveness of the fillcoat layer. The first change was an extensive optical screening of substrates for defects both before and after sputtering of the fillcoat layer. Substrates containing major defects were rejected or the locations and types of defects were recorded so that the PdCr film could be positioned to avoid them. This procedure lead to the discovery that the original fillcoat on 6 Task 5A samples contained numerous defects which could lead to shorts once the PdCr layer was applied. These defects included a network of closed cracks, white beads assumed to be alumina bonded to the fillcoat surface, patches of spalled or buckled alumina, and circular dark depressions which appeared to be formed by a chemical reaction with the alumina by some unknown agent. A successful effort to salvage these samples led to the second change in the test plan.

This second change was the use of a multilayer fillcoat to prevent a single defect from penetrating the full thickness of the fillcoat. The steps used to apply the additional layers included glass bead blasting the original fillcoat surface to remove any loose fillcoat and dislodge the beads described above, sputtering 0.5 μm of alumina, heat treating 1 hour in air at 1255 K, and optical examination of the sample. Two 0.5 μm alumina layers were applied in this manner to bring the total fillcoat thickness to 2.5 to 3.0 μm where the original fillcoat remained intact and 1.0 μm where the original fillcoat had spalled or was removed during glass bead blasting.

The third approach investigated to improve the effectiveness of the fillcoat layer was heating the substrate during fillcoat sputtering. Alumina deposited on a 980 K NiCoCrAlY coated substrate has been shown to have adherence superior to alumina sputtered at room temperature (ref. 11) This procedure reduced the possibility of cracks forming in the alumina as it was heated from room temperature to the test temperature since the fillcoat would be in compression below the sputtering temperature. This procedure should also reduce or prevent the entrapment of argon in the fillcoat during sputtering (ref. 10). Sputtering onto a hot substrate did not eliminate the possibility of shorts caused by debris falling on the substrate during sputtering which created defects in the insulating layer when the debris was removed. Substrates were heated to 870 K or 1070 K using a radiant heater mounted in the sputtering chamber. The substrates were clamped to a Hastelloy-X plate mounted on top of the heater and heated in vacuum to the sputtering temperature at which point the working gas (Ar 20% O_2) was introduced and deposition begun.

Several Hastelloy-X substrates 0.178 cm x 1.27 cm x 1.50 cm on which PdCr film patches (dots) were deposited were also produced to test adherence of Pd-13Cr as well as candidate compensation element materials on various substrate surfaces. In some cases half

the alumina fillcoat surface was given a 200 Å sputtered bondcoat layer of Fe-10.6Cr-11.9Al (FeCrAl Mod 3 evaluated as a possible sensor material during Task 2), whereas on the other half, the sputtered Pd, Pt, or Pd-13Cr was deposited directly onto the alumina fillcoat.

Ten Task 5A samples were also produced on solid alumina substrates to evaluate possible topcoat materials. Alumina was used as a substrate material to eliminate the possibility of shorts to the substrate rendering samples unsuitable for testing. Two thicknesses of alumina substrate were used, the first being 0.254 mm thick and the second being 1.27 mm when the thinner substrates proved too fragile for easy processing. The PdCr grid pattern was sputtered directly onto the alumina substrate, eliminating the fabrication steps needed to produce an insulating layer on Hastelloy-X. The alumina substrates were cleaned in hot freon vapor, then baked for one hour in air at 810 K before deposition of the PdCr film.

5.2.2 Sensor Elements

The sensor elements for resistance measurements at elevated temperatures consisted of a 3 mm x 3 mm sputtered Pd-13Cr grid 4.5 μm thick with a line width and line spacing of 0.127 mm. PdCr grid patterns were prepared by standard "lift off" photolithographic techniques using a positive working photoresist. Samples fabricated at the start of Task 5 had film thicknesses of 6 μm but difficulty was encountered in removing the bridged film between grid legs after dissolving away the photoresist. It was determined that above a critical line spacing to film thickness ratio of 28 to 1 the film could be torn loose without damage to the remaining film. For the 0.127 mm line spacing used in this program, clean removal of the bridged film was achieved with a film thickness of 4.5 μm.

Three PdCr targets were used for preparation of samples tested during this contract. The majority of samples were sputtered from a Pd-14wt%Cr hot pressed target (UTRC target) fabricated for this contract and used at Pratt & Whitney - Engineering Division North (P&W-EDN). This target was found to contain impurities of Al, Mo, and Fe (0.35 - 0.51 wt%). Three samples for target comparison testing were fabricated using a cast Pd-13wt%Cr NASA target at NASA Lewis Research Center. This target did not contain the impurities mentioned above. Sensors deposited on the Task 8 bend bars were sputtered from a cast Pratt & Whitney target at Pratt & Whitney - Engineering Division North (P&W-EDS). This target had an analyzed composition of Pd-13.39wt%Cr with no impurities present in levels exceeding 25 ppm.

Sputtered films are often found to be thermodynamically unstable in the as-sputtered condition and in a high state of stress due to large defects in the crystal structure. In order to produce a stable film and to eliminate the nodular structure seen in the as-sputtered films, the majority of Task 5 samples were heated to elevated temperatures in an inert atmosphere to recrystallize the PdCr. As with previous work in Task 2, recrystallization of the PdCr film was accomplished by a heat treatment at 1370 K for 12 hours in purified argon (O_2<10^{-7}ppm). Two problems were encountered with these recrystallized films. Several samples produced early in Task 5 shorted to the substrate during recrystallization or when heated following recrystallization. During recrystallization the PdCr is apparently able to penetrate defects or areas of thin insulation in the fillcoat causing shorts or later leading to shorts when the sample is heated. The recrystallized film also contained holes 3 μm to 7 μm in diameter believed to have been caused by the loss of exaggerated growth nodules during recrystallization. These holes would lead to difficulties in attempting to later seal the film surface with a protective overcoat layer, since the sides of the holes would not be effectively coated. These problems lead to a decision to delay both the fillcoat stabilization heat treatment and the recrystallization heat treatment until after the sample had been overcoated. This combined heat treatment of an overcoated sample was a failure because it resulted in melting of the PdCr at 1380 K. This melting appeared to be associated with the non-availability of oxygen to convert impurities contained in the PdCr, including aluminum, to oxides. Since the overcoat prevented oxygen from reaching the PdCr, the impurities may have lowered the melting point of the PdCr below 1380 K. It was previously observed that the oxygen content of the heat treatment atmosphere affected the PdCr recrystallization temperature. Samples heat treated at 1370 K with >10^{-6} ppm oxygen present did not recrystallize. Samples produced after the failure of the combined heat treatment were tested without being recrystallized.

For resistance and adherence tests at room temperature before and after thermal cycling without resistance data being taken at elevated temperatures, samples on 0.188 cm x 1.27 cm x 5.00 cm Hastelloy-X substrates were fabricated using the same techniques as for the elevated temperature test samples. Instead of a grid pattern sputtered PdCr lines of various widths were deposited onto these substrates with resistance measurements at room temperature taken from end to end.

5.2.3 Alumina Overcoats

Sputtered alumina overcoats 2.0 μm thick were applied to all Task 5 and 5A samples. These overcoats were applied over the entire sample with the exception of the ends of the leadfilms. Prior to overcoating a 0.5 μm sputtered or ion beam deposited layer

of Pt was deposited over the PdCr at the ends of the leadfilms to prevent oxidation of the PdCr and insure good electrical contact for the clamped leads during thermal cycling. The portions of the leadfilms having a Pt coating were then masked during overcoat application to prevent alumina from being deposited on them thus maintaining the conductive surface.

For application of hot sputtered overcoats, the samples were heated in the sputtering chamber to 570 K in vacuum at which point the chamber was back-filled to a base pressure of 5 millitorr Ar 20% O_2 and sputtering begun. When a 0.15 to 0.20 μm layer of alumina had been applied to protect the PdCr from oxidation during the sputtering process, the sample was heated to the selected substrate temperature while sputtering continued to deposit the remainder of the 2.0 μm thick alumina film.

5.2.4 Topcoats

Various topcoat materials listed in Table 5.2.1 were applied over the alumina overcoats on Task 5A samples to improve the oxidation resistance of the protective layer. The overcoated samples were heat treated at 1140 K in air prior to topcoating to stabilize the alumina overcoat and to eliminate any argon trapped in the overcoat during sputtering. Topcoat materials were applied by transfer tapes, by sputtering, or by ion beam deposition.

Two glass transfer tapes were evaluated as topcoat materials. These tapes consisted of a layer of glass frit and organic binder which were transferred from a carrier film to the sample surface. The glass was then fired to form a fused glass layer 5 μm to 20 μm thick. The first tape tried was G-1004 borosilicate glass * with a suggested firing temperature of 1270 K. This glass was found to react with the alumina overcoat and the PdCr at the firing temperature and therefore was dropped from further evaluation. The second composition was G-1003 lead-alumina-silicate glass * which was fired at 1300 K in air. The resulting topcoat was clear and adherent with a thickness of approximately 8 μm. This material was used to produce one sample for elevated temperature resistance testing.

7070 borosilicate glass topcoats were also fabricated by ion beam deposition. Three samples were produced with topcoat thicknesses of 1.5, 0.4 and 0.25 μm. The 1.5 μm topcoat spalled in some areas while the thinner layers were adherent. These topcoats did not extend to the end of the alumina overcoat on the leadfilms to avoid any direct contact between the glass and the PdCr. Since these topcoats did not have to be heated to fuse the glass, no reactions between the topcoat and the underlying layers were seen.

---

* Vitta Corp., Wilton, CT

Three compositions of sputtered metallic topcoats were also produced. These conductive topcoats were only applied over the grid region to eliminate the possibility of shorts through the overcoat to the PdCr leadfilms. In spite of this precaution the as-sputtered aluminum topcoats were shorted to the grid in at least two locations. Aluminum topcoats of 0.50 μm and 0.25 μm were produced. The 0.50 μm thick topcoat was heat treated in air at 900 K for 50 hours to oxidize the aluminum and remove the shorts prior to testing. Although this heat treatment was successful in oxidizing the topcoat to form a non-conductive layer, stresses created in the topcoat as it oxidized caused it to buckle over sections of the PdCr grid resulting in failure of the grid. The 0.25 μm thick topcoat was heat treated in air at 830 K for 50 hours to oxidize the aluminum. This lower temperature did not completely oxidize the aluminum but did eliminate the majority of the shorts to the PdCr and resulted in an adherent topcoat. A palladium topcoat 0.025 μm thick was applied to sample 8C11-7 but like the aluminum topcoats, resulted in shorts between the conductive topcoat and the Pd-13Cr grid. The third metallic topcoat was 0.25 μm of FeCrAl Mod 3 developed earlier in this contract. The FeCrAl was adherent and, unlike the other conductive topcoats, this sample did not contain any shorts between the topcoat and the PdCr grid as sputtered.

5.3 SUPERALLOY BEND BARS

Nickel base superalloy cantilever bend bars for evaluating complete strain gage systems with compensation grids were prepared by casting and machining to the dimensions shown in Figure 5.3.1. The final design shown in this figure permits these bars to be used in the automated strain gage testing facility at NASA Lewis. The bars were made of P&W alloy 1422, (MAR M-200 + Hf), directionally solidified parallel to the long axis of the bar. This turbine blade alloy was selected because its high strength should ensure that no plastic yielding would occur during our testing to complicate interpretation of the data. The nominal strains parallel to the direction of solidification at 0.5 percent offset yield (the approximate elastic limit) at 1000 K and 1250 K are 8,400 and 5,500 μstrain, respectively. Additional information about the properties of this alloy are given in Table A3 in Appendix A.

Two thin film strain gages were installed on the top surfaces of six test bend bars as shown in Figure 5.3.2. Temperature compensation grids of pure palladium, which are indicated as resistors F+f in the strain gage bridge circuit in Figures B1 and B2 in Appendix B, were positioned on each side of both gages. Drawings A1 and A2 in Appendix A present in more detail the dimensions of the photomasks used to create the compensation and the active grids. Both grids consisted of 0.0127 cm wide conductors spaced 0.0127 cm apart.

The procedures used to prepare the surfaces of the bend bars and to deposit the various sputtered thin films were the same as those used to install Pd-13Cr grids on Hastelloy-X substrates (see Section 5.2) with the following exceptions:

(a) The alumina insulation between the substrate and the metal grid layers was deposited in three different layers in an attempt to reduce the potential for electrical leakage associated with localized defects. The first sputtered alumina layer was approximately 2 μm thick and the second and third layers were each approximately 0.5 μm thick. Because a delay in the completion of Task 5A resulted in the hot sputtered fillcoat and overcoat testing being completed after the start of bend bar fillcoat deposition, the bend bars were not heated during the deposition of these alumina layers. After each layer was deposited, the sample was heated to 1250 K in air and then subjected to a soft glass bead blasting treatment at ambient temperature to remove any poorly adherent alumina. This glass bead blasting was accomplished* using 44 micron beads and a gas pressure of 30 psi. This glass bead treatment was only performed on samples B1, B2, and B3. Following the glass bead blasting, the bars were ultrasonically cleaned in an acetone/Freon mixture to remove any remaining beads or residue.

(b) The Pd compensation grids and leadfilms were sputtered at UTRC prior to sputtering the active Pd-13Cr grids. A 200 Å bondlayer of FeCrAl Mod. 3 was first deposited on the fillcoat followed by 4 μm of Pd. The Pd leadfilms were centered under the PdCr leadfilms and were only half the width of the PdCr. This layout reduced the resistance of the leads compared to the Task 5A leads, and prevented the formation of an 8 μm step at the edge of the leadfilms which might reduce the effectiveness of the overcoat. Further details are shown in Figures A1 and A2 in Appendix A.

(c) The Pd-13Cr active grids were sputtered at P&W-EDS to take advantage of their target which did not contain the impurities present in the UTRC target.

(d) The 2 μm thick alumina overcoats on the first four bend bars (B1-B4) were cold sputtered while the overcoats on the last two bars (B5 and B6) were sputtered with the substrates held at 870 K.

A 0.5 μm 7070 borosilicate glass topcoat was applied to Bend bar B2 by ion beam deposition. Although this topcoat did not have a noticeable effect on the test results for samples with hot sputtered overcoats on Hastelloy-X substrates in Task 5A, it did appear to improve the performance of cold-sputtered overcoats. This topcoat was not added to bars B5 and B6 which had hot-sputtered overcoats.

* S.S. White, Airbrasive 6500 System, Piscataway, N.J.

The first step in the preparation of the bar for the attachment of lead wires was to grit blast a 0.137 cm wide strip across the polished surface of the bar adjacent to the ends of the sputtered leadfilms. A 0.0025 to 0.005 cm thick coat of Metco 443 * was then flame sprayed on this strip followed by a 0.010 cm thick flame sprayed layer of Rockide-H alumina**. The main leads for each gage consisted of three Ni-clad Cu wires 0.025 cm in diameter and approximately 46 cm long with Varglass sleeving. Platinum wires, 0.0075 cm in diameter, were wrapped around and bonded to the bare ends of the Ni-clad Cu wires with Nicobraze-150***. Six of these lead wires were then positioned across the Rockide-H strip with small pieces of masking tape and secured in this position with a flame sprayed coating of Rockide-H. Removing the strips of masking tape and overspraying again with Rockide-H completed the installation of these six wires with the brazed joints embedded within the Rockide-H alumina and the free, uncoated ends of the 0.0075 cm diameter Pt wires extending out over the sputtered thin film leads.

The next step in lead wire installation consisted of connecting 0.0025 cm diameter Pt wires between the individual sputtered leadfilms and the 0.0075 cm diameter Pt wires by a parallel gap welding process. The final step was to carefully incapuslate the 0.0025 cm diameter Pt wires in a ceramic cement ****. Figures 5.3.3 and 5.3.4 are photographs which show complete strain gage installations with the lead wires and thermocouples attached.

Three type K thermocouples were installed on each test bar to measure temperature. One thermocouple was located on the opposite face of the bar from the gages, centered on the bar. The beads of other two thermocouples were located at positions which corresponded to the axial centers of the gages only at the two edges of the bar. The thermocouple wires were 0.020 cm in diameter with Varglass sleeves. The beads of the thermocouples were electrically insulated and held in close contact with the bar using the same flame spraying procedure described above for the Ni clad Cu strain gage lead wires. Spot welded Hastelloy-X tabs were used to hold the thermocouple lead wires in position as shown in Figure 5.3.3.

---

* Metco, Westbury, N.Y. 11590

** Hitec, Ayer, MA

*** Lucas-Milhaupt, Cudahy, WI

**** Micro Engineering II, Upland, CA

5.4 THERMAL CYCLE AND DRIFT TESTING

Electrical resistance measurements of Task 5 and 5A samples were made using a resistively heated tube furnace developed during a prior contract (ref. 2). The facility consists of a 3.81 cm diameter by 20 cm long Inconel tube which is split in half lengthwise to facilitate sample installation. The ends of the heater tube are clamped in water-cooled electrodes which provide up to 900 amperes of AC power. The electrode at one end of the furnace is supported by a ball bearing system which prevents mechanical loads from being applied to the tube as it expands and contracts thermally during use. Power to the furnace is controlled by a commercial closed loop controller and programmer. The programmer is adjusted to provide for constant temperature soaks at elevated temperatures and/or linear heating and cooling cycles at heating rates up to 250 K/min.

A set of B-1900 superalloy clamping bars which extended 5 cm into one end of the furnace provided the clamping force for electrical contacts and physical support of the sample. Electrical contact with the sputtered leadfilms was made through 0.127 mm platinum foils to which 0.254 mm diameter platinum sensing and power leadwires were welded for four-wire measurement of sample resistance. The temperature of the sample was measured by a 0.127 mm ANSI type S (Pt-Pt 10% Rh) thermocouple whose bead (junction) was in contact with the substrate adjacent to the sputtered grid.

A computer, voltmeter, programmable power supply, and a scanner were used to measure the resistance data and to store it on a floppy disk. The standard accuracy of the voltmeter was 20 μV/V (.002% error) which was further improved to 4 μV/V (0.0004% error) by averaging five separate readings. A set of measurements was triggered by a sample thermocouple EMF change equivalent to ±50 K or, if this did not occur, by the passage of ten minutes (drift testing). The following sequence of measurements were made by the computer in order to determine one electrical resistance data point:

1. Sample temperature
2. Voltage across the sample
3. Voltage across precision resistor
4. Repeat reading 2 and 3 for a total of five readings each
5. Sample temperature
6. Repeat readings 2 and 3 with power off for a total of five readings each

Allowing slightly more than the time necessary for voltage "settling" after each reading, a full set of the 12 measurements with the power on required about 2.3 seconds to complete.

Using the average values from repeated measurements of the same type permitted the determination of the values of a number of variables at the same instant of time and tended to reduce the "noise" in the data. Measurements of the voltage drop across the precision resistor in series with the sample were used to accurately determine the current through the sample. This precision resistor was separately mounted on a water-cooled plate away from the furnace to maintain it at a constant temperature.

Voltage measurements with no power through the sample were used to reduce any influence on the data of thermocouple effects due to the use of materials with different compositions in the measurement circuit. Typical currents and voltages through and across the sample were 15 milliamps and 2 volts. Room temperature experiments established that, at this current level, there were no effects on the resistance measurements due to sample heating. The programmable power supply only put current through the sample when a set of measurements was being made. The accuracy of the overall resistance measurement system was estimated to be $\pm$ 8 $\mu\Omega/\Omega$ excluding any error due to temperature gradients in the sample.

5.5 TESTING OF COMPLETE GAGE SYSTEMS ON BEND BARS

The sequence of tests used to evaluate the performance of the six bend bars prepared in Task 8 was designed to make measurements at gradually increasing values of strain and temperature. The sequence began with measurements of the gage factor of each of the two complete strain gage systems installed on each bar at low strains (to 1000 μstrain) at room temperature following the cantilever bending method described in ASTM E251-67. This was followed by apparent strain cycling to the maximum temperature (T_{Max}) selected for that particular bar. The gage factor was also measured at several temperatures up to T_{Max} at low strain (500 μstrain). Drift tests were then to be performed at several temperatures from T_{Max} downward as follows:

50 hours, T_{Max}.
16 hours, 755 K after fast cool (10 minutes) from 920 K.
16 hours, 700 K after fast cool (10 minutes) from 920 K.
16 hours, 645 K after fast cool (10 minutes) from 920 K.

Following each of these drift tests the bar was cooled to room temperature to measure any effect on the thermal coefficient of resistance resulting from the drift test. The provision for heating to and cooling from 920 K before each drift test was added to provide a common reference heat treatment before each subsequent drift test. Finally, the gage

factor at T_{Max} at high strains (to 2000 μstrain) was to be measured. At several points during the sequence and again at the end of all testing, the gage factor was remeasured at room temperature.

The first bar was to be tested for gage factor at room temperature only and then sent to NASA in accordance with the Statement of Work. The second bar was to be tested to a T_{Max} of 920 K. The third bar was to be tested to a T_{Max} of 1000 K and the fourth bar was to be tested to a T_{Max} of 1100 K. If possible, the testing of one bar was to be extended to a T_{Max} of 1250 K. The fifth bar was to be tested for gage factor at room temperature only and then also sent to NASA in accordance with the Statement of Work. The sixth bar was to be tested to a T_{Max} selected with the concurrence of NASA after the testing of the first four bars had been completed. Because a number of the bars were not suitable for testing because of problems encountered during fabrication, the testing plan was modified so that after finishing the test program to the first T_{Max} temperature, the same samples were used for testing to higher T_{Max} temperatures to gather as much data as possible from the samples available.

Loading of the bend samples was accomplished using the Pratt & Whitney cantilever bend testing machine shown in Figure 5.5.1. Testing at elevated temperatures was accomplished by use of a Marshall furnace which fitted over the test bar mounted in the test machine. The furnace was capable of 1250 K operation and had an 8-cm diameter cylindrical interior 30 cm long. The heat-up times to reach the test temperatures were typically about one hour. Special reinforced end fixtures were used to isolate the region of high strain. The amplitude of deflection was determined by the computer-controlled motion of a stepping-motor-driven arm. The deflection was about three millimeters for 500 μstrain, and repeatable within 0.03 millimeters (1 percent at 500 μstrain).

As shown in Figure 5.3.2, two independent strain gage systems were installed beside each other on the top surface of the each test bar. Three ANSI type K thermocouples and a reference commercial static strain gage were also installed on each bend bar as described in Section 5.3. A commercial strain gage was located on the opposite side of the test bar, directly under the two test gages, which permitted a reliable initial measurement of strain to be made to compare with the strain calculated on the basis of test bar dimensions and deflection. The reference gage did not survive the high temperature testing and was not replaced. The strains obtained at high temperatures were assumed to be the same function of deflection as at low temperatures. The possibility of the bar yielding plastically at temperature was nil because the elastic limit of MAR M 200 + Hf is appreciably higher than any strain imposed in this testing. Previous tests with this apparatus and similar test bar

geometry have shown that the temperature was uniform within 17 K over the 7.6 cm centered on the midpoint between the grips (ref. 12).

A Hastelloy X test bar instrumented with four commercial strain gages on one side was used to determine the overall accuracy of the gage factor determination using the automated testing system at room temperature. The repeatability of gage factor was within one percent when several repetitions of a strain measurement were made without changing the test conditions and within two percent when the bar was removed and reinstalled between measurements. Gage factors in tension and compression, at 500 μstrain and at 1000 μstrain, were the same within two percent. Agreement with the manufacturer's specified gage factor was also within two percent, as determined from the calculated strain. All percentage figures are two sigma error bands, based on at least four repetitions of each measurement. The uncertainty of gage factor determinations in this work is therefore estimated to be the square root of $2^2 + 2^2 + 2^2 = 3.5$ percent at room temperature.

The measurement and control system used an existing digital data acquisition system controlled by a desktop computer to provide acquisition and storage of the desired strain gage bridge data (output voltages and excitation voltages). The data system was programmed to acquire and store sample measurements at rates up to five per second. The system also provided subsequent automatic data reduction and output in the form of tables and plots of calculated gage factor, apparent strain, and drift for each strain gage.

The strain gage data was acquired using the bridge circuit shown in Figure B1 of Appendix B using a constant 5 volt power source and the three-wire connection method to minimize lead wire and lead film resistance. The following quantities were measured at each test point for each thin film strain gage:

e^+	Output voltage for positive excitation
e^-	Output voltage for negative excitation
E^+	Excitation voltage for positive excitation
E^-	Excitation voltage for negative excitation

For each strain level and temperature, the bar was deflected (strained) twice in each direction (tension and compression) in a 0 + 0 - 0 + 0 - 0 sequence. For each strain gage, an average gage factor was calculated for each direction, strain level, and temperature based on the four measurements in the deflection sequence. The standard deviation was also calculated for the four measurements. A separate ground lead wire welded to the bare metal of each test bar also permitted automatic measurements of the insulation leakage to substrate ground.

Table B1 of Appendix B defines and lists all of the terms used in the adjustments and calculations in this program associated with strain measurement of a compensated strain gage system. The following procedure was designed to adjust the temperature compensation where A & B are the 10 turn potentiometers, C is the fixed resistor and R is the gage resistance as shown in Figures B1 and B2 in Appendix B. The procedure assumes that the temperature compensation element (F) changes resistance with temperature at about the same rate (ohms/Kelvin) as the strain gage element (R) so that the bridge ratio (m) is near 1:1. The procedure was altered appropriately when a bridge ratio far from 1:1 was necessary, due to a larger or smaller than expected compensation element resistance as sputtered (see Sect. 6.3).

1. Measure the strain element resistance R with a low current ohmmeter (0.01 Amp. or less). Select C (ohms) and set A (ohms) and B (ohms) so that (A+F) = B = C = R within 5 percent.

2. At room temperature adjust B for optimum bridge balance, i.e., output voltage e corresponding to less than 50 μstrain indicated.

3. At high temperature (920 K) observe that there is a large bridge unbalance voltage e. Remove this unbalance, while still at high temperature as follows:

4 Adjust A and B in the same direction by equal amounts until the unbalance is again less than 50 μstrain indicated. The direction will be such that A increases the unbalance and B decreases it.

5. Repeat 2 and 3 until no further adjustment is needed. No iteration will be needed if the four bridge arms were initially nearly equal at room temperature (step 1)..

An example of initial and final settings of A and B is given below. The quantities f and r in the table are the changes in resistance due to temperature in the compensation arm and the strain element arm of the bridge, respectively. In this example it was assumed that C = R = 100 ohms and that E = 1 volt. EC and ER are then the voltages across the bridge arms containing resistor C and R (gage), respectively, where (e = EC-ER).

	B ohms	A+F ohms	f ohms	r ohms	EC volts	ER volts	e volts	Change in e Due to Temp	Approx. Apparent Strain (με) For G = 2
Before Adjustments									
Room Temp.	100	100	0	0	.5	.5	0	0	0
High Temp.	100	100	19	20	.5	.5021	.0021	.0021	4200
After Adjustments									
Room Temp.	95	95	0	0	.5128	.5128	0	0	0
High Temp.	95	95	19	20	.5128	.5128	0	0	0

The temperatures of the gages were measured using ungrounded ANSI Type K thermocouples cemented to the substrate with a thin layer of cement for good thermal contact and electrical isolation. The temperature was recorded to the nearest tenth of a Kelvin unit even though the uncertainty due to calibration bias might be several units. This requirement arises because the thermal coefficient of resistance of the compensated gage may be about 30 $x10^6$/K, the effective gage factor about 1.5, and it was desired to construct a lookup table for apparent strain change due to temperature change with a resolution of about 2 μstrain. The temperature resolution requirement is then about (2) (1.5)/(30) = 0.1K.

The bridge equation for a dual-element, self-compensated strain gage bridge has been examined in both the present NASA program and in a concurrent NASA program, NASA/P&W Contract NAS3-25410. The derivation presented in Appendix B results in the equation:

$$e' = K[U^*x + L^* + V^* + c'] \qquad (1)$$

In this equation e' is the ratio of bridge output voltage e to bridge excitation voltage E, K is the bridge sensitivity factor (bridge factor), U* is gage factor, x is the strain, L* and V* are functions of temperature and c' is the fractional change in calibration arm resistance C when the shunt calibration switch is activated. (c' = 0 except when the shunt calibration procedure is being used.)

The quantities L* and V* need further comment. L* is the apparent residual fractional change (dimensionless) in gage arm resistance due to temperature after compensation. V* is the error term due to thermocouple emf's in the bridge. Both are

functions of temperature. The quantity V* is unique in that its algebraic sign is independent of the polarity of bridge excitation voltage. Therefore V* may be measured (and eliminated in calculations) by measuring bridge output with positive excitation (e+) and again with negative excitation (e-). KV* is half the difference between e+ and e-.

The following procedures for various measurement subroutines are all based on the use of equation (1) above:

Determining Bridge Sensitivity (Bridge Factor) K by Shunt Calibration

Without shunt c' and positive bridge excitation, Eqn, (1) becomes

$e'1 = K[U^*x + L^* + V^*]$

With a known shunt c' and a positive bridge excitation, Eqn. (1) becomes

$e'2 = K[U^*x + L^* + c' + V^*]$

Measure e'1 and e'2. Calculate $K = (e'2 - e'1)/c'$
Measure resistance to ground with + and - polarity.
Flag readings less than 600,000 ohms.

Determining Gage Factor, U*

With no shunt cal c', no strain, $T = T_{test}$, bridge excitation +, Eqn. (1) becomes

$e'1 = K[L^* + V^*]$

With no shunt cal c', strain x, $T = T_{test}$, bridge excitation +, Eqn. (1) is

$e'3 = K[U^*x + L^* + V^*]$

Measure e'1 and e'3. Calculate $U^* = (e'3 - e'1)/(Kx)$
Measure resistance to ground with + and - polarity.
Flag readings less than 600,000 ohms.

Determining L* (ΔR/R) (Apparent Resistance Change Due to TCR and Delta TCE) and V* (Apparent Resistance Change Due to Thermocouple Effects)

At x = 0, known temp., no c', e+, Eqn. (1) becomes

$e'+ = K(L^* + V^*)$

For e'-, $e'- = K(L^* - V^*)$

Measure e'+, e'-, and T. Calculate $\Delta R/R = L^* = [(e'+) + (e'-)]/2K$
Calculate $V^* = [(e'+) - (e'-)]/2K$
Flag V* values greater than 0.0001

Construct look up table of L* versus temperature.
Measure resistance to ground with + and - polarity
Flag readings less than 600,000 ohms.

Measuring Gage to Ground Resistance

In the bridge circuit of Figure B1 in Appendix B placing the "USE-CHECK" switch to "CHECK" disconnects all four external connections to the strain gage bridge and connects a floating ohmmeter circuit to measure resistance to test bar ground (0.5 volts applied) at the common lead of the gage and compensation element on the test bar, The "OHMMETER POLARITY" switch permits performing the measurement with either a positive or a negative 0.5 volts.

To avoid possible ground loops due to electrical leakage through the insulation between the gages and the metal substrate under the gages, the test bar must not be in contact with any other metal parts in the experiment. One lead wire was welded to the metal substrate ground to permit measurement of resistance to metal substrate ground.

The data recorded were the ohmmeter applied voltage EE (Volts), and the ohmmeter circuit output voltage E1 (volts, across the resistor R1). The resistance from gage to test bar ground RG ohms was then calculated from:

$$RG = (R1)\,(EE) / (E1). \qquad (2)$$

6.0 RESULTS

6.1 SAMPLES WITH COLD SPUTTERED ALUMINA OVERCOATS

During task's 5 and 5A 34 samples on alumina or Hastelloy-X substrates having alumina fillcoats and overcoats sputtered at room temperature were produced. Many of these samples were not tested due to various defects or failures during fabrication. A summary of these samples is shown in Table 6.1.1 for samples produced on Hastelloy-X substrates and Table 6.1.2 for samples produced on alumina substrates. Thirteen of these samples were tested for thermal coefficient of resistance and stability (drift) at temperatures to 1250 K. Several of these samples also included various topcoats to aide in sealing the overcoat. A summary of the results of these tests is shown in Table 6.1.3.

6.1.1 Samples without Topcoats

Two samples on Hastelloy-X substrates overcoated with 2.5 μm to 3.5 μm of alumina were tested during Task 5. These samples differed in that sample 8-40 was heat-treated to recrystallize the PdCr prior to overcoating (see Section 5.2.2), whereas sample 8-81 was not recrystallized. Sample 8-40 was drift tested at 1100 K but shorted to the substrate after 20 hours. During this test the sample resistance rose rapidly with a total drift of 700,000 μΩ/Ω after 20 hours. A 50 hour drift test at 1100 K resulted in a total drift of -54,500 μΩ/Ω for sample 8-81 and a final drift rate of -185 μΩ/Ω/hr. These results led to the decision to discontinue attempts to produce recrystallized PdCr films since the as-sputtered films appear to be more stable at elevated temperatures. The thermal coefficient of resistance of sample 8-81 increased 35% from 149 μΩ/Ω/K to 202 μΩ/Ω/K as a result of the 1100 K drift. Both the negative drift and the increase in thermal coefficient of resistance indicate that significant change in composition is taking place as the PdCr oxidizes. Optical examination of the sample revealed circular defects in the alumina overcoat over the PdCr grid. These defects consisted of patches of debonded overcoat 0.076 to 0.100 mm in diameter allowing oxidation of the underlying PdCr. In addition the left leg of the grid had detached from the substrate with delamination taking place between the sputtered alumina fillcoat and the grown oxide layer on the NiCoCrAlY. A direct comparison of these results to uncoated PdCr was not possible since previously tested uncoated samples had been tested at 1250 K.

Five samples on alumina substrates with alumina overcoats, but without additional topcoats, were tested during Task 5A. A summary of the results of these tests is shown in

Table 6.1.3. Two of these samples (5A-A-1, 5A-A-2) contained PdCr films sputtered from a target at NASA Lewis for comparison with material sputtered using the UTRC target. The as-sputtered thermal coefficient of resistance (alpha) of these samples varied from 139.4 μΩ/Ω/K to 131.4 μΩ/Ω/K for the UTRC material and was 134.2 μΩ/Ω/K for both samples sputtered at NASA Lewis.

Two samples sputtered using the UTRC target (8CII-10, 8CII-13) and two sputtered at NASA (5A-A-1, 5A-A-2) were tested for stability at 1100 K for 50 hours. All samples showed a negative drift over the 50 hours with the results plotted in Figure 6.1.1. The decreasing resistance is probably due to several processes, including stabilization of the as-sputtered structure and the formation of Cr_2O_3 under the overcoat removing chromium from the alloy. The decreasing rate of drift may signify that the Cr_2O_3 being formed is filling cracks or other defects in the overcoat, slowing the movement of oxygen through the overcoat. Total drift for these samples ranged from -17,400 μΩ/Ω to -19,068 μΩ/Ω for the UTRC material and from -22,883 μΩ/Ω to -23,689 μΩ/Ω for the NASA Lewis material. Final drift rates were also higher for the NASA Lewis material with an average of 205 μΩ/Ω/hr vs. 106 μΩ/Ω/hr for the UTRC material. The thermal coefficient of resistance of the UTRC samples increased an average of 15.4% as a result of the drift test whereas the NASA material increased an average of 12.2%. These results represent a significant improvement over results from sample 8-81 on Hastelloy-X tested during Task 5 (above). Optical examination of the samples following the 1100K drift test showed no signs of overcoat spalling or cracking. The differences in results between the UTRC PdCr and the NASA PdCr were minimal with the exception of final drift rate. This difference may have been caused by the integrity of the overcoat or by differences in target composition (Section 5.2.2).

The four Task 5A samples tested at 1100K were subsequently tested for stability at 1250 K. All these tests were plagued by erratic data caused by high clamp resistance. Sample 8CII-13 had a drift of -20,000 μΩ/Ω in 10 hours before the resistance began to increase due to high clamp resistance. The thermal coefficient of resistance for this sample increased 146% to 394.3 μΩ/Ω/K as a result of 50 hours at 1250K. All samples which were held at 1250K for more then 8 hours exhibited overcoat defects. These defects in the samples sputtered using the UTRC target consisted of blisters in the overcoat (Figure 6.1.2). The samples sputtered at NASA Lewis did not contain these blisters but instead had regularly spaced transverse linear cracks in the alumina overcoat over the legs of the PdCr grid. Each crack extended completely across the grid leg, ending at the edges of the PdCr. It was not determined if these cracks coincided with cracks in the underlying PdCr grid. The lack of blisters on these samples can not be explained by differences in overcoat fabrication since

both types of samples had overcoats applied at Pratt & Whitney. The only known difference between the samples was the target used for the PdCr sputtering. The UTRC target did contain impurities of Al, Mo, and Fe which were not found in the NASA target. The presence of these impurities could explain the blister formation in the UTRC samples.

6.1.2 Samples with Topcoats

Five samples with a variety of topcoats over the alumina overcoat were also tested as part of Task 5A. Sample 8CII-9 was topcoated with G-1003 glass transfer tape. Drift at 1100 K was random with maximum excursions of +10,800μΩ/Ω and -14,900μΩ/Ω. Alpha increased 101% to 301.2 μΩ/Ω/K as a result of this test. The random drift and a relatively small change in room temperature resistance combined with the large change in thermal coefficient of resistance indicates that oxidation of the PdCr was not the only process occurring during the drift test. This conclusion was supported by examination of the sample following testing which revealed signs of a reaction between the lead-alumina-silicate topcoat and the overcoat, as well as between the topcoat and PdCr.

Two samples were topcoated with sputtered aluminum. Topcoat thicknesses were 0.50 μm for sample 5A-A-3 and 0.25 μm for sample P87-1-5. Topcoating resulted in a decrease in sample resistance of 9% for sample 5A-A-3 and 57% for sample P87-1-5 due to shorting of the grid through the conductive topcoat. During a 900K heat treatment of sample 5A-A-3 to oxidize the topcoat, the grid resistance rose 15.6%, but an open circuit developed in the grid during cool-down. The open circuit was associated with a region where the topcoat had cracked and folded either due to differences in CTE between Al, Al_2O_3 and PdCr, or a volume change in the topcoat as the aluminum oxidized or reacted with the PdCr at defects in the overcoat. Sample P87-1-5 was heat treated at 835 K instead of 900 K, which succeeded in raising the grid resistance to its as-sputtered value without causing any breaks in the PdCr film. During the first cycle to 1100 K, however, the PdCr film again shorted to the topcoat causing the grid resistance to drop 50%. Alpha measured during this cycle was 191 μΩ/Ω/K, indicating a change in sample composition due to a reaction between the PdCr film and unoxidized aluminum during the 835 K heat treatment. Optical examination of the sample following this cycle revealed the same type of defect as seen in sample 5A-A-3 (above). Sample P87-1-5 was heated to 1250 K which increased the resistance between the topcoat and PdCr to >20 MegΩ and appeared to completely oxidize the topcoat, but resulted in an open grid circuit when the sample cooled to ambient temperature.

Two samples were topcoated with ion beam deposited 7070 borosilicate glass. Topcoat thicknesses were 0.25 μm for sample P87-1-1 and 0.40 μm for sample P87-1-2. Alpha, measured during the third cycle to 1100 K was 154.7 μΩ/Ω/K and 147.3 μΩ/Ω/K for P87-1-1 and P87-1-2 respectively. These values are slightly higher then those obtained from testing of overcoated samples on alumina substrates, which averaged 135.5 μΩ/Ω/K. The difference in alpha between samples sputtered on the two substrate materials could be due to the higher CTE of the Hastelloy-X vs. alumina. The CTE difference is 10.1 μin/in/K which is very close to the average difference in alpha of 10 to 12 μin/in/K if a gage factor of 1.3 to 1.5 is used to convert μΩ/Ω to μin/in. This gage factor is based on data for Pd-13%Cr from Task 8 of this contract. The results of 50 hour drift tests at 1100 K are shown in Fig. 6.1.3. Total drift over the 50 hours was -40,400 μΩ/Ω for P87-1-1 with a minimum drift rate of -164 μΩ/Ω/hr at 16 hours, and a final drift rate of -306 μΩ/Ω/hr. Sample P87-1-2 had a lower total drift (-24,400 μΩ/Ω), and a lower final drift rate (-249 μΩ/Ω/hr), indicating that the thicker topcoat offered better oxidation protection at 1100 K without delaminating or spalling. Alpha measured after the 1100 K drift test for sample P87-1-2 was 182 μΩ/Ω/K, a 24% increase over the pre-drift alpha. Post drift measurement of alpha for sample P87-1-1 was not possible due to an error in furnace programming.

Both samples were heated to 1250 K for a 50 hour drift test, but again the data from sample P87-1-1 was not usable due to the furnace programming error. Total drift of sample P87-1-2 at 1250 K was -309,700 μΩ/Ω, with a final drift rate of -432 μΩ/Ω/hr. Alpha following drift testing was 610 μΩ/Ω/K, an increase of 314% over alpha at the start of testing.

Insulation resistance measurements were also taken on both samples during testing at 1100 K. The insulation resistance dropped below 20 MegΩ at 675 K for sample P87-1-1, and at 860 K for sample P87-1-2. Insulation resistance of sample P87-1-1 at 1100 K was initially 130 KΩ but decreased during drift testing stabilizing at 19 KΩ after 3.5 hours. Sample P87-1-2 had an initial insulation resistance of 0.89 MegΩ at 1100 K, increasing to 1.0 MegΩ after 5 hours. Changes in insulation resistance during the initial stage of drift testing are believed to be caused by the formation of oxides at point defects in the fillcoat causing an increase in resistance, or the formation of cracks in the fillcoat causing a decrease in resistance.

Optical examination of both samples showed the topcoats to be intact following 1250 K testing with no major defects present. The alumina overcoat on both samples contained a network of tight cracks, similar to those seen on overcoated samples on alumina substrates. There were no additional cracks, bubbles, or spalled patches seen in the glass topcoats.

One sample (P87-1-6) was topcoated with 0.25 μm of sputtered FeCrAl Mod. 3. The conductive topcoat was not shorted to the PdCr and was not given any heat treatment prior to resistance testing. Total drift during 50 hours at 1100 K was -47,589 μΩ/Ω with a final drift rate of -724 μΩ/Ω/hr. The thermal coefficient of resistance increased 47% to 209 μΩ/Ω/K as a result of the drift test. At 1250 K the sample resistance decreased rapidly, with a total drop of -252,000 μΩ/Ω after 20 hours, at which point the test was stopped. The thermal coefficient of resistance measured during cooling was 608 μΩ/Ω/K, indicating substantial oxidation of the PdCr film.

Optical examination of the sample following testing revealed that patches of the overcoat and topcoat had spalled from the PdCr film during testing, leaving the sample with a scalloped surface. This spalling appeared to result from shear stresses in the overcoat causing fracture to occur within the overcoat, and not from delamination due to poor bonding to the PdCr. In areas where the overcoat had not spalled, the FeCrAl topcoat remained adherent to the overcoat.

6.2 SAMPLES WITH HOT SPUTTERED ALUMINA

6.2.1 Samples with Fillcoats and Overcoats Sputtered at 870 K

Three samples fabricated on Hastelloy-X substrates with fillcoats and overcoats sputtered with the substrates at 870 K were tested at temperatures to 1100 K. Two of these samples (P87-4-3, P87-4-5) also contained a 0.4 μm 7070 borosilicate glass topcoat. Because of the severe degradation of previously tested sputtered samples at 1250 K, it was decided to drop the 1250K drift tests in favor of tests at a temperature below 1100 K. The temperature chosen was 1000 K, since a demonstration of stability at this temperature would represent a significant improvement over the currently existing technology.

All three samples were initially cycled twice to 1000 K at 50 K/min to determine alpha in the as-sputtered condition and to confirm film adherence. Alpha as-sputtered varied from 130 μΩ/Ω/K to 139 μΩ/Ω/K for the three samples which was in good agreement with samples having overcoats and fillcoats sputtered at room temperature. Thermal coefficient of resistance data for all samples with hot sputtered fillcoats and overcoats is summarized in Table 6.2.1. Following these cycles the samples were heated to the first drift temperature for a 50 hour drift test. In the case of the first two samples (P87-4-4 & P87-4-5) this drift temperature was 1000 K. Total drift over the 50 hours was -13,250 μΩ/Ω for sample P87-4-4 without the glass topcoat, and -18,0900 μΩ/Ω for sample P87-4-5 with a glass topcoat (Fig. 6.2.1). Although it had a higher total drift, the sample with the glass topcoat had a

final drift rate of -89 μΩ/Ω/hr as opposed to -110 μΩ/Ω/hr for sample P87-4-4 without the topcoat. Drift results for all the samples having hot sputtered fillcoats and overcoats are summarized in Table 6.2.2. These results appear to indicate that the sputtered overcoat/topcoat systems contain defects which allow some initial oxidation of the PdCr film. As the drift test proceeds, these defects are minimized as pathways for passage of oxygen through the overcoat are filled with chromium oxide. As the defects are eliminated the drift rate decreases. The total drift over 50 hours would therefore seem to be a measurement of the magnitude of the defects occurring in the overcoat, whereas the final drift rate is an indicator of the effectiveness of the chromium oxide in sealing these defects. Resistance to the substrate was 6.55 MegΩ to 7.26 MegΩ at 1000 K for sample P87-4-4, and 6.1 MegΩ for sample P87-4-5.

Following this initial drift both samples were again cycled to 1000 K to check the effect of 50 hours at 1000 K on alpha. As can be seen from Table 6.2.1 alpha increased 15% and 20% for P87-4-4 and P87-4-5 respectively. This increase is presumably due to the lower percentage of chromium in the alloy due to the formation of chromium oxide.

Both samples were next subjected to a second drift test for 50 hours at 1100 K (Fig 6.2.2). Both samples reacted the same as they had at the lower drift temperature. Resistance initially dropped as defects formed at the higher temperature; probably cracks in the overcoat; caused the formation of additional chromium oxide. Both the total drift and final drift rate were lower then at the lower drift temperature. Alpha measured after this drift again rose from the pre-drift value, but only by an additional 6.5% and 5.0% for P87-4-4 and P87-4-5 respectively. These data indicate that at 1100 K both the hot sputtered overcoat and the hot sputtered overcoat with a 7070 glass topcoat are effective in reducing oxidation of the PdCr film. Resistance to the substrate was 3.70 MegΩ at 1100 K for sample P87-4-4.

Since the high drift rate observed when these samples were first soaked at an elevated temperature was believed to be caused by the passage of oxygen through cracks or other defects in the overcoat which were then sealed by the formation of chromium oxide, a second drift at 1000 K was performed after the 1100 K drift. The data from these drift tests are shown graphically in Figure 6.2.3. As expected the drift rates and total drift were much lower then for the initial drift test at this temperature. The lack of a decrease in resistance at the start of the test is an indication that no additional defects are being formed in the fillcoat or topcoat. As can be seen from Figure 6.2.3, the total drift over 50 hours at temperature is within the ±200 μstrain goal of the contract. As with the other tests on these samples, little difference in performance is seen between samples with and without the glass topcoat. This

third drift resulted in no significant change in alpha measured to 1100 K before and after the test. This is also an indication that no additional oxidation of the PdCr occurred. Examination of these samples following testing showed no signs of overcoat or topcoat spalling or cracking.

The series of drift tests for sample P87-4-3, which like sample P87-4-5 had a 0.4 μm 7070 glass topcoat over the hot sputtered overcoat, were run at higher temperatures then the first two samples to see if a stable structure could be produced at 1100 K. The first drift test was performed at 1100 K instead of 1000 K. Like the initial tests on the previous samples, P87-4-3 experienced a sharp decrease in resistance during the first 5 hours of the test. Unlike the previous samples, the drift rate became positive after 20 hours at 1100 K (Fig. 6.2.4). The process of oxidation of the PdCr and sealing of the defects with chromium oxide appears to take place at an increased rate at this higher temperature as would be expected. The fact that the total negative drift is the same for samples tested at 1000 K and 1100 K would seem to confirm that an equal amount of chromium oxide is formed in this process, but that the process is complete after 15 hours at 1100 K, while it is still occurring at a slow rate after 50 hours at 1000 K. Alpha measured after the drift test had increased 19% over the pre-drift value which in the same range as the previous samples, and is another indication of the same level of PdCr oxidation. The process responsible for the positive drift after 20 hours at 1100 K is not known. Heating the sample directly to 1100K appears to be a more effective method for sealing the defects, since the previous samples which were held at 1000K for 50 hours prior to the 1100 K test were still experiencing a negative drift after 50 hours at 1100 K.

Another indication that sealing the cracks at 1100 K is more effective then at a lower temperature, is that during the next drift test on sample P87-4-3 at 1150 K, no initial decrease in resistance was seen (Fig. 6.2.5). Thus it appears that no additional chromium oxide was formed at 1150 K. Also the small increase in alpha as a result of this drift (2.4%) is a sign that very little additional oxidation took place. The positive drift rate at 1150 K was higher then the final drift rate at 1100 K for this sample. Again the process causing this positive drift is not known. Since this sample did have a glass topcoat, it is possible that some glass diffused through cracks in the overcoat during the initial 1100 K drift and is reacting with the PdCr. This positive drift was not seen however in the other topcoated sample which was initially held at the lower temperature of 1000 K.

The final drift test on sample P87-4-3 at 1100 K also produced a positive drift with a lower drift rate then the initial 1100K test. This drift rate was constant throughout the test however, indicating that the process causing it was not stabilizing. The total drift over the 50 hours was 720 μΩ/Ω or approximate 550 μstrain (Fig. 6.2.6). As seen in Table 6.2.1 there was no significant change in alpha as a result of this drift test.

6.2.2 Samples with Fillcoats and Overcoats Sputtered at 1070 K

Only one sample (P87-6-2) with the fillcoat and overcoat sputtered at 1070 K was suitable for resistance testing. The thermal coefficient of resistance after 2 cycles to 1100 K was 136.5 μΩ/Ω/K, which is consistent with the previously tested samples having 870 K fillcoats and overcoats. Resistance to ground which was low after sputtering of the overcoat, did not improve during this test and this may have contributed to slightly erratic drift data at 1100 K (Fig. 6.2.7). Total drift during 50 hours was -21,500 μΩ/Ω, with an average drift rate of zero over the final 15 hours. The thermal coefficient of resistance following this drift test was 160 μΩ/Ω/K. The higher total drift for this sample compared with those having fillcoats and overcoats sputtered at 870 K is believed to be due to a higher incidence of fillcoat defects, which were partially repaired during the drift. This assumption is supported by the fact that the room temperature insulation resistance had increased from <200 Ω to 12 KΩ after the drift test.

This sample was next heated to 1200 K for a 50 hour drift test (Fig. 6.2.8). The test plan for this sample included this higher temperature in an attempt to stabilize the sputtered materials prior to subsequent drift tests at lower temperatures. Insulation resistance at 1200 K increased to 380 KΩ. After 20 hours at 1200 K the sample resistance started to decrease sharply. At 40 hours the test was stopped due to the continued high negative drift rate (-3,000 μΩ/Ω/hour). Insulation resistance at room temperature measured at the termination of the drift test was 123 KΩ, compared to 12 KΩ prior to the test. This drift test had increased alpha to 201 μΩ/Ω/K, an increase of 25%. At this point testing was discontinued due to the obvious deterioration of this sample. The sample was instead examined to determine the cause of its poor performance compared to the previously tested samples with 870 K fillcoats and overcoats.

SEM examination revealed the presence of cracking and spalling of the hot sputtered overcoat at the edges of the PdCr film. The overcoat also appeared to contain a groove extending along the step in the overcoat caused by the the edge of the underlying PdCr film. As sputtering of the overcoat proceeded, the alumina deposited on the edge of the PdCr apparently grew outward, masking the fillcoat next to the PdCr. As deposition proceeds outward from the edge of the PdCr, and upward from the fillcoat, a crevice is formed in the completed overcoat which extends upward and outward from the edge of the PdCr. During elevated temperature testing in air, oxygen may penetrate through cracks or defects in this thin region and initiate local oxidation of the PdCr. As oxides form on the PdCr, the increased volume of the film exerts an upward pressure on the film and increases the likelihood of additional cracking at the crevice. Spalling of the alumina overcoat may

have occurred after 20 hours at 1200K coinciding with the sharp drop in sample resistance, or during cooling from 1200 K. Upon cooling compressive stresses occur in the alumina overcoat due to the higher CTE of the Hastelloy-X substrate. At the edge of the sputtered PdCr grid legs, the groove in the overlying alumina overcoat removes support to balance these compressive forces on one side and spalling of the alumina overcoat may occur. Although this groove in the overcoat may also occur in overcoats sputtered at 870 K, this type of overcoat failure was not seen in previously tested Task 5A samples. The increased compressive forces which build up in the alumina during cooling from 1070 K as opposed to 870 K, may be enough to cause cracks to form at the bottom of the groove. At 1100 K, oxidation of the PdCr due to these cracks is slow, but the rate of oxidation increases at 1200 K and causes additional cracking as suggested above. All previous testing on Task 5A samples had been at temperatures of 1150 K or lower. No other overcoat defects were seen, including the cracking and blisters previously seen on overcoated samples on alumina substrates heated to 1250 K.

6.3 RESULTS FROM THE TESTING OF COMPLETE SYSTEMS ON BEND BARS

The results of the efforts to fabricate twelve complete strain gage systems with Pd compensation grids on six bend bars are summarized in Table 6.3.1

During the preparation of bar B1 an accident occurred during the soft grit blast cleaning step after the deposition of one of the alumina fillcoat layers. The powder feed contained some agglomerates apparently because of high humidity which resulted in occasional erratic behavior. One of the alumina fillcoat layers was damaged before the problem was appreciated. Some of the alumina was lost and significant areas of the Pd film sputtered on top of the alumina were torn away when the photo mask was removed so that this bar could not be tested.

During deposition of the Pd compensation grids on bar B3, the Pd sputtering target "burned through" and the Pd films became contaminated with In and Cu from the backing plate. Attempts were made to clean away the contaminated Pd with the photomask still in place in order to repair the sample. The ion beam etching removed enough of the mask so that remasking was required. After the ion beam etching had been competed and the sample treated to remove the rest of the mask, it was discovered that the ion beam etching had harmed the fillcoat or perhaps exposed previously cracked fill coat. A dark residue, apparently from photomask material, had infiltrated the alumina, also remained and could not be removed. No further attempts to repair this sample appeared warranted so this bar also was not tested.

During the fabrication of bar B4 it was observed that the compensation grid in one of the gages was electrically open and the compensation grid in the second gage had too high a resistance to test (19.4 Ω). Bend bars B2, B5 and B6, however, were suitable for testing.

The first experiments to evaluate the behavior of a complete Pd-13Cr strain gage system on a bend bar began by making measurements of the apparent strain of the two gages on bar B2 as a function of temperature. External changes of the compensation resistor in the circuit diagrams shown in Figures B1 and B2 of Appendix B were then made to determine experimentally the optimum value of resistance to be added to the adjacent leg of the Wheatstone bridge. A general summary of the most interesting data obtained in testing gages #1 and 2 of bar B2 is presented in Table 6.3.2.

The initial ratio of the resistance of the sputtered Pd compensation grid to the resistance of the PdCr gage required a high value be selected for the fixed resistor (A in Appendix B, Figure B2) in the adjacent leg of the bridge in order to provide correct compensation for temperature. As indicated in Table 6.3.2, a value of 226 Ω was chosen which resulted in a bridge ratio of 3:1 rather than the desired ratio of 1:1. This means that common-mode changes in lead wire resistance versus temperature were not canceled, and the lead wires became part of the temperature compensation.

The initial four temperature cycles made to adjust the thermal compensation for gage #1 on bend bar B2 for minimum sensitivity to temperature are shown in Figure 6.3.1. The experimental behavior and the circuit adjustments for gage #2 were very similar. When gage#1 was first heated to 920 K, the resistance curve was nonlinear but then became relatively linear upon cooling with a positive slope. The data for the second thermal cycle duplicated that of the first cooling. Because of the positive slope of the resistance curve, the value of the external fixed resistor was then decreased from 226 to 179 Ω. As shown by the third thermal cycle in Figure 6.3.1, this decreased the slope but not not by a sufficient amount. The adjustable compensation resistance was then decreased to 138 Ω which resulted in the very low sensitivity to temperature shown by cycle four. It was of note that second, third and fourth cycles each showed small peak values of $\Delta R/R$ at a temperature of about 790 K.

Bar B2 was then subjected to a fifth testing cycle which included a 50 hours soak at 920 K. This long exposure resulted in the large negative drifts in resistance for gages #1 and 2 shown in Figure 6.3.2. No additional external adjustments of the fixed resistances in the adjacent leg of the Wheatstone bridge were made to compensate for these changes which made the resistance vs temperature curves for both gages have appreciably negative slopes.

In the sixth testing cycle, bar B2 was reheated to 920 K and then soaked for 16 hours at 760 K during cooling. The seventh and eighth testing cycles were similar except that the 16 hour soaks after heating to 920 K were at 700 and 650 K, respectively. Figures 6.3.3, 6.3.4, and 6.3.5 show the changes that occurred in the bridge output during these lower temperature soaks. Note that the two bridges showed almost identical behavior and that the direction of change was upward in the reverse direction from that at 920 K shown in Figure 6.3.2.

Figure 6.3.6 shows resistance vs temperature data for gage #1 measured throughout the three cycles (6,7,8) mentioned above. A large positive correction factor, linear with temperature has been added to the data to increase the sensitivity of the ordinate scale.The data shows that changes in the heating and cooling traces after the drift at these three relatively low temperatures were all removed by reheating to a temperature of about 830 K. Above 830 K, all of the curves had essentially the same resistance vs temperature behavior.

Bar B2 was then held at 1000 K for 50 hours (cycle 9) and then subjected to an additional 16 hour drift run at 700 K (cycle 10) under the same conditions as before. A summary of the data obtained for gage #1 for cycles nine and ten is presented in Figure 6.3.7. The major effect was an additional large negative drift of approximately -120 x 10^{-3} Ω/Ω at 1000 K. The 16 hour drift at 700 K had smaller effects but again appeared to affect the reproducibility of the thermal cycle data at lower temperatures as shown in Figure 6.3.7 by the divergence of the cycle 10 heating and cooling curves below 450 K. The data for gage #2 was similar.

A subsequent 50 hour drift test of bar B2 at 1100 K (cycle 11) resulted in positive drifts of +115 and +125 x $10^{-3}\Omega/\Omega$ for gages #1 and #2, respectively. During the last few hours of these drifts, however, each gage began to drift in the reverse direction. Figure 6.3.8 show a plot of the data for Gage #1.

Bar B2 was then subjected to a 16 hour drift at 700 K (cycle 12) to determine if the 1100 K soak would result in a lower drift rate at 700 K compared to the earlier drift at this temperature. This 700 K drift was followed by a 50 hour soak again at 1000 K (cycle 13). During the 50 hours at 1000 K, the $\Delta R/R$ values again decreased by approximately -35 and -85 x 10^{-3} Ω/Ω for gages #1 and #2, respectively. In the last thermal cycle the bar was heated to 1000 K and cooled with a 16 hour drift soak at 700K during the cool down (cycle 14). The output of the bridge versus temperature is shown in Figure 6.3.9. Gage #2 apparently shows some discontinuity upon heating at about 800 K. Both gages were still

operational and appear fairly insensitive to temperature on this very coarse scale. The drastic cumulative changes that had occurred in the system after these experiments led us to a decision to end the experiments on this bar.

Measurements of gage factors versus temperature were made after the fourth and the eighth cycles of testing. The detailed results are presented in Table 6.3.3. A plot of the data for the measurements after the fourth cycle, before all of the large drifts in bridge output were experienced, is presented in Figure 6.3.10. The factor appears to drop fairly linearly from values of about 1.55 at room temperatures to about 1.4 at 920 K. The gage factor measured on bar B2 at room temperature is lower then that reported for cast Pd-13Cr earlier in this contract (1.8) (ref. 7). The compensating grid in the opposite leg of the bridge has some strain sensitivity which lowers the gage factor of a compensated gage.

Bar B5 was prepared by the same procedure as Bar B2 except that the alumina overcoat was sputtered with the bar heated to about 870 K. The behavior of bar B5 was similar to that of bar B2. The bridge as fabricated, however, was approximately balanced with a bridge ratio of approximately 1:1 as intended. A general summary of data obtained from this bar is presented in Table 6.3.4.

Figure 6.3.11 shows the behavior of gage #1 during the first heating and cooling cycle of bar B5 to 920 K and also the data for the second cycle which included a one hour soak at 920 K. Gages #1 and #2 showed negative drifts of -64×10^{-3} and -85×10^{-3} Ω/Ω, respectively, during the one hour hold at 920 K.

In order to reduce the thermal sensitivity of the system, the fixed resistances in the adjacent arms of the bridges (A in Appendix B, Fig. B2) were increased to produce bridge factors of 5.54:1 and 5.52:1 for gage #1 and 2, respectively, before the third cycle to 920 K. As can be seen in Table 6.3.4, the temperature experienced during the first and second cycles resulted in the resistances of the compensation grids approximately doubling in value.

The data obtained for bar B5 during the third cycle indicated that the compensation effects were not sufficient and the value of the fixed resistance in the adjacent arm of the bridge (resistor A) was increased again. As shown in Table 6.3.5, the adjustment made before the fourth cycle resulted in bridge factors of 5.77:1 and 6.60:1 for gage #1 and 2, respectively. These changes reduced the thermal sensitivity as shown in Figure 6.3.12 but permanent negative changes in resistance occurred in even the few minutes the gages were held at 920 K while the furnace temperature changed direction and during the one hour

soak at 920 K. It was decided at this point that no additional attempts would be made to adjust the compensation.

During the fifth heating and cooling cycle bar B5 was held for 50 hours at 920 K and large apparent negative drifts were observed in both gages as shown in Figure 6.3.13. Figure 6.3.14 shows the associated heating and cooling curves for gage #1. The cooling curve is not linear. As can be seen in Table 6.3.4, after the fifth cycle the resistance of the compensation grid has increased from an original value of 11.8 Ω to 175.9 Ω. This increase in resistance was most likely due to oxidation of the Pd. Examination of the sample following the completion of testing showed that the overcoat covering the Pd grid had spalled during testing.

During sixth cycle bar B5 was heated to 760 K and soaked there for 16 hours before cooling. As shown in Figure 6.3.15, gage #2 gage showed fairly reproducible results on this coarse scale but gage #1 did not. The bar was then heated to 700 K and soaked for 16 hours before cooling. Figure 6.3.16 shows the constant temperature drift results during the seventh cycle and that both gages drifted in the same positive direction as the gages on bar B2 shown in Figure 6.3.4.

During the eighth cycle, bar B5 was heated to 920 K and then held for 16 hours at 660 K during the cooling portion of the cycle. The data presented in Figure 6.3.17 shows that both gages exhibited some open loop behavior but tended to come back to the same values they each originally had at room temperatures. At this point it was concluded that the gages had drifted so far that taking further data did not appear warranted. In order to permit comparisons between this bar and bar B2, however, bar B5 was subsequently exposed to a 50 hour drift exposure at 1000 K, a 16 hour exposure at 700 K, a 50 hour exposure at 1100 K, and finally a 16 hour exposure at 700 K.

Gage factors measurements are presented in Table 6.3.5 for both gages on bar B5 at room temperature before any thermal cycles were made and then at several temperatures after the fourth, and the eighth thermal cycle. Plots of gage factors in tension and compression for both gages after the fourth cycle of tests are presented in Figure 6.3.18. The values measured are generally similar to those for bar B2 presented in Table 6.3.3 and Figure 6.3.10.

Figure 6.3.19 is a photograph showing the condition of the two gages on bar B2 some time after the completion of all elevated temperature testing. Large sections of the alumina overcoat are missing from the Pd grids while the PdCr grids appeared to be properly coated. An enlarged view of the bottom left side of gage #1, the gage on the left in

Figure 6.3.19, is shown in Figure 6.3.20. The photograph on the top in Figure 6.3.20 shows in incident light that the overcoat is filled with cracks. The PdCr grid line appears to be in good condition while the Pd shows obvious indications of reaction and spalling of the overcoat. Although the Pd was still continuous at the completion of testing, it was poorly attached when the photograph in Figure 6.3.19 was taken and important sections of the Pd grids were missing. It could then be observed that the cracks shown in Figure 6.3.20 were apparently only in the overcoat because no cracks were observed in the alumina fillcoat which had been under the Pd.

An overview photograph of gage #1 on bar B5 at the completion of all testing is presented in Figure 6.3.21. All of the Pd is present but all of the overcoat which covered the Pd is gone. The alumina overcoat has also spalled away from the PdCr leads along the step formed in the PdCr when it was sputtered on top of the pure Pd additions to the leadfilms. Also, some blisters are evident in the leadfilms, almost completely concentrated in the areas of the leads defined by the strips of Pd underneath the PdCr. There was also evidence of some very small areas of distress in the overcoat on the PdCr at spots along the edges of the grids. The one major loss can be seen at the top of the left loop of PdCr in Figure 6.3.21.

Bar B6 was prepared for evaluation by the NASA Lewis Research Center. Measurements of gage factors at room temperature at United Technologies are presented in Table 6.3.6. In these determinations, the output of the two sputtered gages were compared directly to the output of a commercial gage positioned on the opposite side of the same bar, as shown in Figure 5.3.4. The two sputtered gages on the opposite side of the bar experienced strains which were equal but opposite in sign from those of the reference gage. For reasons which are not understood, the data from gage #1 was erratic and the gage did not function properly. Gage #2 gave more consistent results but showed more variance than the commercial gage. The two sputtered gages may perform better after stabilization heat treatments.

7.0 DISCUSSION OF RESULTS

7.1 SAMPLES ON HASTELLOY-X AND ALUMINA SUBSTRATES

Palladium-13wt% Chromium was chosen as the best sensor material for incorporation into the final strain gage system based on its stability and the fact that it exhibited a linear resistance vs. temperature curve to 1250 K. A typical curve for overcoated sputtered Pd-13Cr is shown in Figure 7.1.1. As seen in this figure if a straight line is drawn beside the curve it does reveal some degree of nonlinearity. When a compensation element is added to the strain gage system, lowering the overall alpha from 173 μΩ/Ω/K to a much lower value, this nonlinearity could become significant. The magnitude of this departure from linearity is more clearly seen if difference between the actual curve and the straight line is plotted vs. temperature. This type of curve is shown for drop-cast Pd-13Cr and sputtered Pd-13Cr in Figures 7.1.2 and 7.1.3 respectively. These data were generated by calculating alpha from the starting temperature to the maximum temperature. For each test temperature the difference shown in the plot is (actual dR/R) - (alpha x temperature). This procedure forces the data point at the maximum temperature to be zero. The curves for both drop-cast and sputtered material show a maximum deviation from linearity at approximately 800 K. The deviation appears greater for the drop-cast material only because the maximum temperature is higher causing zero deviation at 1250 K instead of 1100 K. Assuming a gage factor of 1.4 at 1100 K (Section 6.3) this deviation would be +1430 μstrain during heating to 1100 K. Since the nonlinearity is seen in both drop-cast and sputtered material it appears to be a material property and not related to strains generated in the sputtered film as it is heated or due to oxidation effects. This nonlinearity could be due to residual impurities in both the sputtered and cast material.

The sample with fillcoat and overcoat sputtered at 1070 K experienced an overcoat failure at the edge of the underlying Pd-13Cr grid. This failure was attributed to a crevice formed in the alumina at the edge of the PdCr as the overcoat was being deposited. Poor coverage of the PdCr at its edge was also believed to have caused problems in previous samples. All samples were prepared using a positive acting photoresist which covered the entire substrate surface with the exception of the sensor pattern. After deposition of the PdCr the photoresist was dissolved and the free PdCr film broken loose from the adherent gage by agitation in an ultrasonic solvent bath. This procedure left a sharp torn edge on the remaining film. A possible improvement on this procedure would be to deposit the PdCr over the entire substrate surface, then masking the strain gage pattern with photoresist and using ion beam etching to remove the unwanted PdCr film. This procedure would be expected to leave a slightly tapered edge on the PdCr which should not present a problem when overcoating.

The integrity and performance of the alumina insulating layer recommended at the start of this contract was not viewed as a problem area. The successful use of this insulating system in thin film thermocouple development has been documented (ref. 9) As work on the contract proceeded, it became obvious that there were several problems which needed to be overcome before consistent reliable insulating layers could be produced to effectively insulate the PdCr film from the underlying substrate.

The as-sputtered alumina films which were deposited on cold substrates in an argon-20% oxygen atmosphere were found to be oxygen rich, containing 51.9 wt.% oxygen as opposed to 47.1 wt.% for stoichiometric alumina. The as-sputtered alumina films also contained 1.2 wt.% argon. Sputtered alumina containing appreciable concentrations of argon have been shown to undergo significant shrinkage when heated above 1070 K as the trapped argon is released (ref. 10). It is assumed that the loss of oxygen from the oxygen rich film would also cause shrinkage, resulting in cracking of the overcoat or insulating layer. Cracks were seen in both insulating layers and overcoats when heated to 1250 K. An example of cracks in an overcoat after heating to 1250 K for 10 hours in air is shown in Figure 7.1.4. Analysis of the alumina film after heating showed that all the argon was removed from the film after heating to 1140 K in air for 30 min. but excess oxygen still remained after 10 hours at 1250 K (2.5 wt% excess). The heat treatment atmosphere was found to have a large influence on the amount of film shrinkage. Heat treating a batch of 4 overcoated samples at 1140 K for 30 min. in argon resulted in severe film shrinkage and cracking (Fig. 7.1.4), whereas the same heat treatment in air only caused minor shrinkage and a system of tight cracks which resulted in acceptable insulating properties. The reason for the severe cracking in the argon atmosphere has not been explained.

Another continuing problem was the formation of spot defects in the sputtered alumina films by particulate foreign material falling onto the substrate during deposition, heat treatment, or handling and storage. Particles which were present during deposition acted as masks, resulting in thin areas in the film. It can be expected that in order to consistently produce a defect free insulating layer a strict clean room environment will need to be employed at each step of fabrication.

A third problem encountered with sputtered insulating layers was the growth and loss of exaggerated growth nodules, resulting in holes in the film. Because the sputtered alumina layer was deposited on top of the rough grown oxide surface, the sputtered alumina exhibited nodular growth. The presence of oxide protrusions or possibly particles on the grown oxide surface resulted in occasional nodules which were much larger then the

surrounding film. These nodules appeared to be poorly adhered to the underlying material and were dislodged during expansion and contraction of the film as it was heat treated.

The above defects in the overcoat layer resulted in sample failure due to shorts between the topcoat and grid when any conductive topcoat was applied to improve the effectiveness of the overcoat. The only exception was one FeCrAl topcoat which was effectively insulated from the grid as-sputtered and during testing to 1100 K. Eliminating the defects in the overcoat would therefore not only improve its effectiveness, but also allow the possible application of conductive topcoats such as platinum which should be effective to higher temperatures then the 7070 glass chosen as the best topcoat at the end of Task 5A.

As reported in Section 5.2.1 multilayer fillcoats were utilized to overcome observed defects in the sputtered alumina fillcoat. Of the 6 Task 5A samples employing multi-layer fillcoats, one had a low insulation resistance as sputtered, which improved to an acceptable level after heating to 1100 K. The three samples which were tested at 1100 K had insulation resistances ranging from 19 KΩ to 9 MegΩ at 1100 K. These results indicate that although this technique did enable some of these samples to be tested, a more extensive series of tests are needed to evaluate its effectiveness.

Several Task 2 and 5A samples which had the insulation resistance monitored to 1250 K showed an unexpected increase in resistance above 1100 K. This increase, which was reversible on cooling, does not follow the properties of bulk alumina, which steadily decreases in resistivity over this temperature range. The fact that the resistance of the alumina decreased as the sample was cooled back to 1100 K rules out an increase due to the formation of additional oxide filling defects in the insulating layer. These results reflect the fact that this is a complex insulating layer including the grown oxides on the NiCoCrAlY and is still not completely understood.

Hot sputtering at 870 K proved to be the most effective means of improving the overcoat and fillcoat layers. Of 6 samples with the alumina overcoats and fillcoats sputtered at 870 K, three failed prior to testing. None of these failures was associated with low insulation resistance. Of the 3 samples which were tested, all had good insulation resistance at 1100 K (3 - 5 MegΩ). In addition these three samples also had low drift rates compared to samples with cold sputtered alumina layers as reported in Section 6.2. All 6 of these samples had the alumina layer applied in one sputtering step. Because of the scheduling overlap of sample preparation, no samples were produced which had hot sputtered overcoats and fillcoats applied using the multilayer techniques described above. Combining these two techniques would offer the possibility of further improving the performance of these alumina films as insulation materials or oxidation barriers.

Scanning electron microprobe analysis of an alumina film sputtered at 870 K showed that the sputtered alumina was very close to stoichiometric (47.2 vs. 47.1 wt.%) but still contained 0.5 wt.% argon compared with 1.2 wt.% when cold sputtered. Considering this data and earlier results obtained from alumina layers prepared on unheated substrates, the apparent advantages of hot sputtering the alumina at 870 K can be summarized:

a) Reduces the thermal expansion mismatch between the alumina and a nickel base superalloy substrate so that the alumina should be in compression below 870 K.
b) Reduces the shrinkage of the alumina at elevated temperatures due to the loss of excess oxygen.
c) Reduces shrinkage of the alumina due to the loss of entrapped argon at elevated temperatures.

7.2 BEND BAR TESTING

Testing of complete strain gage systems on bend bars revealed a number of unexpected problems. It is believed that the effects of these problems could be avoided or greatly reduced in further work. The most serious difficulty was the failure to appreciate that when Pd is used with surface to volume ratios characteristic of thin films, oxidation of Pd would cause major problems if the oxidation protection afforded by the alumina overcoat was compromised due to cracking or spalling of the overcoat. For fine powders of pure Pd, oxidation can begin at temperatures as low as about 570 K. Oxidation of Pd tends to reverse beginning at about 870 K and the metal reverts to pure Pd at about 1190 K (ref. 13). This problem should not have arisen if we had selected Pt instead of Pd for use as the temperature compensation grid. Palladium was originally selected after considerable discussion as the compensation material because it was felt that it might form a (somewhat) stronger, more reliable bond with the alumina fillcoat. In Task 5 adhesion experiments sputtered Pt films had experienced problems in bonding to alumina fillcoats. Although a bondlayer of sputtered FeCrAl had appeared to improve adherence of both Pt and Pd, the Pt did spall on some samples after heating to elevated temperatures.

An examination of the data for bend bars B2 and B5 shows that large negative drifts occurred, especially during the first 50 hour drift test at 1000 K. At the conclusion of these runs and the 16 hour drift runs at lower temperatures, it was observed that the Pd grids had darkened significantly and no longer had metallic lusters. A more detailed examination of the bars following the conclusion of all testing showed that the alumina overcoat had spalled from the Pd grids although it was adherent adjacent to the Pd as well as over the PdCr grids. At what point in the test sequence the overcoat spalled is not known, although

the large increase in Pd resistance for both bar B5 gages at room temperature after cycle 5 (below) indicates that the overcoat was not intact at that point. A measurement of the resistance of the compensation grid of bar B5 showed that its resistance had increased from an initial value of 11.8 to 20.8 Ω for gage #1 and from 12.6 to 25.1 Ω in the case of gage #2. After the fifth cycle of bar B5, which consisted of a 50 hour soak at 1000 K, the resistances of the Pd compensation grid had increased to 175.9 and 62.8 Ω for gage #1 and gage #2, respectively. The effect on gage output to be expected from an increase in the resistance of the compensation grid would be to cause an apparent decrease in resistance of the active strain gage which is what was observed.

A possible explanation for the observations of positive drifts during drift runs at lower temperatures, the data shown for example in Figures 6.3.3, 6.3.4, 6.3.5, and 6.3.16, is that the oxide which formed during the 920 K drift in the Pd compensation grid is tending to dissociate restoring some Pd to the films at lower temperatures. At the highest temperature, 760 K, the effect occurs rapidly and saturates when the equilibrium concentration of oxide is reached. At lower temperatures, the equilibrium concentration of oxide is less but the kinetics are slower so that the process does not reach equilibrium within the 16 hour periods over which we ran the experiments.

At much higher temperatures, Pd oxide again begins to dissociate (ref. 13). An examination of the data in Tables 6.3.2 and 6.3.4 shows that after the completion of the exposures to the highest temperature, (1100 K), the resistances of the temperature compensation grids had returned to essentially the same values that they had initially.

The observations that the protective alumina overcoats on the Pd were either severely damaged or completely removed by these thermal exposures is also understandable. The volume changes that must have occurred when the Pd absorbed oxygen and the pressures that must have been created when the oxide became unstable must have been appreciable.

The observations here of problems with the oxidation of thin films of pure Pd are consistent with the reports of similar problems by scientists at NASA Lewis in their studies of the Pd-13Cr alloy in wire form (ref. 14,15). Their 0.0004 cm diameter wires were encased in flame sprayed alumina with various additives which would not generally be expected to form as effective a barrier to oxidation as dense, properly prepared sputtered films. The presence chromium in the alloy is apparently effective in obtaining a good bond of sputtered Pd-13Cr with the alumina overcoat and in reacting at defects in the film to form chromia which tends to seal up leaks in the film and prevent continued oxidation.

A particular failing in processing procedures was demonstrated by the spalling of the overcoat on the PdCr leadfilms on both bend bars. The spalled areas were all associated with the edges of the strips of Pd sputtered underneath the PdCr. In the lift-off photoresist process used during this contract the film is sputtered onto a substrate which has been masked with photoresist. Unwanted areas of films are removed by dissolving the photoresist mask from under the sputtered film, then allowing the unwanted films to tear away from the adherent films sputtered directly onto the substrate. Unfortunately, this tearing process tends to leave ragged edges and thin fins of sputtered material along these edges which are not bonded to the substrate. It is very difficult to overcoat these edges with an alumina overcoat film which will reliably seal these edges and prevent oxidation attack. In further work we intend to avoid this method of forming thin film grids and to use the ion beam etching technique. Use of this techniques will produce grids with tapered edges that are smooth and well bonded to the substrate which should provide tight bonds to protective overcoat layers.

A bridge voltage of 5 volts was used to obtain data from the strain gages mounted on bend bars B2, B5, and B6. For a balanced bridge with a bridge ratio of 1:1 the voltage across the individual strain gages was therefore 2.5 volts which would require the 94 Ω gages to dissipate 1.33 watts/cm^2 when this voltage was applied. This is within the published range of 1-3 watts/cm^2 suggested for moderate accuracy with gages on steel (ref. 16). These recommended limits are for voltages constantly applied to the bridge. In our experiments the bridge voltage was only applied when a sequence of measurements were being taken, typically for a total time of about 3 seconds. This would reduce the amount of heat that needed to be dissipated. The thickness of the grown plus sputtered alumina insulation layers were approximately equal to the thickness of organic cement (2 μm) recommended in reference 16. The range of heat dissipation values recommended in reference 16 also assumed the presence of an adhesive backing for the gage, typically about 25 μm thick, which was not present on our gages. Although the thermal conductivity of the oxide layer separating the sputtered PdCr from the metallic substrate is lower then that of the commercial cement and adhesive backing, the oxide layer is only one tenth the thickness of the cement plus adhesive.

Because the resistivity of pure Pd in the compensation grid was initially only about one-twentieth of that of the Pd-13Cr grid, we would not expect power dissipation problems to occur in these films even though the resistance of this grid did increase appreciably during our testing. We conclude that the effects of I^2R heating in our strain gage systems were probably not significant compared with other effects observed.

The alumina fillcoat layers on the bend bar samples all tended to be darker than expected, typically with a brownish cast. These effects were first observed upon removal of the photoresist after sputtering the Pd compensation grids at UTRC. This discoloration was not observed with any of the PdCr gages installed on Hastelloy-X substrates, even with samples that were prepared using the same three layer procedure as that used in preparing the fillcoats on the bend bars.

One explanation for this discoloration is that the sputtered alumina fillcoats contain cracks and fine crevices, especially between the nodules, from which it is extremely difficult to remove all traces of photoresist. We were not able to completely clean these bend bar samples even with additional long soaks in fresh acetone/Freon solutions in an ultrasonic bath and by severe physical scrubbing with "Q tips" and acetone. This does not explain why the same discoloration was not observed on the Hastelloy-X substrates prepared during Tasks 5 and 5A. As described in Table 6.3.1, attempts to remove the photomask on bar B-3 by electron beam etching after the PdCr target became contaminated were so unsuccessful that this sample was lost from the testing program. In this instance, some polymerization of residual mask material may also have occurred in the electron beam.

It was observed in bar B1, where there was some delamination of the fillcoat because of an accident during the soft grit cleaning step, that the discoloration was only associated with the alumina layers that had been in direct contact with the photoresist. Newly exposed alumina layers underneath the top layers did not show this discoloration.

It is difficult to attribute problems in removing the photoresist in a simple way to polymerization and overheating of the mask by the plasma. The bend bars were well clamped to a water-cooled hearth during sputtering and the bars had appreciable thermal inertia. Also, even before the sputtering step, observations of discoloration were made in areas where the mask had been dissolved and where sputtered films of Pd were to be sputter deposited.

Test bars B5 and B6 were extreme examples of the discoloration problem. Both of these samples had hot sputtered alumina overcoats. During this overcoating process, the samples were heated in a 80/20 argon/oxygen environment with a base pressure of about 10 millitorr. During the heating and sputtering processes, some of the residual photomask material could have partially decomposed (oxidized) or polymerized in the plasma.

The reason this problem was encountered is not clearly understood. It probably would not have occurred if the fillcoat was prepared by hot sputtering or if the samples had been heated to 1250 K in air after chemically cleaning away the photoresist. The presence of this contamination under the sputtered sensor films was probably detrimental to their behavior during subsequent testing.

The failure of many of the gages in this program before testing could be initiated emphasizes that the fabrication of thin film strain gages requires the accomplishment of many steps and that each step must be done properly to obtain a useful gage. The yield of useable gages must be significantly increased. This should come with further experience. The subject of better control during processing and the identification of critical parameters should be pursued in further work. This work has shown the potential for these gages to be successfully used to 1100 K in the near term, with use to the original goal of 1250 K still a reasonable possibility.

8.0 SUMMARY AND CONCLUSIONS

A research program was conducted to identify and evaluate a new static strain gage sensor alloy that could be used up to 1250 K on blades and vanes in a gas turbine engine running on a test stand. The Pd + 13 weight percent Cr alloy that was developed is single phase and metallurgically stable up to 1250 K. When prepared as a thin film, so much of the Cr content was consumed to form a protective chromium oxide coating that the alloy requires the use of a protective overcoat film. It was discovered that sputtered alumina films as normally prepared would not protect the Pd-13Cr films from oxidation and, furthermore, these alumina films were also not adequate to properly insulate the sensor films electrically from the substrate. Major improvements in the properties of alumina films were observed when they were prepared by hot sputtering. Sputtering on substrates at 873K avoids the formation of significant thermal expansion tensile stresses and reduces the entrapment of argon from the carrier gas.

The high thermal coefficient of resistance of the Pd-13Cr alloy, 173 $\mu\Omega/\Omega/K$, necessitated the use of a temperature compensation grid in an adjacent arm of the Wheatstone bridge. The testing of complete strain gage systems using pure Pd for this compensation revealed that oxidation of the Pd grid was a significant problem at elevated temperatures. Hot sputtered alumina overcoats did not adhere to thin films of pure Pd to provide protection from this attack. At the current state of development, it is believed possible to prepare compensated thin film PdCr static strain gages which should perform up to 1100 K. Additional work is needed to confirm this conclusion and to extend the range of use to higher temperatures.

A more specific summary of the conclusions and recommendations from this effort are as follows:

A. Gage Performance

1. Current technology should permit properly prepared and protected thin film Pd-13Cr strain gages to operate to 1100 K in air. Additional work is needed to confirm this conclusion, to improve the fabrication yield, and to extend the range of use to higher temperatures.

2. Total drifts over 50 hour periods of uncompensated Pd-13Cr strain gages with hot sputtered insulation insulation and overcoat films were approximately 150 and 500

μstrain at 1000 K and 1100 K, respectively, after prestabilization treatments at temperatures approximately 100 K higher.

3. The use of PdCr films as strain gages requires the addition of a compensation grid in the adjacent leg of the Wheatstone bridge which decreases the effective gage factor at room temperatures from about 1.8 to 1.55. The gage factor decreases linearly with temperature to about 1.45 at 920 K.

4. Hot sputtered alumina overcoat films were adherent and protective when sputtered on Pd-13Cr grids but were not adherent and protective on pure Pd compensation grids.

5. Complete Pd-13Cr strain gage systems prepared using Pd compensation grids showed large negative drifts when exposed to temperatures in the range 900 to 1000 K due to oxidation of the Pd. At 1100 K this effect begins to reverse, apparently because of the dissociation of the oxide.

B. Gage Preparation

1. When Pd-13Cr is prepared as a sputtered film it requires a protective overcoat to prevent unacceptable oxidation. Alumina films sputtered on unheated substrates did not adequately prevent oxidation at elevated temperatures.

2. Significant improvements in overcoat and substrate insulation films of alumina were obtained by depositing these films on substrates heated to 870 K.

3. Sputtering alumina at 870 K resulted in close to stoichiometric aluminum : oxygen ratios, a reduction in entrapped argon (0.5 vs. 1.2 weight percent cold sputtered), and a reduction in the maximum thermal expansion mismatch strain between the substrate and the sputtered film.

4. We recommend the use of platinum for the compensation grids in further work which should eliminate the oxidation problem that was encountered in this effort.

5. Because of grid dimensions and the high cohesive strengths of sputtered PdCr, film thickness were limited to about 5 microns with the lift-off photoresist process used in this work. This fabrication approach resulted in torn edges which provide preferential sites

for oxidation. In further work, we recommend the use some other technique, such as ion beam etching, to make the grid arrays which would permit forming thicker films with tapered edges which should be more effectively protected by sputtered overcoat layers.

9.0 REFERENCES

1. Hulse, C.O., Stetson, K.A., Grant, H.P., Jameikis, S.M., Morey, W.W., Raymondo, P., Grudkowski, T.W. and Bailey, R.S.: Advanced High Temperature Static Strain Sensor Development Program, NAS CR-179520, 1987.

2. Hulse, C.O., Bailey, R.S. and Lemkey, F.D.: High Temperature Static Strain Gage Alloy Development Program, NASA CR-174833, 1985.

3. Stetson, K.A.: Demonstration Test of Burner Liner Strain Measuring System, NASA CR-174743.

4. Stetson, K.A.: Demonstration of a Laser Speckle System on Burner Liner Cyclic Rig, CR-179509.

5. Lant, C.T. and Barranger, J.P.: Progress in High Temperature Speckle-Shift Strain Measurement System, Hologram Interferometry and Speckle Metrology Proceedings, Soc. for Exp. Mech, Inc., Nov. 1990, p 203.

6. Dennis, A.J. and Fulton, G.B.: Advanced Structural Instrumentation, U.S. Air Force, WRDC-TR-90-2020, Vol. I and II, 1990.

7. Hulse, C.O., Bailey, R.S., Grant, H.P. and Przybyszewski, J.P.: Review of Current NASA Thin Film Static Strain Gage Research at United Technologies, Fourth Annual Expo. International, Kansas City, 1989.

8. Hulse, C.O., Bailey, R.S., Grant, H.P. and Przybyszewski, J.S.: High Temperature Static Strain Gage Development Contract, CR-180811, 1987.

9. Grant, H. P. and J. S. Przybyszewski: Thin Film Temperature Sensor. NASA CR-159782, 1980.

10. Gardner R. A., P. J. Peterson, T. N. Kennedy: Stability of RF-Sputtered Aluminum Oxide. J. Vac. Sci. Technol., vol. 14, no. 5, pp. 1139 - 1145, 1977.

11. Godefroy, J.C., C. Gageant, D. Francois, and M. Portat: Sputtered Alumina Layers and Platinel Thermocouples for High Temperature Surface Thermometers. Evaluation of Their Electrical and Mechanical Characteristics. ONERA, BP 72, 92322 Chatillon Cedex, France, 1987.

12. Anderson, Lee et. al., Unpublished final report, P&W Aircraft, NASA Lewis Contract NAS3-25410, High Temperature Strain Gages for Hypersonic Aircraft Development Applications, 1991.

13. Cole, S.S. Jr.: Oxidation and Reduction of Palladium in the Presence of Silver, Jour. Am. Ceramic Soc.,vol. 68, no.4, C-106, 1985.

14. Lei, J.-F.: Test of PdCr Wire Resistance Static Strain Gauge to 700°C, High Temperature Symposium, Electrochemical Soc., Montreal, 1990.

15. Zeller, M.V. and Lei, J.-F.: Surface Analysis Studies of the Oxidation of PdCr Strain Gage Material, High Temperature Symposium, Electrochemical Soc., Montreal, 1990.

16. Tech. Note TN-502, Measurements Group, Inc., Raleigh, N. Carolina, p.3, 1979.

Table 5.2.1

Task 5A Topcoat Materials

Material	Application Method	Thickness	Comments
Borosilicate Glass	Ion Beam Deposition	0.25 - 1.5 μm	
Borosilicate Glass	Transfer Tape	5 - 20 μm	Requires firing at elevated temperature
Aluminum	Sputtering	0.25 - 0.50 μm	Heat treatment to convert to Al_2O_3
Palladium	Sputtering	0.025 μm	
FeCrAl Mod. 3	Sputtering	0.025 μm	

Table 6.1.1

TASK 5/5A Fabrication and Test Remarks
Samples with Cold Sputtered Overcoats on Hast-X Substrates

Sample #	Overcoat	Topcoat	Remarks
8-39	3.0μm Al_2O_3	None	Sample lost; fixture collapsed during overcoat sputtering
8-40	3.0μm Al_2O_3	None	Al_2O_3 on tabs : high contact resistance may have contributed to high drift. Sample shorted to substrate after 20 hrs. at 1100K.
8-41	0.5μm Al_2O_3	None	Shorts to substrate as sputtered - repaired. Overcoat spalled from areas of grid. Not tested.
8-42	0.5μm Al_2O_3	None	Shorts to substrate as sputtered - repaired. Overcoat spalled from areas of lead films. Shorted to substrate during first cycle to 1100K.
8-81	3.5μm Al_2O_3	None	Not recrystalized. Resistance to substrate 400-600 Ω during drift at 1100K. Shorted to substrate after 36 hrs. at 1100K.
8-82	3.5μm Al_2O_3	None	PdCr melted during recrystalization heat treatment at 1373K after overcoat applied.
P87-1-5	3.0μm Al_2O_3	0.25μm Al	Topcoat shorted to grid as sputtered. Topcoat oxidized at 835K/50 hrs. Topcoat still conductive and shorted to grid after 835K. Heating to 1250K oxidized topcoat but grid open on next cycle.
P87-1-1	3.0μm Al_2O_3	0.25μm 7070 glass	Insulation res. 130KΩ at 1100K; dropping to 19KΩ after 3.5 hrs at 1100K, then constant for remaining 46.5 hrs.
P87-1-6	3.0μm Al_2O_3	0.25μm FeCrAl	Grid shorted to sub. at defect #7. Resistance topcoat - grid >20 MegΩ.
P87-1-2	3.0μm Al_2O_3	0.4μm 7070 glass	Insul. res. >20 MegΩ after 1st cyc. Large drift at 1100K and 1250K.
P87-1-3			Insulation resistance 1.0 MegΩ during 1100K drift.
P87-1-4			PdCr partially delaminated during removal of mask. New PdCr blistered during heat treatment
			PdCr partially delaminated during mask removal . Repair failed.

Table 6.1.2

TASK 5/5A Fabrication and Test Remarks
Samples with Cold Sputtered Overcoats on Alumina Substrates

Sample #	Overcoat	Topcoat	Remarks
8CII-1	3.5μm Al_2O_3		Thin alumina substrate cracked during testing at 1100K
8CII-2	3.5μm Al_2O_3	1.5 μm 7070 glass	Delamination of topcoat and PdCr after first cycle to 1100K
8CII-3	3.5μm Al_2O_3		Not tested. PdCr spalls when heated to 1100K
8CII-4	3.5μm Al_2O_3		Overcoated PdCr detached from substrate during 1140K/air.
8CII-5	3.5μm Al_2O_3		Broken after sputtering.
8CII-6	3.5μm Al_2O_3		Not tested. PdCr spalls when heated to 1100K
8CII-7	3.5μm Al_2O_3	Pd	Topcoat shorted to grid. Broken attempting to remove shorts.
8CII-8	3.5μm Al_2O_3		Broken during shipment.
8CII-9	3.5μm Al_2O_3	G1003 glass	Post-test exam. indicated glass reacted with Al_2O_3 & PdCr.
8CII-10	3.5μm Al_2O_3		Overcoat intact after 50 hrs. at 1100K. Tests at 1250K stopped due to high contact resistance.
8CII-11	3.5μm Al_2O_3		Severe shrinkage and cracking of overcoat after 1140K/argon
8CII-12	3.5μm Al_2O_3		Broken during shipment
8CII-13	3.5μm Al_2O_3		During 1250K drift, resistance dropped for 8 hrs. then increased
8CII-14	3.5μm Al_2O_3		Severe shrinkage and cracking of overcoat after 1140K/argon
8CII-15	3.5μm Al_2O_3		Severe shrinkage and cracking of overcoat after 1140K/argon
8CII-16	3.5μm Al_2O_3		Severe shrinkage and cracking of overcoat after 1140K/argon
8CII-17			Portion of one lead film detached after sputtering
8CII-18	3.5μm Al_2O_3		Not tested. PdCr spalls when heated to 1100K
8CII-19	3.5μm Al_2O_3		Not tested. PdCr spalls when heated to 1100K
5A-A-1 *	3.5μm Al_2O_3		Grid open after 20 hrs at 1250K.
5A-A-2 *	3.5μm Al_2O_3		Large transverse cracks in overcoat on grid after 50 hrs/1250K
5A-A-3 *	3.5μm Al_2O_3	Al	Grid open after topcoat oxidation at 900K. Topcoat cracked and folded.

* NASA Target

Table 6.1.3

TASK 5/5A TEST RESULTS
Samples with Cold Sputtered Overcoats

Sample #	Substrate	Topcoat	Initial Alpha (μΩ/Ω/K)	Total Drift 1100K (μΩ/Ω)	Minimum Drift Rate 1100K (μΩ/Ω/hr)	Alpha After 1100K (μΩ/Ω/K)	Alpha After 1250K (μΩ/Ω/K)
8-40	Hastelloy-X	None	218	+700,000 (20 hrs.)	+12,500		
8-81	Hastelloy-X	None	149	-54,500 (37 hrs)	-185	202	
P87-1-5	Hastelloy-X	0.25μm Al	189				
P87-1-1	Hastelloy-X	0.25μm 7070 glass	155	-40,500	-306		1,940
P87-1-6	Hastelloy-X	0.25μm FeCrAl	143	-47,600	-724	209	
P87-1-2	Hastelloy-X	0.40μm 7070 glass	146	-23,600	-249	193	
P87-1-3	Hastelloy-X		Not Tested				
P87-1-4	Hastelloy-X		Not Tested				
8CII-1	Alumina	None	139				
8CII-2	Alumina	1.5 μm 7070 glass	144				
8CII-9	Alumina	8.0 μm G1003 glass	150	-14,900/+10,800	random	301	
8CII-10	Alumina	None	138	-19,000 (50 hrs)	-88	160	
8CII-13	Alumina	None	131	-17,400 (50 hrs)	-124	152	394
5A-A-1	Alumina	None	134	-22,900 (50 hrs)	-182	148	
5A-A-2	Alumina	None	134	-23,700 (50 hrs)	-228	153	1400

Table 6.2.1

Changes in Thermal Coefficient of Resistance
Task 5A Samples with Hot Sputtered Overcoats & Fillcoats

SAMPLE	TOPCOAT	ALPHA AS SPUTTERED (μΩ/Ω/K)	FIRST DRIFT TEMP (K)	ALPHA AFTER 1ST DRIFT (μΩ/Ω/K)	SECOND DRIFT TEMP (K)	ALPHA AFTER 2ND DRIFT (μΩ/Ω/K)	THIRD DRIFT TEMP (K)	ALPHA AFTER 3RD DRIFT (μΩ/Ω/K)
P87-4-4 *	None	133	1000	153	1100	163	1000	165
P87-4-5 *	0.4 μm 7070 glass	130	1000	157	1100	165	1000	166
P87-4-3 *	0.4 μm 7070 glass	139	1100	166	1150	169	1100	169
P87-6-2 **	None	136	1100	160	1200	201		

* Fillcoat & overcoat sputtered at 870 K

** Fillcoat & overcoat sputtered at 1070 K

Table 6.2.2

Drift Data
Task 5A Samples with Hot Sputtered Overcoats & Fillcoats

SAMPLE	TOPCOAT	DRIFT	TEMP (K)	TOTAL DRIFT (μΩ/Ω)	FINAL DRIFT RATE (μΩ/Ω/hr)
P87-4-4 *	None	1st	1000	-13,250	-110.0
		2nd	1100	-10,900	-13.6
		3rd	1000	+200	+2.5
P87-4-5 *	7070 glass	1st	1000	-18,040	-89.0
		2nd	1100	-11,190	-35.5
		3rd	1000	+184	-0.7
P87-4-3 *	7070 glass	1st	1100	-10,160	+33.9
		2nd	1150	+5,810	+68.6
		3rd	1100	+720	+13.4
P87-6-2 **	None	1st	1100	-21,470	0.0
		2nd	1200	-72,000 (40 hrs.)	-3,060 (40 hrs.)

* Fillcoat & overcoat sputtered at 870 K

** Fillcoat & overcoat sputtered at 1070 K

Table 6.3.1

Summary of Efforts to Fabricate
Twelve Complete Gage Systems on Six Bend Bars

Bar	Gage	Results
B1	#1	Large areas of all three leads damaged by grit blast cleaning, Pd and fillcoat spalled away.
	#2	Damaged by Grit blasting accident, sections of active & compensation grid torn loose during mask removal. Could not be repaired.
B2	#1 & 2	OK, Tested
B3	#1 & 2	Pd target "burned through", In and Cu contamination. Attempts to repair by ion etching harmed fillcoat and left insoluble residue.
B4	#1	Compensation grid open, not tested
	#2	Compensation grid had high resistance, not tested.
B5	#1 & 2	OK, Tested. Alumina overcoat sputtered at 873K.
B6	#1 & 2	OK, Measured Gage Factor at R.T., sent to NASA. Alumina overcoat sputtered at 870 K.

Table 6.3.2
Summary of Data for Bar B2

	Gage #1						Gage #2					
	Bridge Ratio	Bridge Factor	Gage Resist. (Ω)	Comp. Resist. (Ω)	Fixed Resist. (Ω)	Lead Resist. (Ω)	Bridge Ratio	Bridge Factor	Gage Resist. (Ω)	Comp. Resist. (Ω)	Fixed Resist. (Ω)	Lead Resist. (Ω)
Initial Value	3:1	5.52	80.8	14.1	226	4.25	3:1	5.52	79.8	14.1	226	4.15
For 3rd Cycle	2.4:1	5.02			179		2.4:1	5.02			179	
For 4th Cycle	1.9:1	4.63			138		1.9:1	4.63			138	
After Testing			66.1	14.3		3.75			66.6	15.8		2.95

Table 6.3.3
Gage Factor Results For Bar B2

	Gage #1					Gage #2				
	Temp (K)	GF Comp.	Var. c (%)	GF Tension	Var. t (%)	Temp (K)	GF Comp.	Var. c (%)	GF Tension	Var. t (%)
After Cycle 4 ± 500 μstrain	310.00	1.52	17.45	1.51	19.37	310.00	1.57	16.94	1.56	18.74
	651.60	1.44	0.86	1.43	0.53	651.60	1.48	0.58	1.47	0.55
	706.10	1.43	3.69	1.42	2.81	706.10	1.47	3.70	1.47	2.95
	759.60	1.42	2.71	1.42	1.96	759.60	1.47	3.20	1.45	1.91
	922.30	1.36	17.58	1.35	11.07	922.30	1.41	21.17	1.40	16.08
	318.20	1.52	3.58	1.51	5.14	318.20	1.56	3.43	1.56	4.91
After Cycle 8 ± 500 μstrain	300.40	1.46	3.99	1.44	3.63	300.40	1.45	4.40	1.45	3.73
	919.80	1.29	5.42	1.28	0.89	919.80	1.31	4.09	1.30	3.54
	320.70	1.43	2.31	1.42	2.74	320.70	0.00	57.08	0.00	145.00
± 1000 μstrain	300.60	1.45	0.40	1.44	1.07	300.60	1.45	0.57	1.43	1.49
	920.50	1.30	5.98	1.30	1.96	920.50	1.33	6.42	1.32	2.08
	320.70	1.43	0.59	1.42	0.33	320.70	0.00	243.74	0.00	139.60
± 1500 μstrain	300.80	1.46	0.17	1.43	0.67	300.80	1.46	0.37	1.42	1.20
	919.90	1.32	5.62	1.29	2.58	919.90	1.34	5.62	1.31	2.98
	320.20	1.44	1.13	1.41	0.32	320.20	0.00	91.62	0.00	60.00
±500 μstrain	297.00	1.45	2.66	1.44	2.15	297.00	1.43	1.78	1.44	1.28
	297.00	1.44	1.03	1.43	3.24	297.00	1.43	1.78	1.40	6.21
	650.80	1.38	13.87	1.32	10.49	650.80	1.41	19.82	1.33	17.01
	705.80	1.39	10.94	1.31	8.22	705.80	1.42	10.74	1.31	15.28
	760.10	1.38	7.26	1.34	13.68	760.10	1.39	10.99	1.33	9.89
	999.20	1.34	48.45	1.32	42.69	999.20	1.35	49.31		338.74
	318.30	1.39	17.03	1.39	18.26	318.30	0.00	125.19	0.00	101.94
After Cycle 10 ± 500 μstrain	297.00	1.27	9.84	1.24	6.72	297.00	1.26	5.24	1.26	7.15
	649.00	1.15	6.39	1.16	5.70	649.00	1.15	7.87	1.15	9.63
	703.20	1.15	8.70	1.16	11.03	703.20	1.17	9.79	1.17	12.26
	757.20	1.35	54.70	1.12	4.51	757.20	1.31	46.72	1.13	5.29
	1093.90	1.03	112.07	3.63	80.88	1093.90	3.80	91.11	4.70	65.54
	317.50	1.23	29.41	1.25	36.81	317.50	1.97	195.85	1.20	128.64
After Cycle 12 ± 500 μstrain	295.50	1.57	1.28	1.56	1.65	295.50	1.90	94.38	1.45	70.11
	649.60	1.43	2.08	1.98	57.64	649.60	1.52	97.64	1.47	97.87
	703.60	1.44	5.51	1.41	6.72	703.60	1.42	17.55	1.36	33.92
	757.20	1.42	3.88	1.40	15.39	757.20	1.38	25.85	1.26	9.10
	1245.00	1.42	46.10	1.31	65.73	1245.00	2.12	142.10	1.67	111.42
	317.30	1.87	2.18	1.86	2.69	317.30	2.38	144.57	1.50	89.27

Table 6.3.4
Summary of Data for Bar B5

	Gage #1						Gage #2					
	Bridge Ratio	Bridge Factor	Gage Resist. (Ω)	Comp. Resist. (Ω)	Fixed Resist. (Ω)	Lead Resist. (Ω)	Bridge Ratio	Bridge Factor	Gage Resist. (Ω)	Comp. Resist. (Ω)	Fixed Resist. (Ω)	Lead Resist. (Ω)
Initial Value	1:1	4.0	92.5	11.8	80.7	5.8	1:1	4.0	93.3	12.6	80.7	5.65
For 3rd Cycle	3.1	5.54	89.9	20.8	249.2	5.5	3:1	5.54	91.3	25.1	248.8	4.8
For 4th Cycle	3.25:1	5.77			273		4.19:1	6.60			357	
After 5th Cycle			96.8	175.9	273	3.65			100.5	62.8	357	2.85
After Testing			66.6	9.7	273	3.85			41.1	11.2	357	2.9

Table 6.3.5
Gage Factor Results For Bar B5

	Gage #1					Gage #2				
	Temp (K)	GF Comp.	Var. c (%)	GF Tension	Var. t (%)	Temp (K)	GF Comp.	Var. c (%)	GF Tension	Var. t (%)
Prior to any thermal cycles										
± 500 μstrain	297.6	1.12	10.79	1.22	6.10	297.6	1.00	11.80	1.25	7.75
± 1000 μstrain	297.8	1.02	4.80	1.13	11.49	297.8	0.90	21.23	0.98	27.37
± 1500 μstrain	298.0	1.05	3.72	0.95	30.44	298.0	0.84	17.79	0.51	51.41
	297.4	1.69	1.96	1.68	0.78	297.4	1.76	0.28	1.76	1.23
After Cycle 4	653.6	1.55	4.23	1.55	1.31	653.6	1.64	2.29	1.65	1.58
	706.4	1.54	0.59	1.53	0.21	706.4	1.61	2.20	1.63	0.89
± 500 μstrain	759.3	1.53	5.12	1.52	8.43	759.3	1.60	1.21	1.63	8.92
	916.9	1.43	108.93	1.42	108.99	916.9	1.55	88.94	1.54	93.45
	335.8	1.65	3.40	1.63	5.25	335.8	1.71	3.30	1.71	3.98
After Cycle 8	299.3	1.31	5.52	1.29	1.18	299.3	1.63	7.22	1.62	5.25
	914.6	1.15	4.29	1.14	14.01	914.6	1.39	7.58	1.41	7.65
± 500 μstrain	335.8	1.22	17.96	1.22	27.62	335.8	1.59	7.93	1.57	13.79
	299.5	1.31	2.33	1.28	0.71	299.5	1.61	1.54	1.61	1.22
± 1000 μstrain	914.9	1.15	3.04	1.11	12.68	914.9	1.38	7.09	1.38	7.25
	333.9	1.22	22.46	1.21	27.41	333.9	1.58	5.39	1.57	9.67
	299.5	1.30	1.56	1.28	0.44	299.5	1.62	1.18	1.61	0.22
± 1500 μstrain	914.6	1.15	3.74	1.07	11.89	914.6	1.37	6.34	1.36	7.01
	331.8	1.23	20.04	1.20	21.02	331.8	1.59	3.31	1.57	7.65

Table 6.3.6

Room Temperature Gage Factor Measurements on Bar B6
(Four measurements at each strain level)

Reference Gage		Gage #1		Gage #2	
Mean Strain (μstrain)	Variation (%)	Mean Gage Factor	Variation (%)	Mean Gage Factor	Variation (%)
-507	0.2	0.55	69	1.24	9.8
+505	0.3	1.12	13	1.22	3.2
-1,014	0.5	1.00	30	1.24	5.0
+1,014	0.5	0.25	129	1.17	1.6
-507	0.3	0.27	108	1.27	14
+506	0.4	0.48	61	1.22	3.1
-1,014	0.3	1.03	7.9	1.24	4.2
+1,006	0.4	0.13	28	1.21	3.4

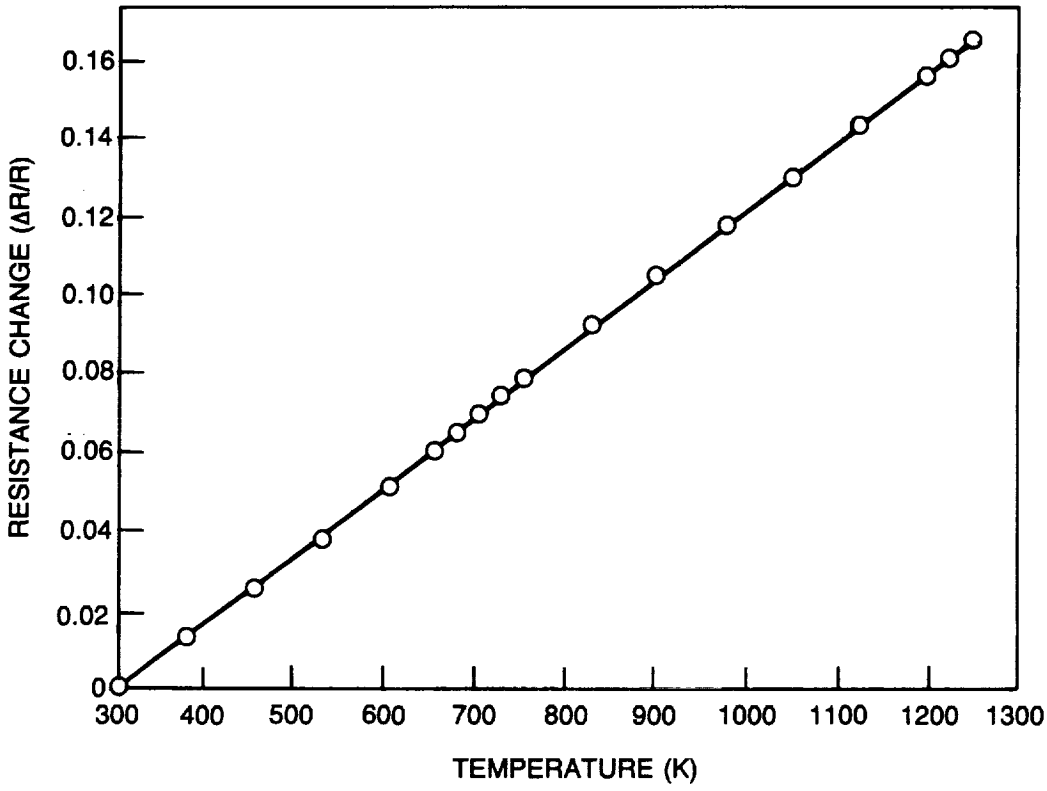

Figure 3.1 Change in resistance vs temperature at 50 K/min in argon of splat cast Foil Pd-13Cr (wt%)

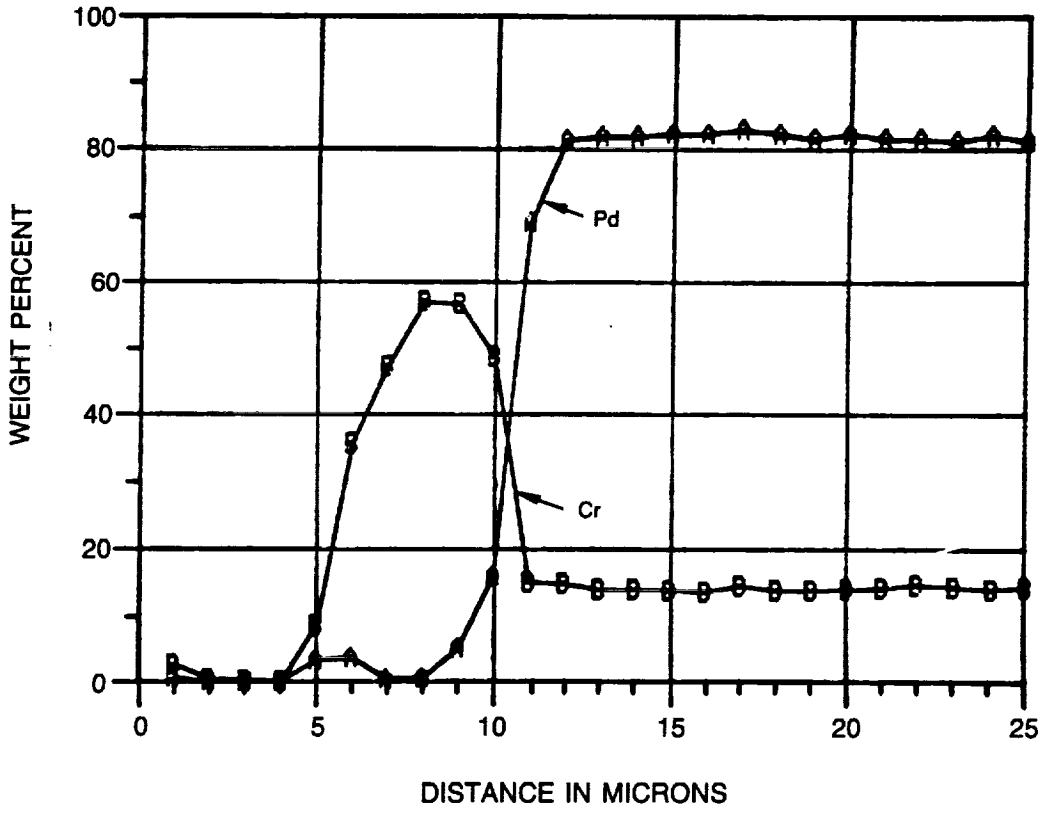

Figure 3.2 Elemental composition profiles at the surface of Pd-13Cr (wt%) sample after 40 hours in air at 1250 K

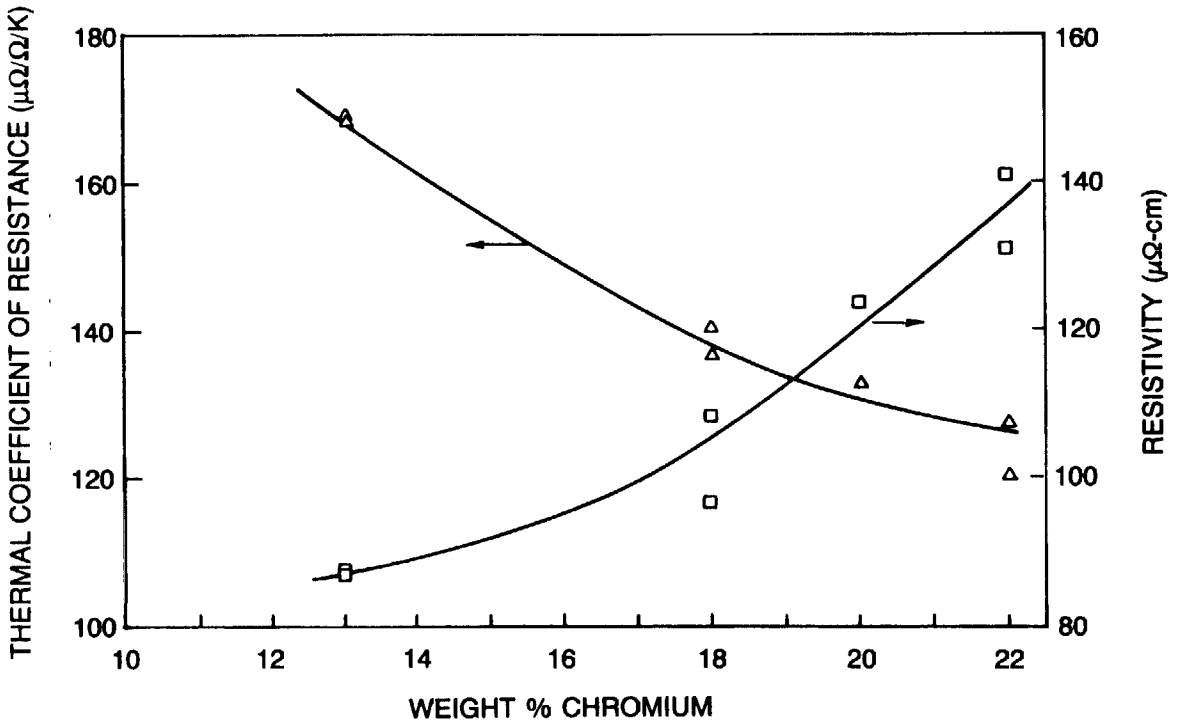

Figure 3.3 Resistivity and thermal coefficient of resistivity of PdCr alloys

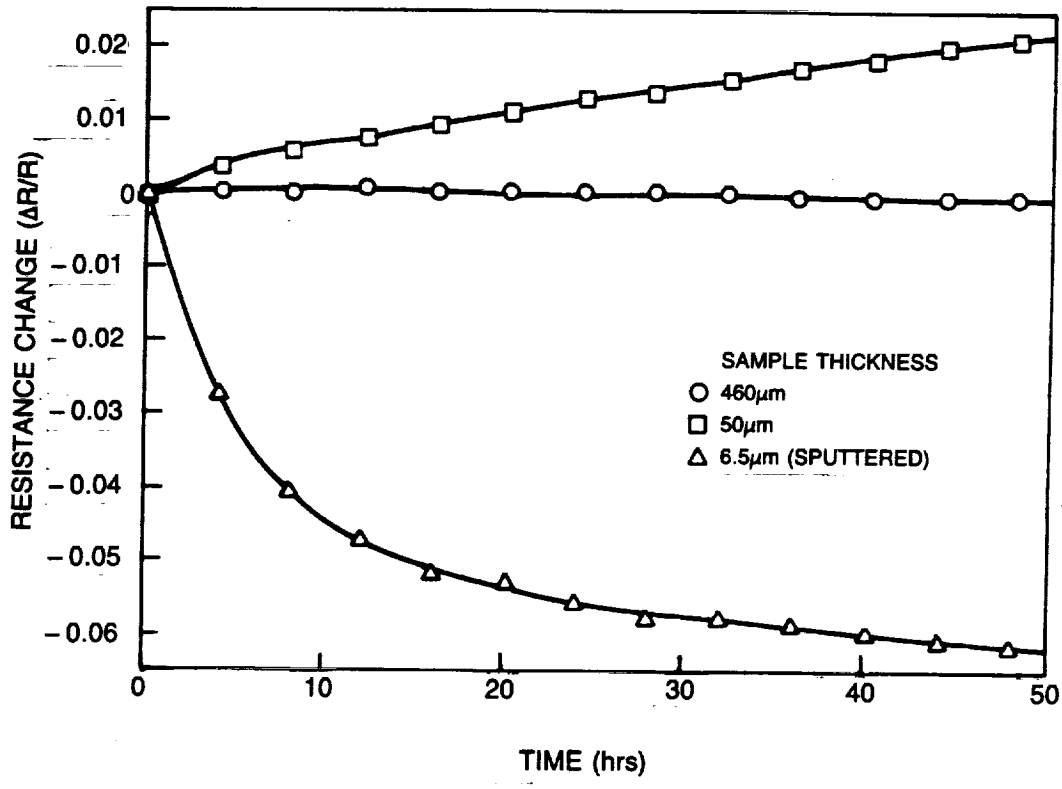

Figure 3.4 Effect of sample thickness on drift in resistance of Pd-13Cr (wt%) in air at 1250 K

a) UNIFORM NODULES

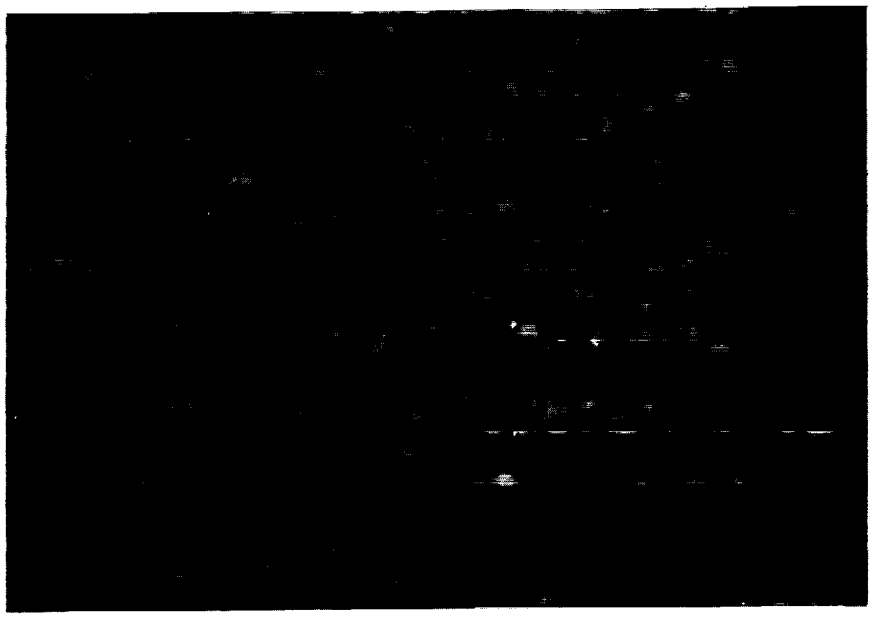

b) SOME EXAGGERATED NODULES

Figure 3.5 As-sputtered Pd-13Cr (wt%) on NiCoCrAlY coated Hastalloy-X

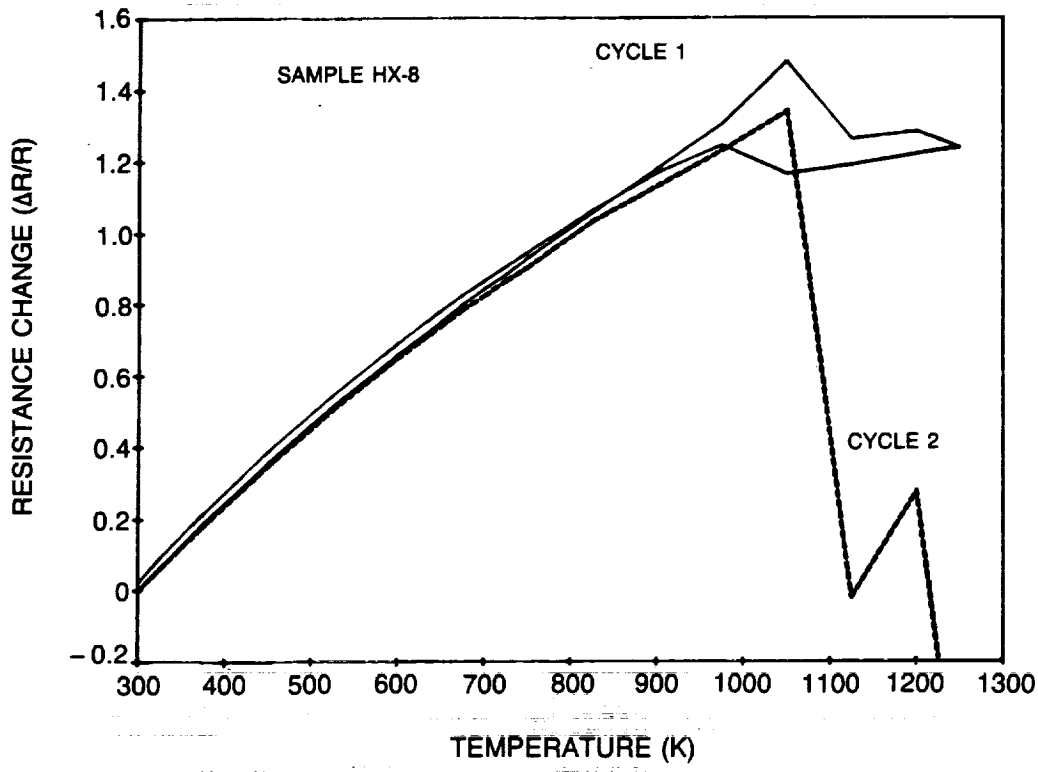

Figure 3.6 Resistance vs temperature for sputtered Pd-13Cr (wt%) pretreated 10 hrs in air at 1370 K

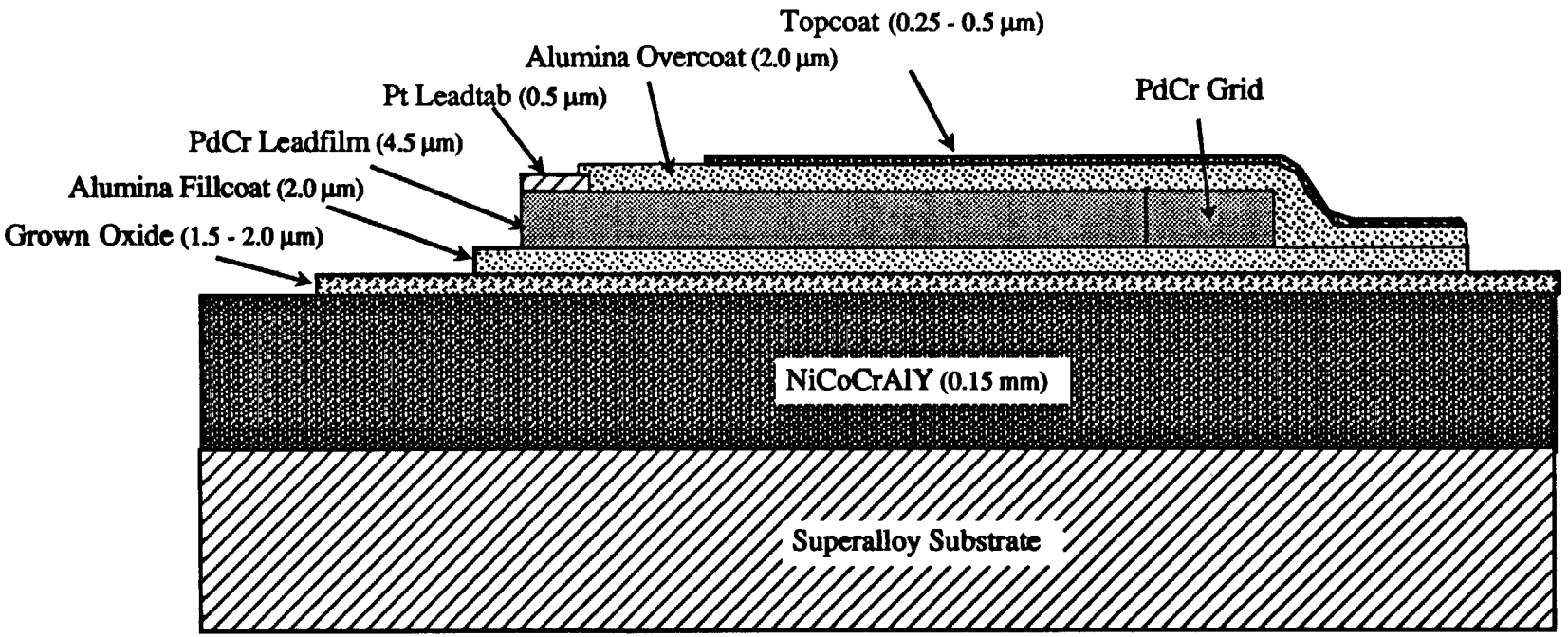

Figure 5.1.1 Layers constituting a typical elevated temperature test sample on Hastelloy-X

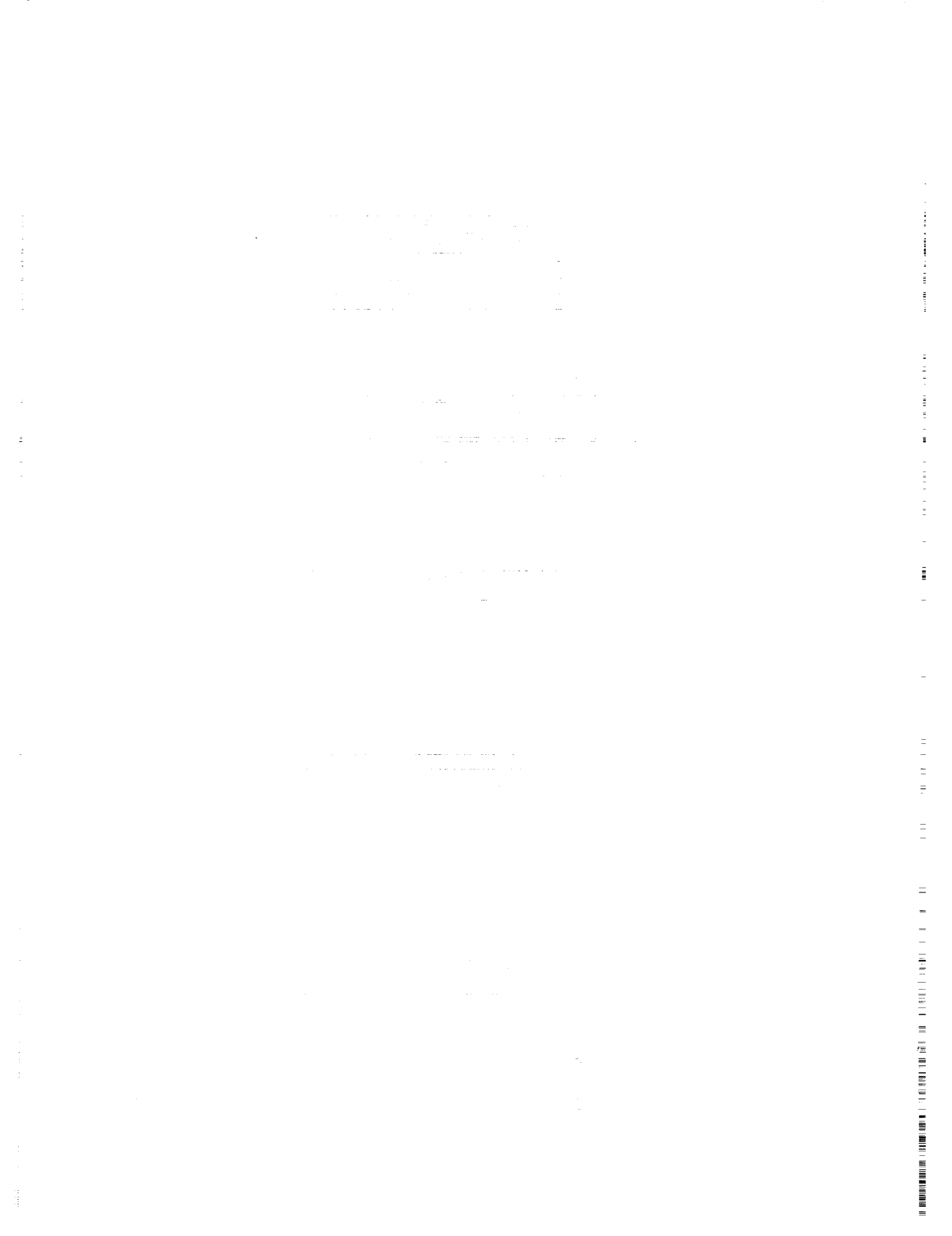

1. ALL DIMENSIONS IN CENTIMETIMERS (INCHES).
2. TOLERANCE ± 0.025 CM (± 0.010 in.) EXCEPT WHERE NOTED.
3. THICKNESS OF TEST BAR IS 0.32 ± 0.01 CM (0.125 ± 0.005 in.).
4. MATERIAL IS PWA 1422 DS. LONG GRAINS PARALLEL ℄ .
5. FINISH 0.4 MICROMETER (15 MICROINCH AA) BOTH SIDES OF TAPERED SECTION. TYPE 6A SHOT PEEN BEFORE POLISHING.
6. BREAK ALL CORNERS AND EDGES 0.08 CM (0.03 in.)
7. USE ANTI-GALLING COMPOUND WHEN CLAMPING FOR FATIGUE TEST.
8. COATING: PWA 273 + PWA 270. SEE SPECIAL INSTRUCTIONS.

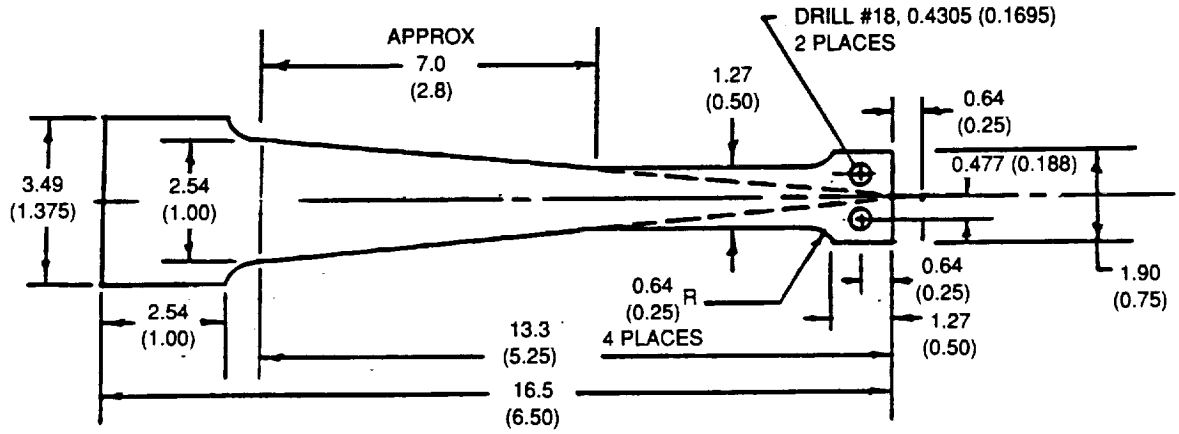

Figure 5.3.1 Design of test bars

PRECEDING PAGE BLANK NOT FILMED

91-9-45-1

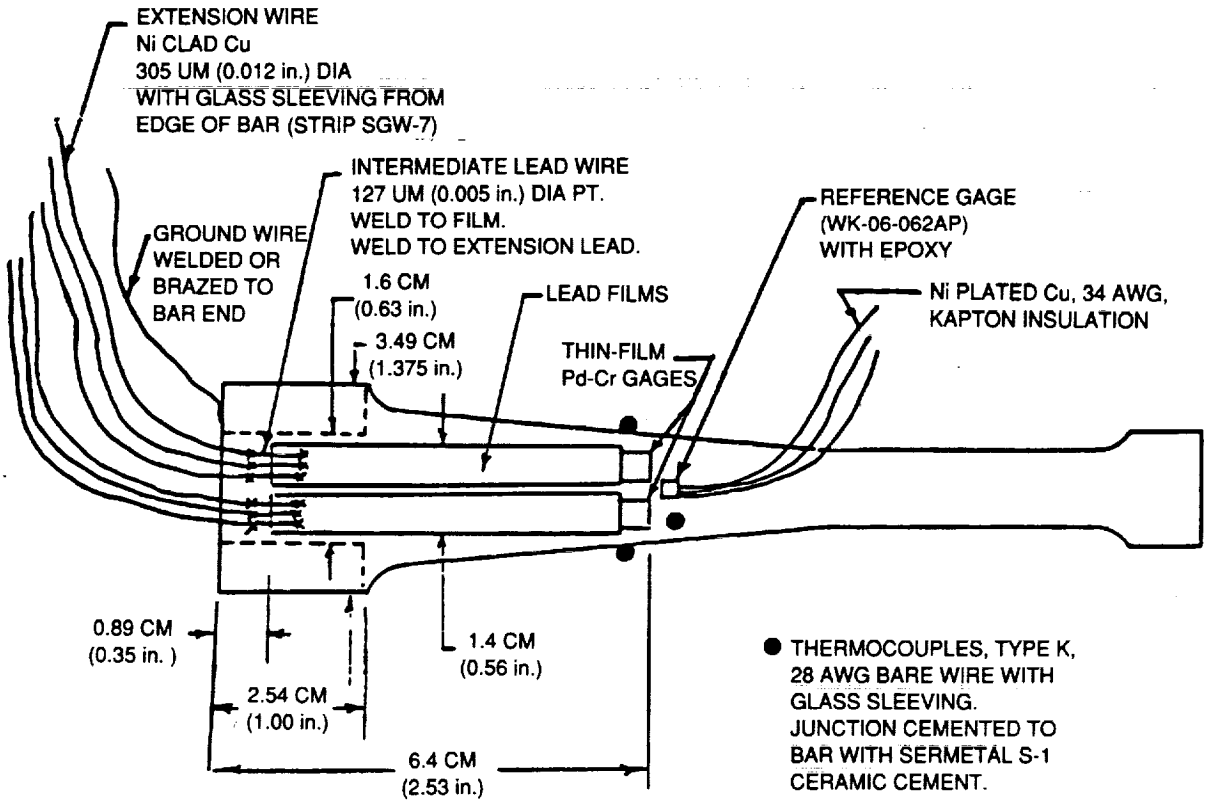

Figure 5.3.2 Gage and thermocouple layout on test bar

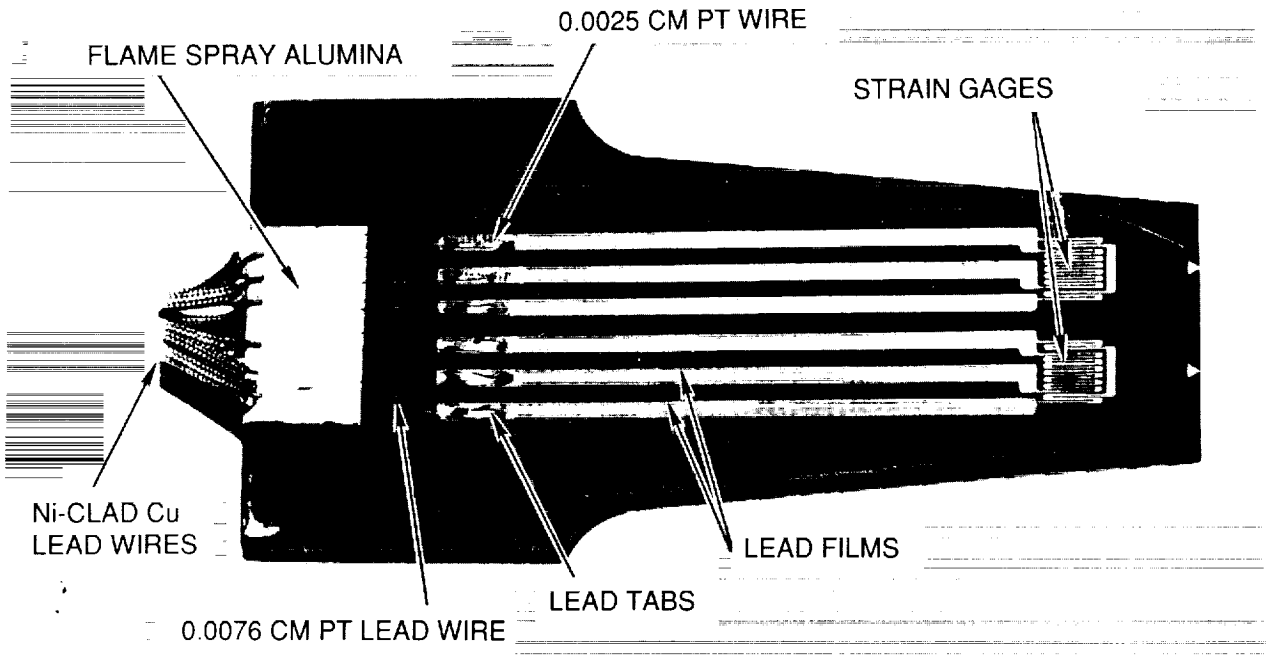

Figure 5.3.3 Two sputtered PdCr strain gage systems installed on Bend Bar B6

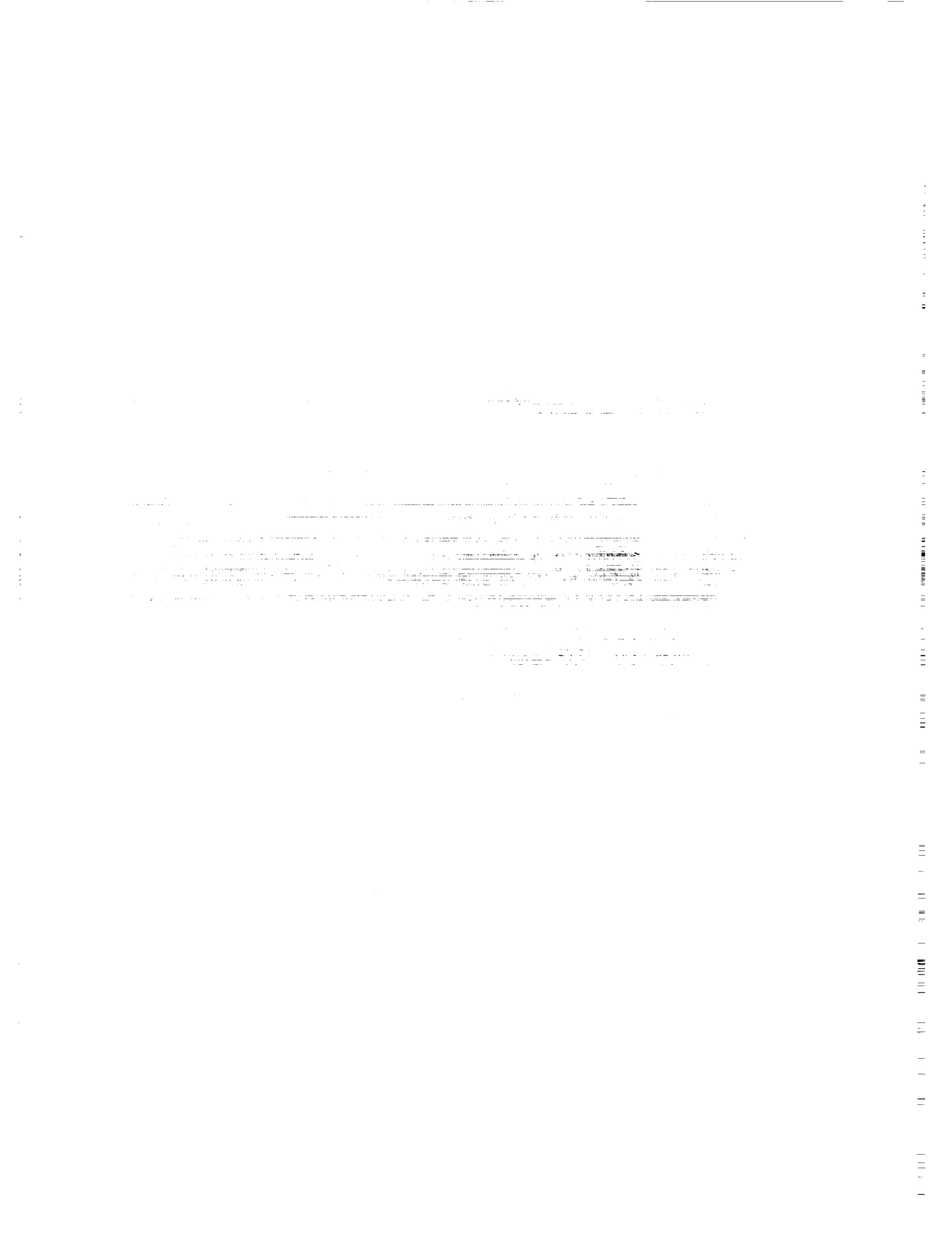

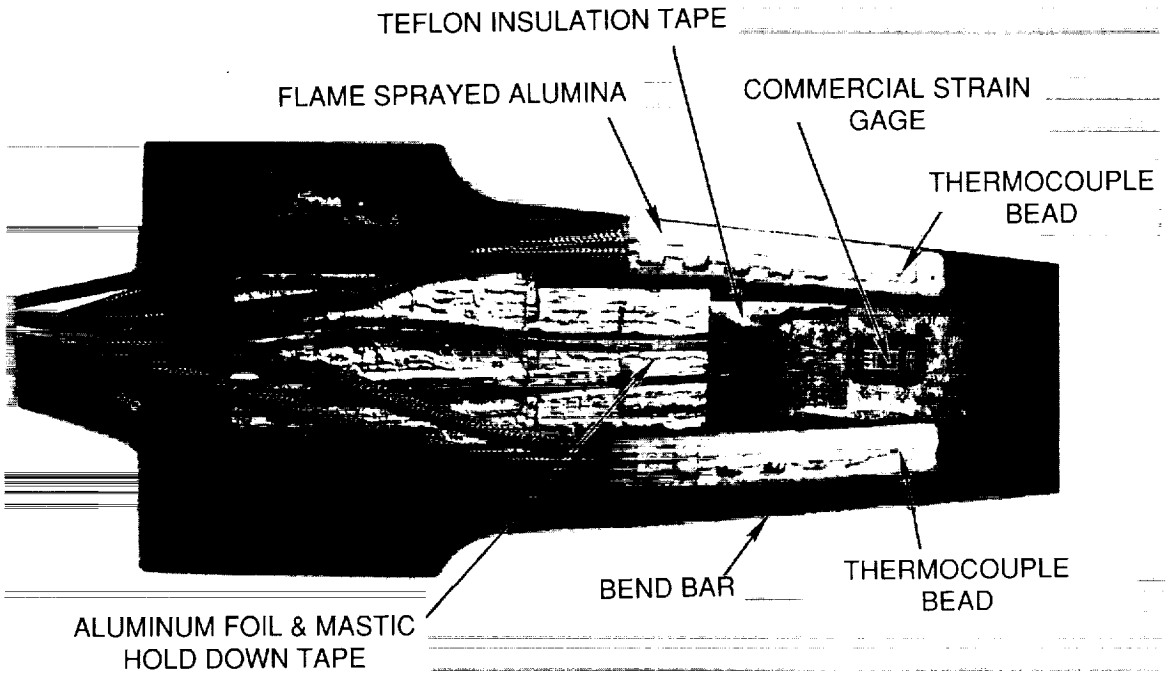

Figure 5.3.4 Commercial strain gage and two thermocouples mounted on bottom of Bend Bar B6

ORIGINAL PAGE
BLACK AND WHITE PHOTOGRAPH

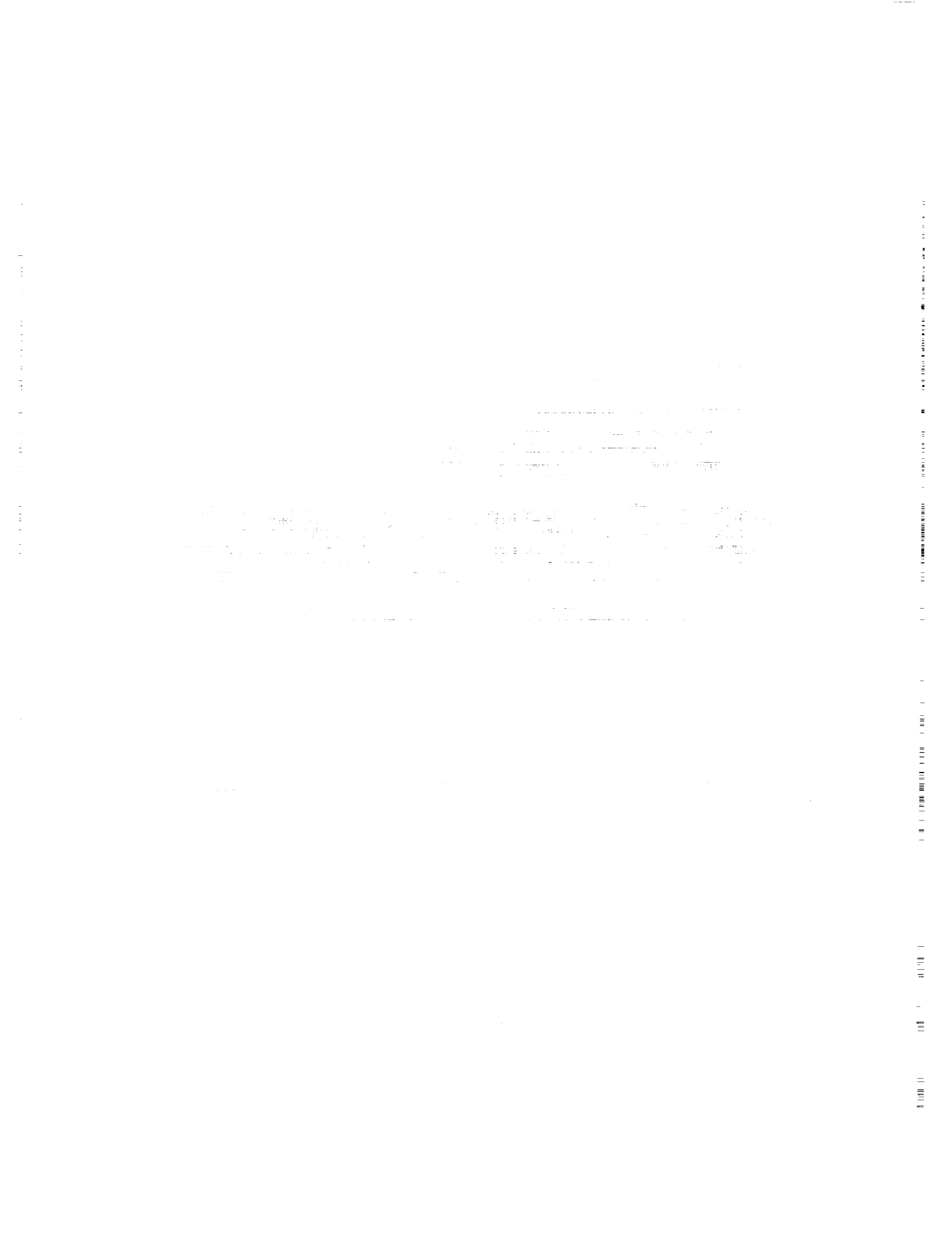

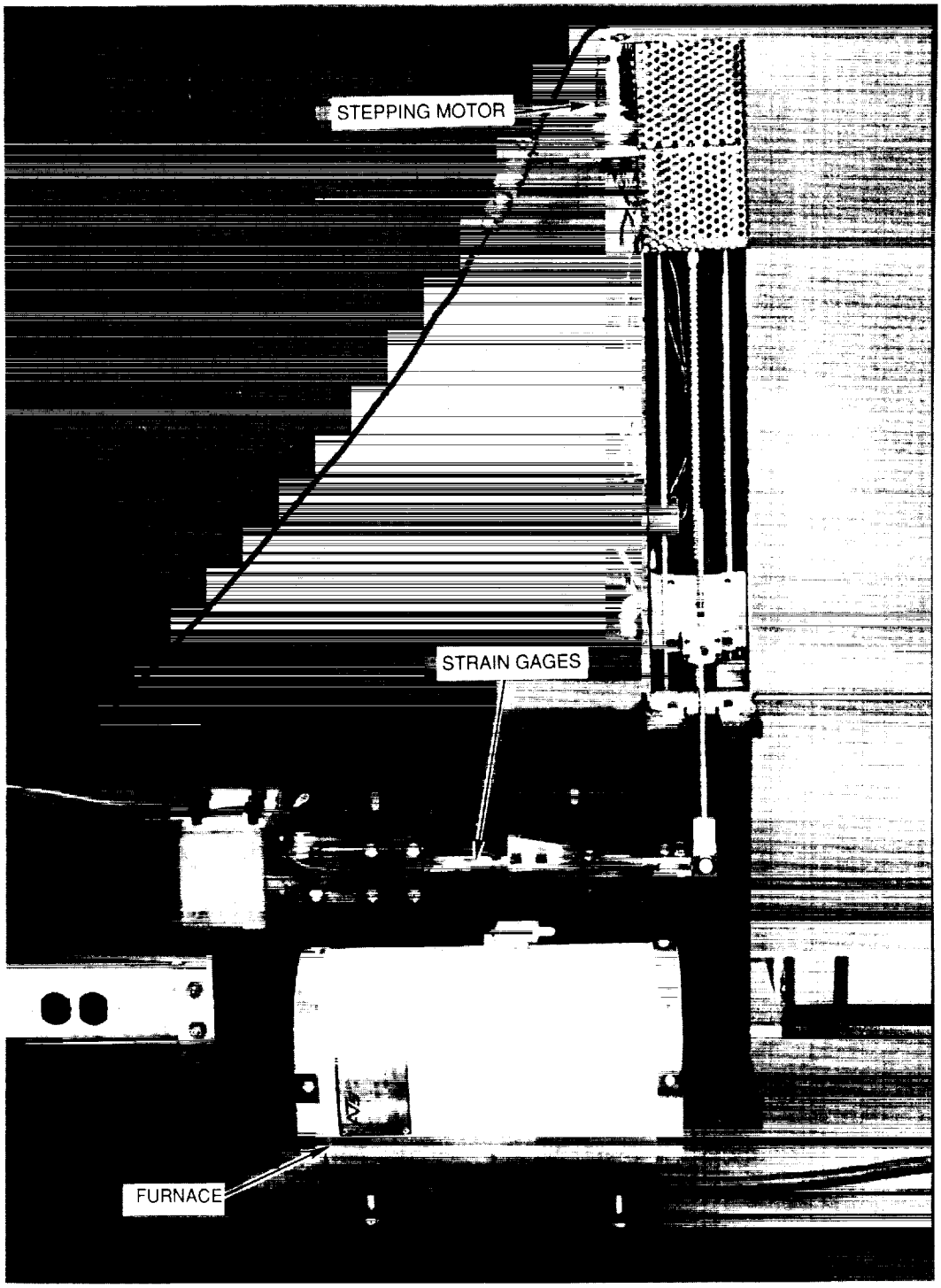

Figure 5.5.1 **Cantilever bend bar testing facility with furnace adjacent**

91-9-45-6

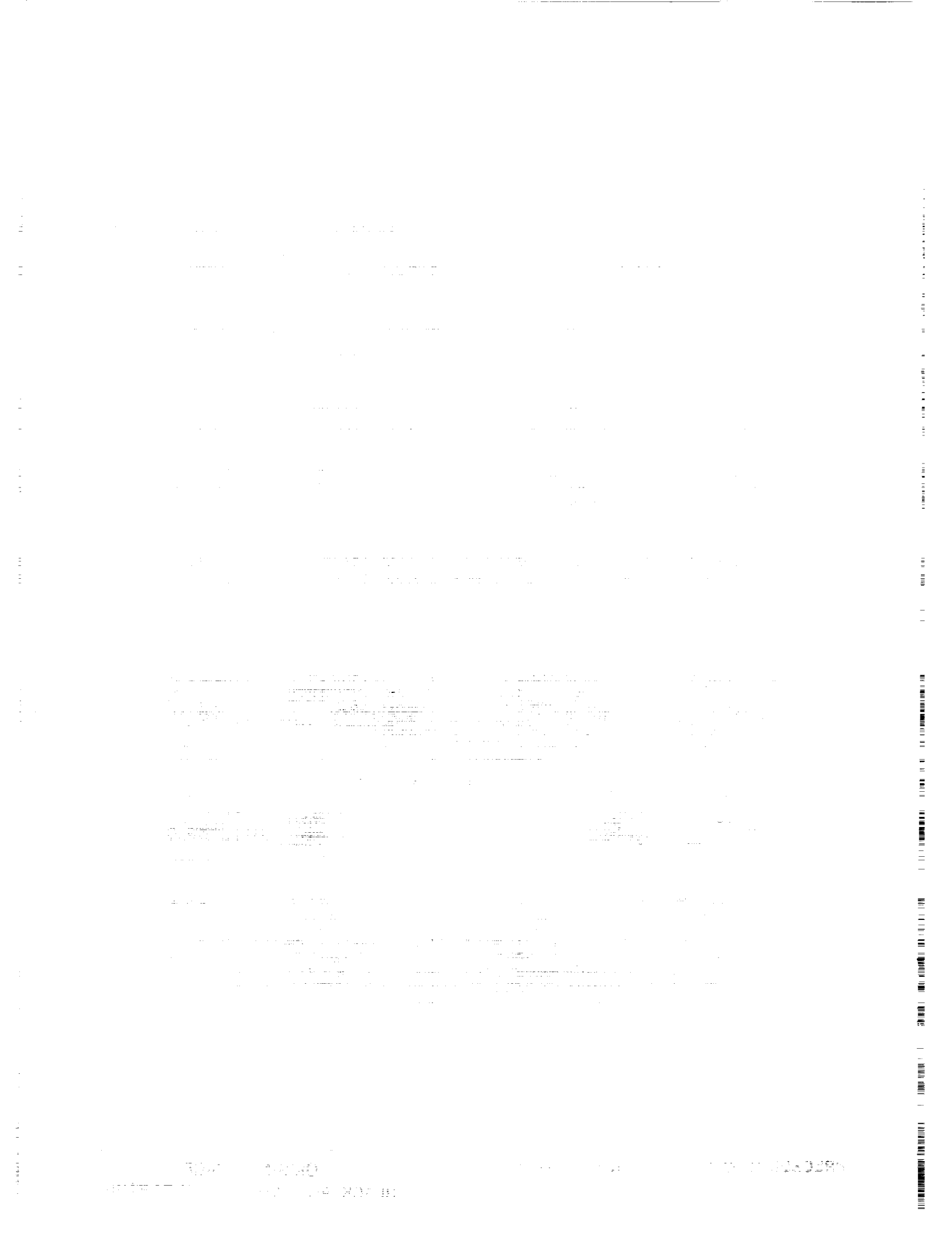

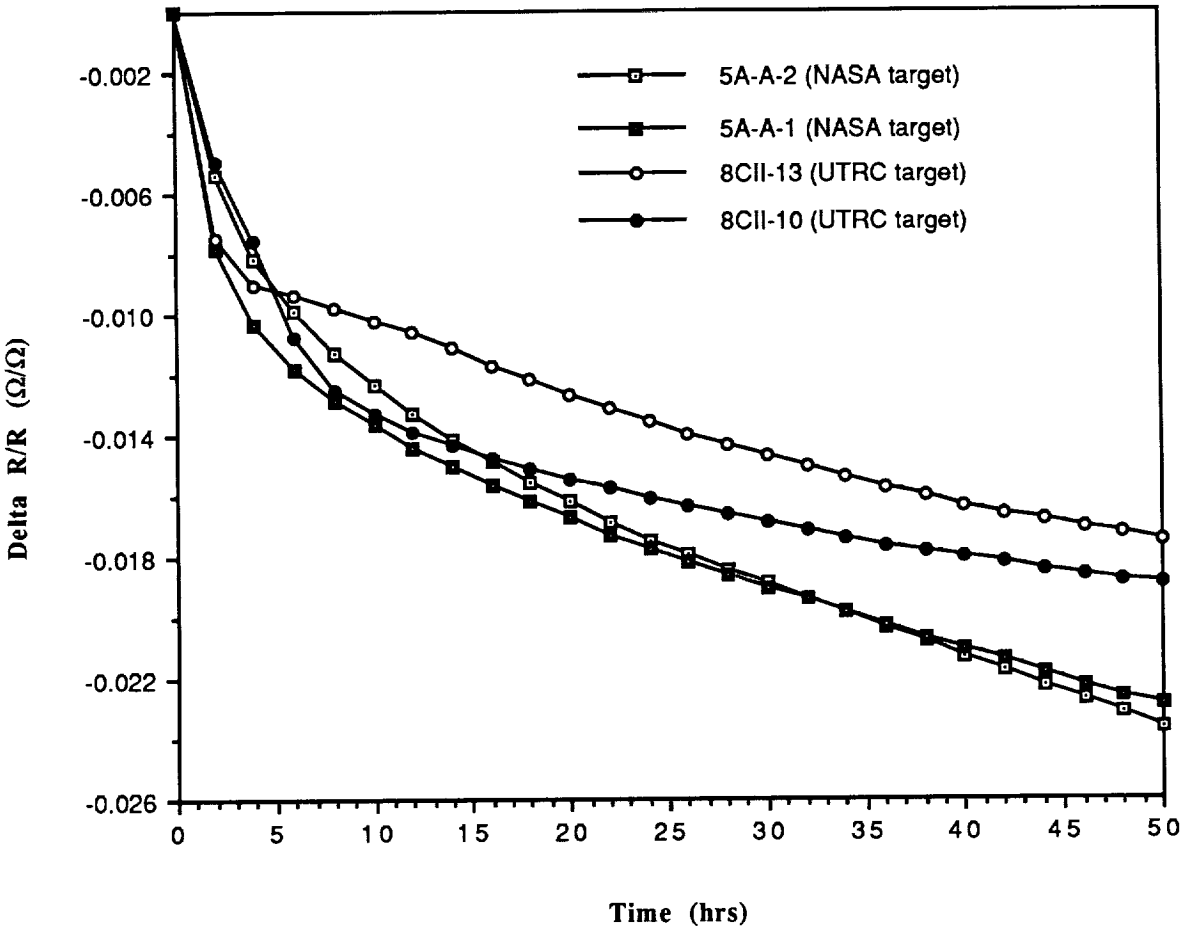

Figure 6.1.1 Electrical resistance drift at 1100 K
Task 5A samples with R.T. fillcoats & overcoats

a) FRACTURED BLISTERS

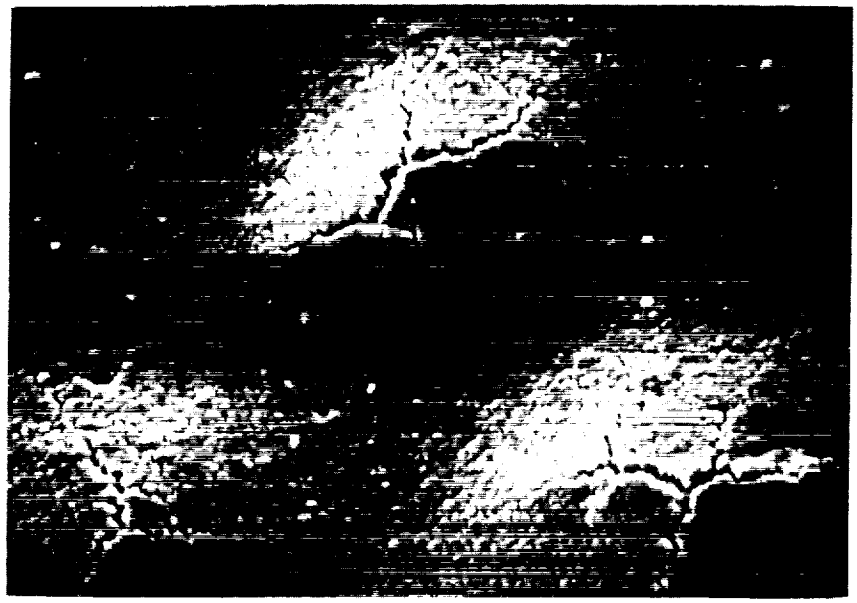

3.3μm

b) TYPICAL AREA

20μm

Figure 6.1.2 SEM micrographs of alumina overcoat after 10 hours at 1250 K in air

91-9-45-7

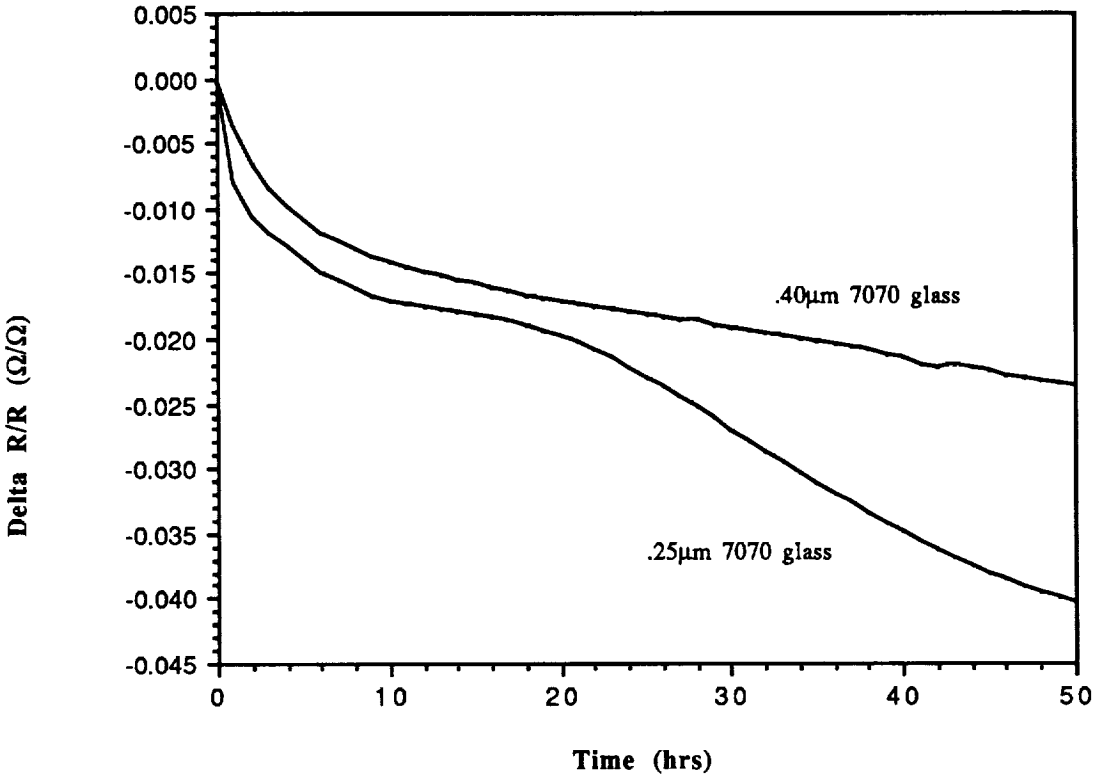

Figure 6.1.3 Electrical resistance drift at 1100 K
Samples with R.T. overcoats & 7070 glass topcoats

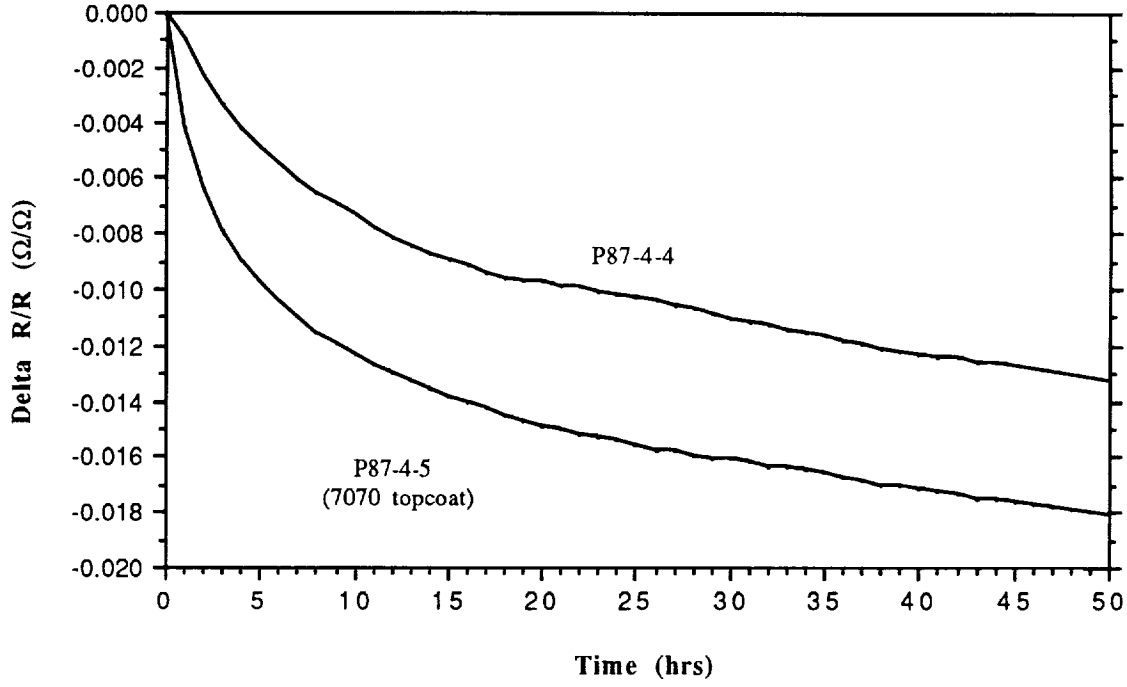

Figure 6.2.1 Electrical resistance drift at 1000 K
Task 5A samples with 870 K fillcoats & overcoats

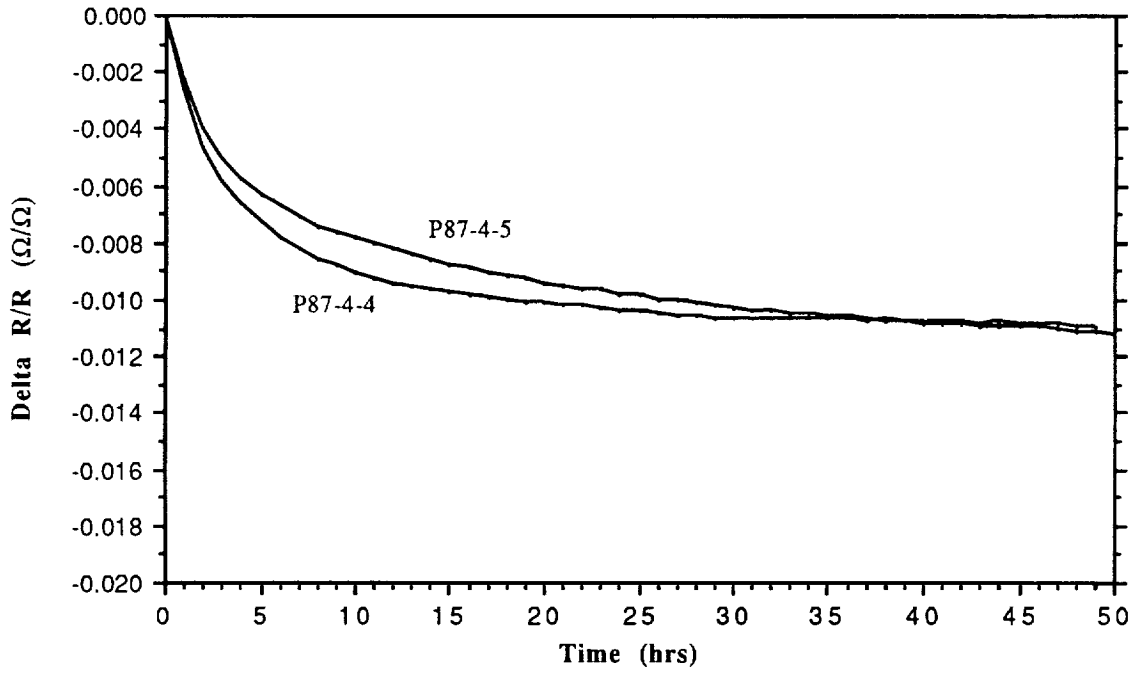

Figure 6.2.2 Electrical resistance drift at 1100 K after 1000 K/50 hrs
Task 5A samples with 870 K fillcoats & overcoats

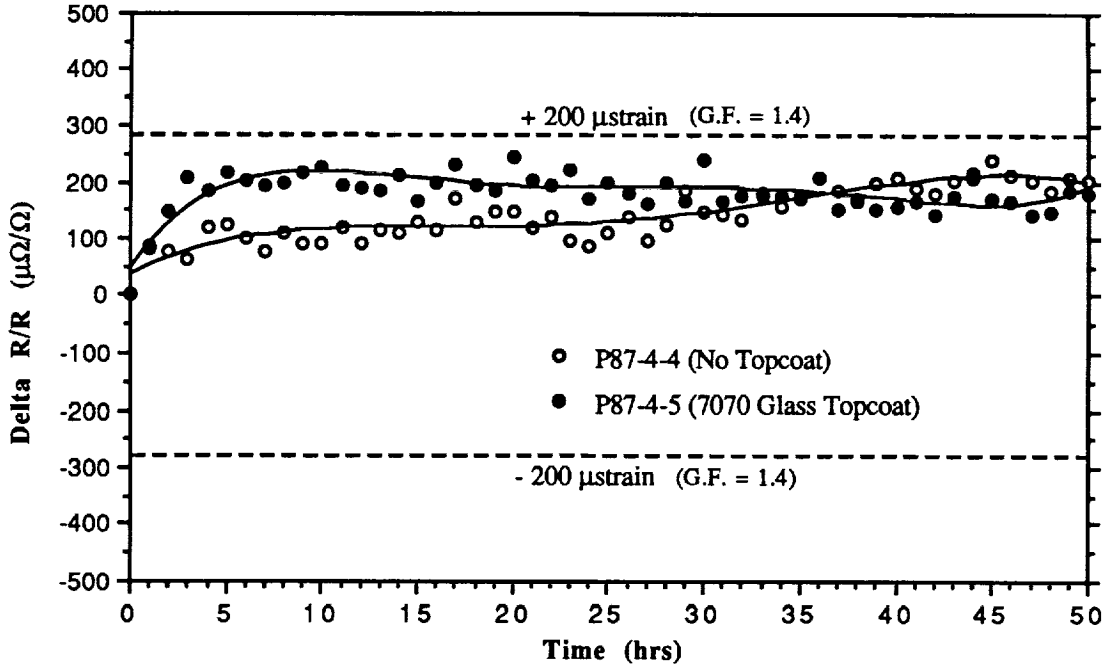

Figure 6.2.3 Electrical resistance drift at 1000 K
Task 5A samples with 870 K fillcoats &overcoats
(After 1100 K/50 hrs. & 1100K/50 hrs.)

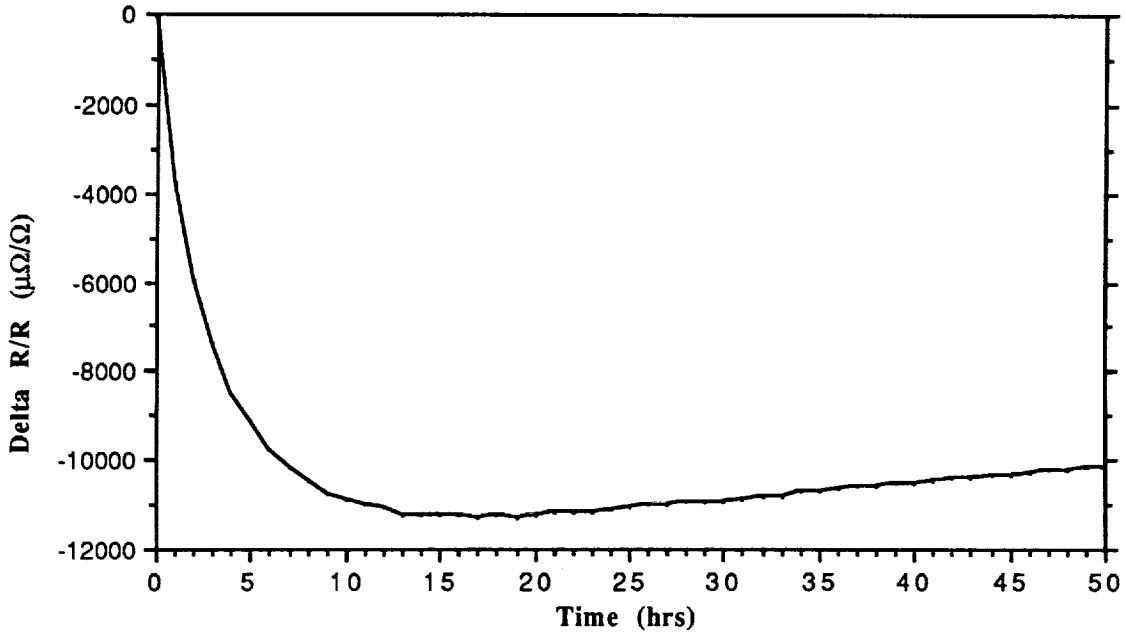

Figure 6.2.4 Electrical resistance drift at 1100 K
Sample P87-4-3

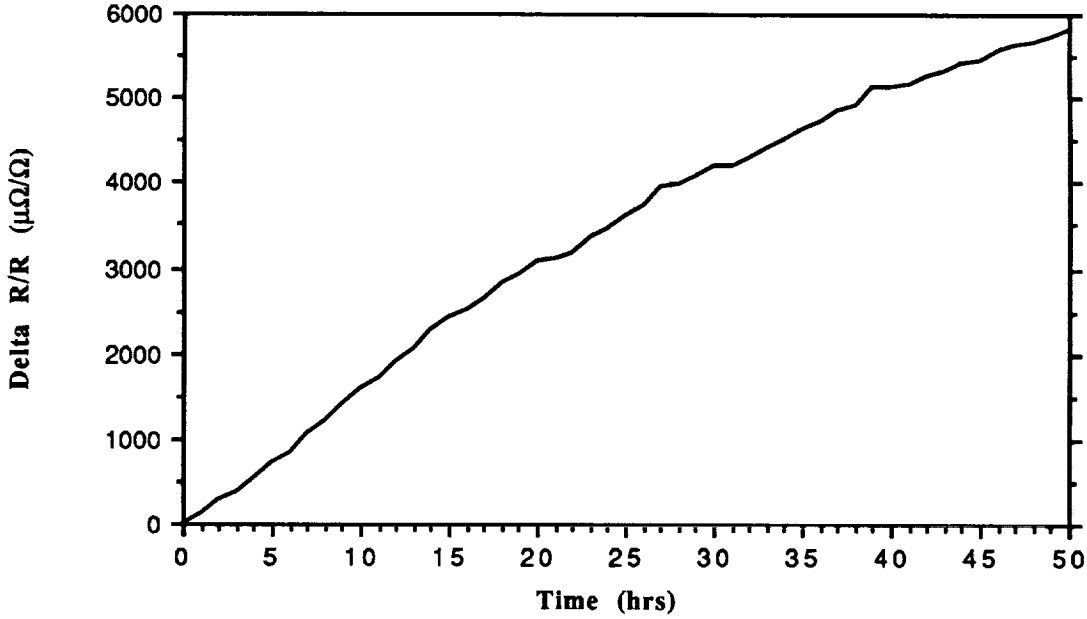

Figure 6.2.5 Electrical resistance drift at 1150 K
Sample P87-4-3
(After 1100 K/50 hrs)

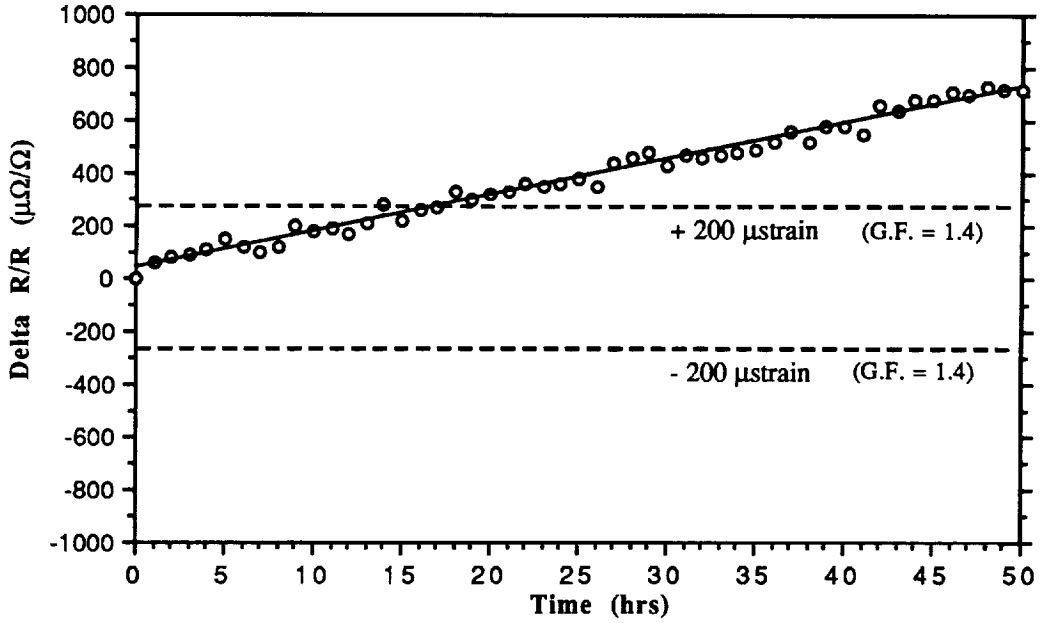

Figure 6.2.6 Electrical resistance drift at 1100 K
Sample P87-4-3
(After 1100 K/50 hrs. & 1150 K/50 hrs.)

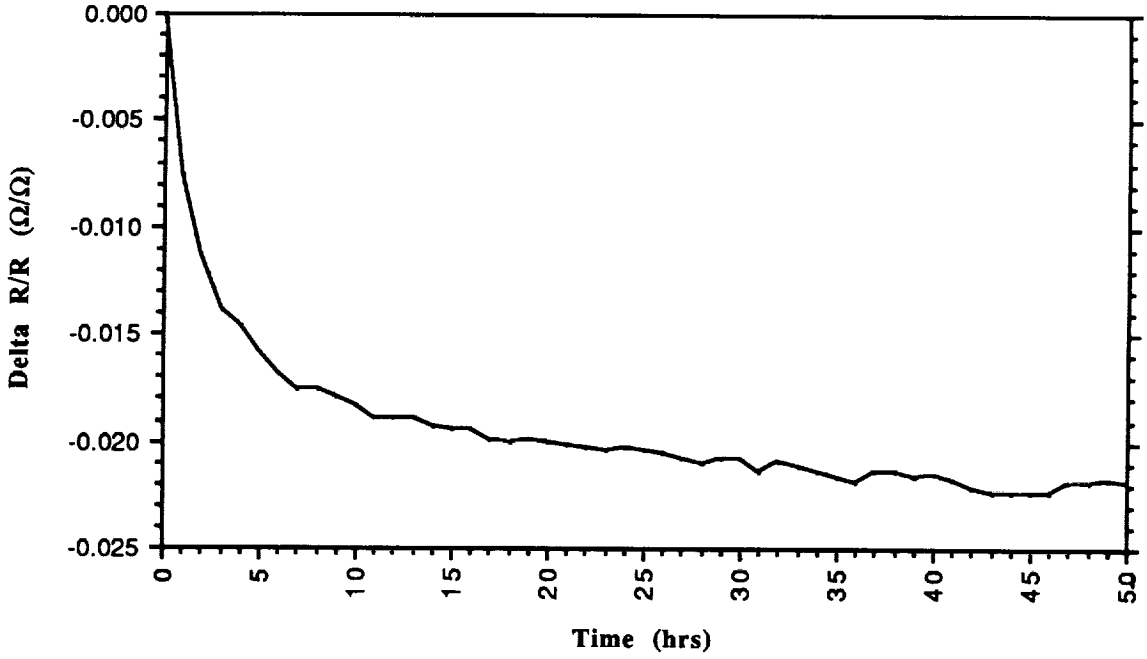

Figure 6.2.7 Electrical resistance drift at 1100 K Sample P87-6-2

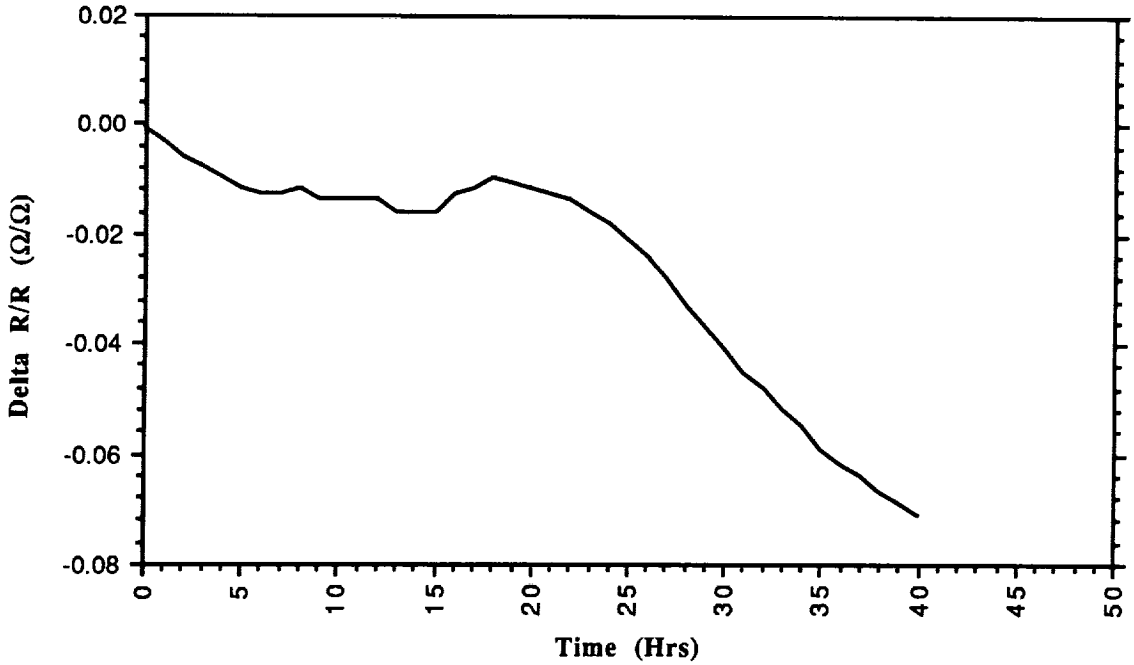

Figure 6.2.8 Electrical resistance drift at 1200 K after 1100 K/50 hrs. Sample P87-6-2

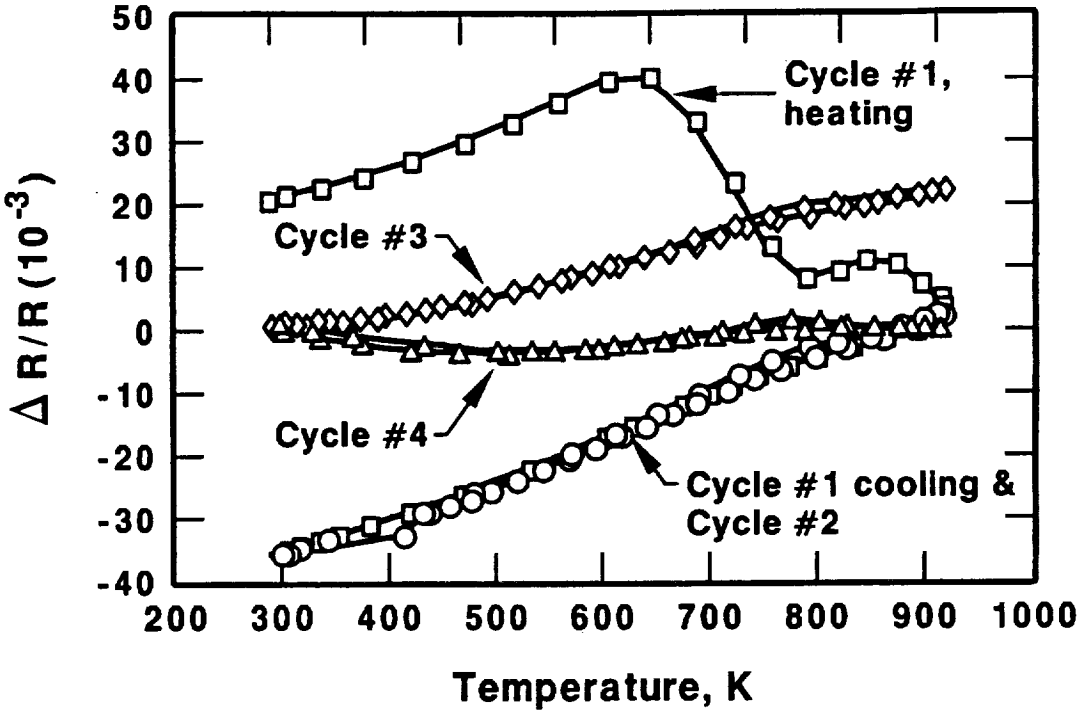

Figure 6.3.1 Effect of changes in external compensation on the strain gage resistance during first four thermal cycles, Gage 1, Bar B2.

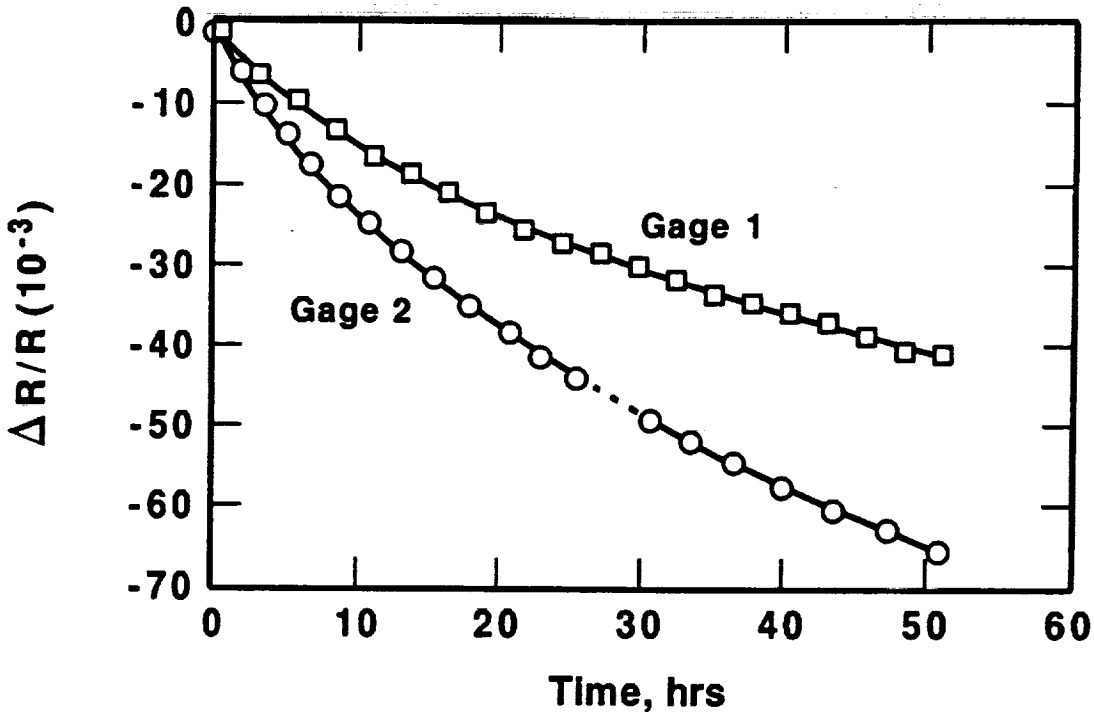

Figure 6.3.2 Decrease in resistance of strain gages on Bar B2 during 50 hour soak at 920 K

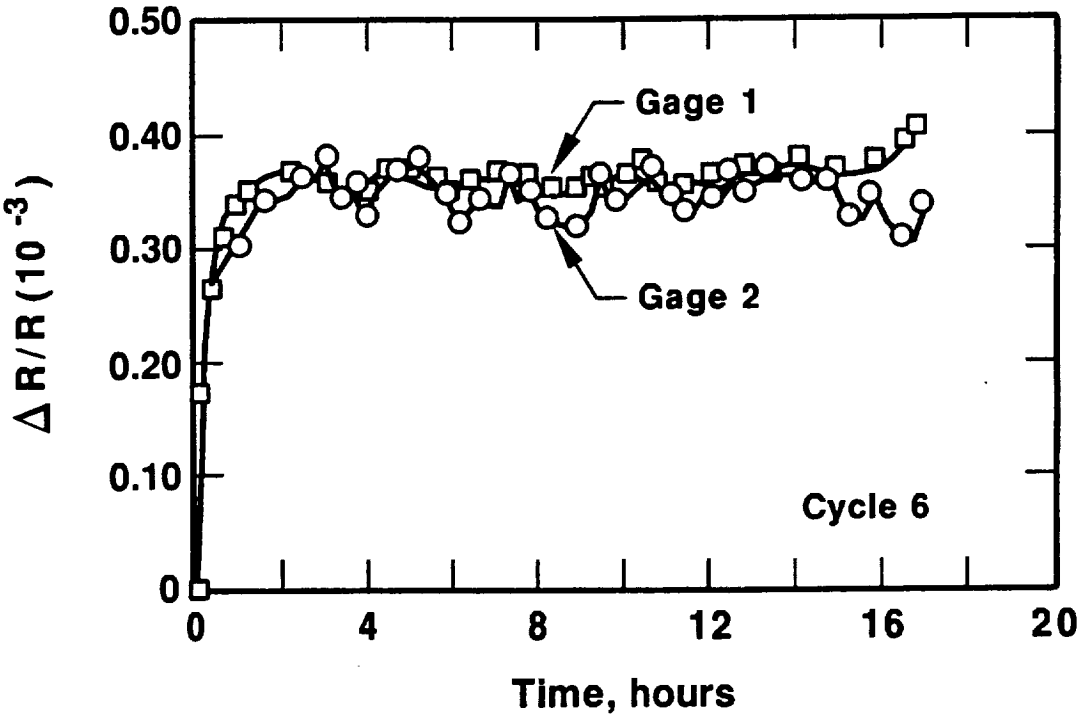

Figure 6.3.3 Drift of strain gages on Bar B2 during initial soak at 760 K

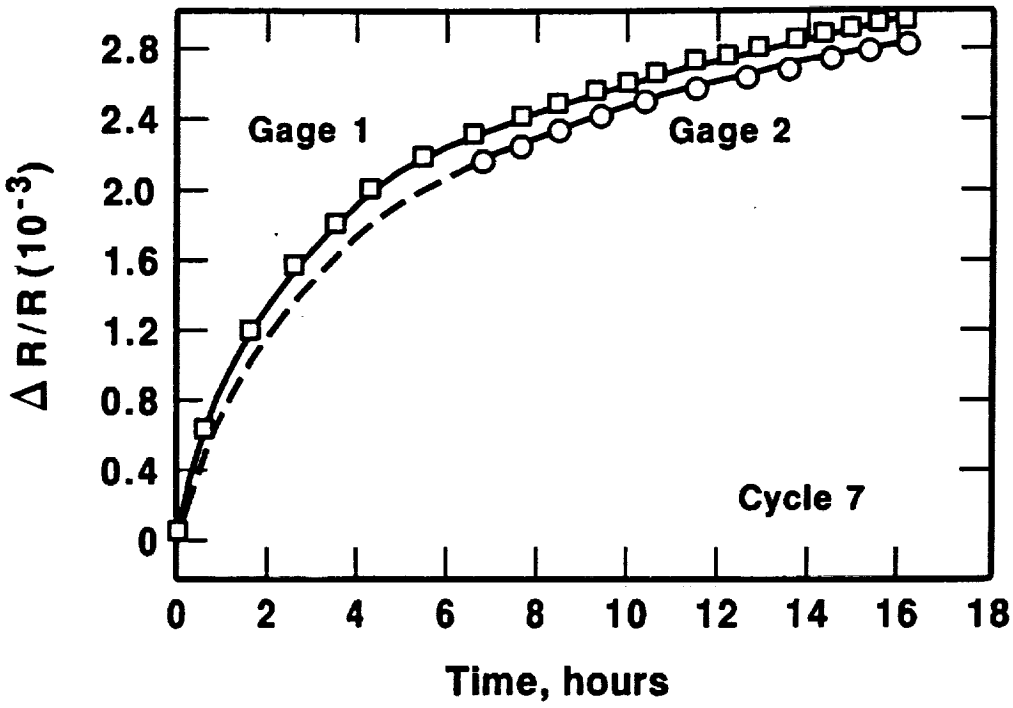

Figure 6.3.4 Drift of strain gages on Bar B2 during initial soaks at 700 K

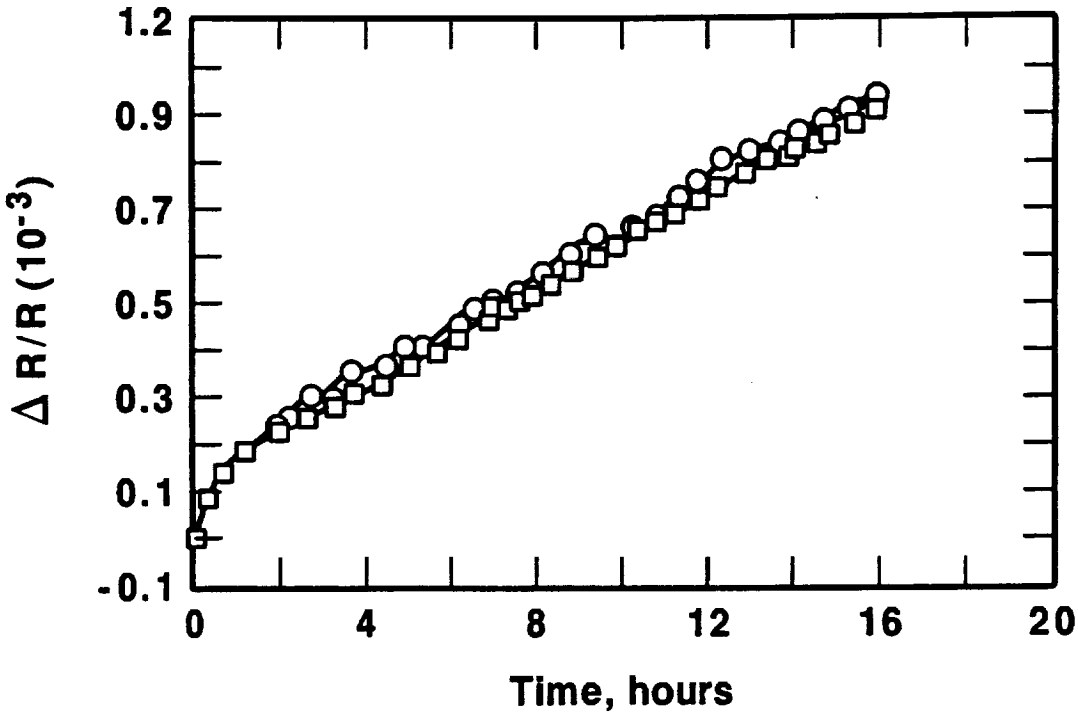

Figure 6.3.5 Drift of strain gages on Bar B2 during initial soaks at 650 K

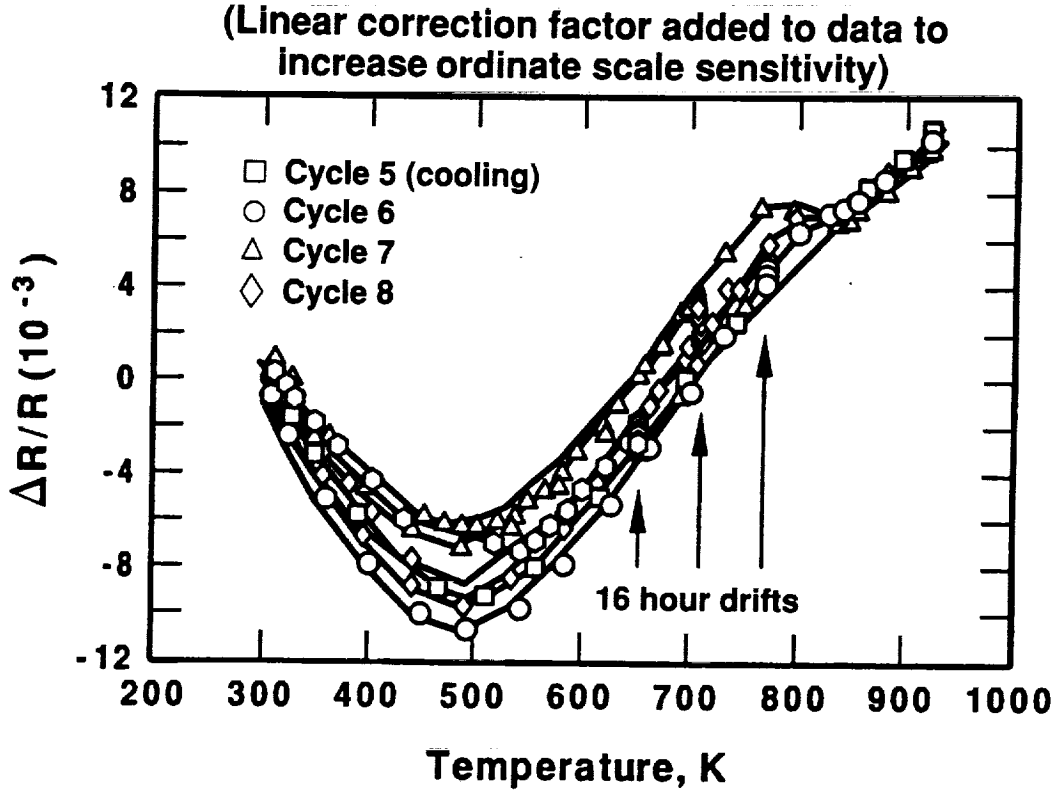

Figure 6.3.6 Changes in strain gage resistance vs temperature of Gage 1 on Bar B2 showing effects of drift soaks at 760, 700 and 650 K

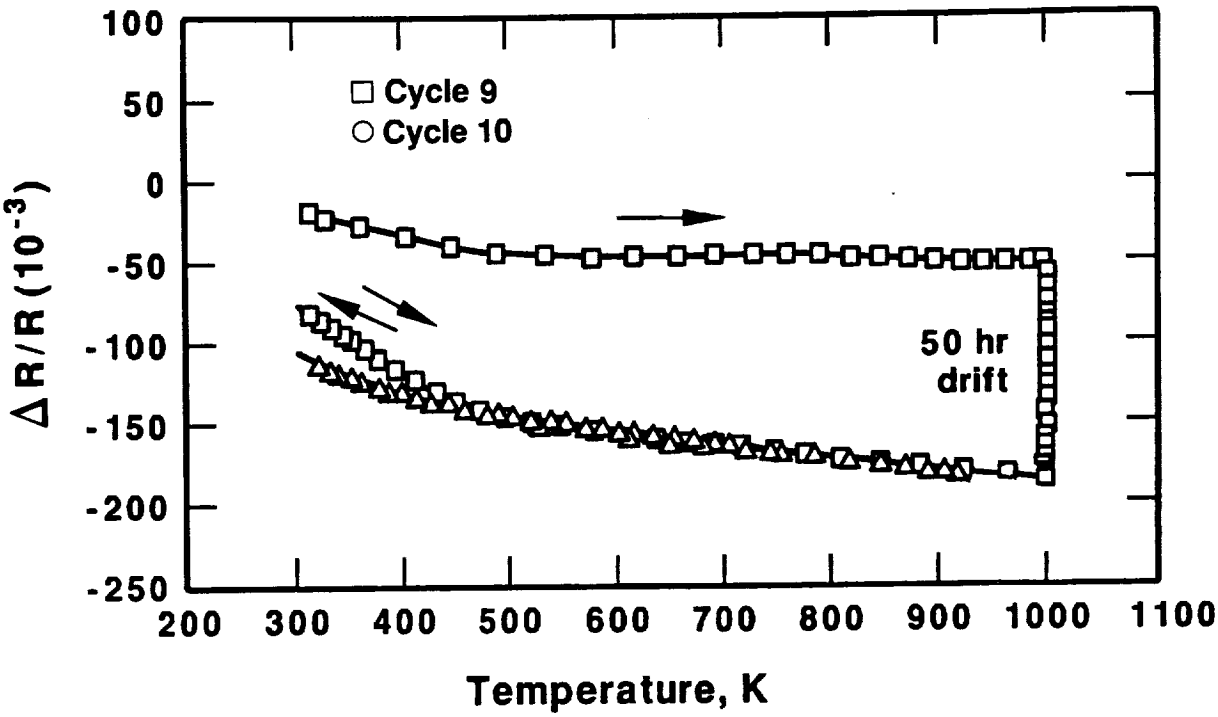

Figure 6.3.7 Effect of strain gage resistance of a 50 hour drift test at 1000 K followed by 16 hour drift test of Gage 1 on Bar B2 at 700 K

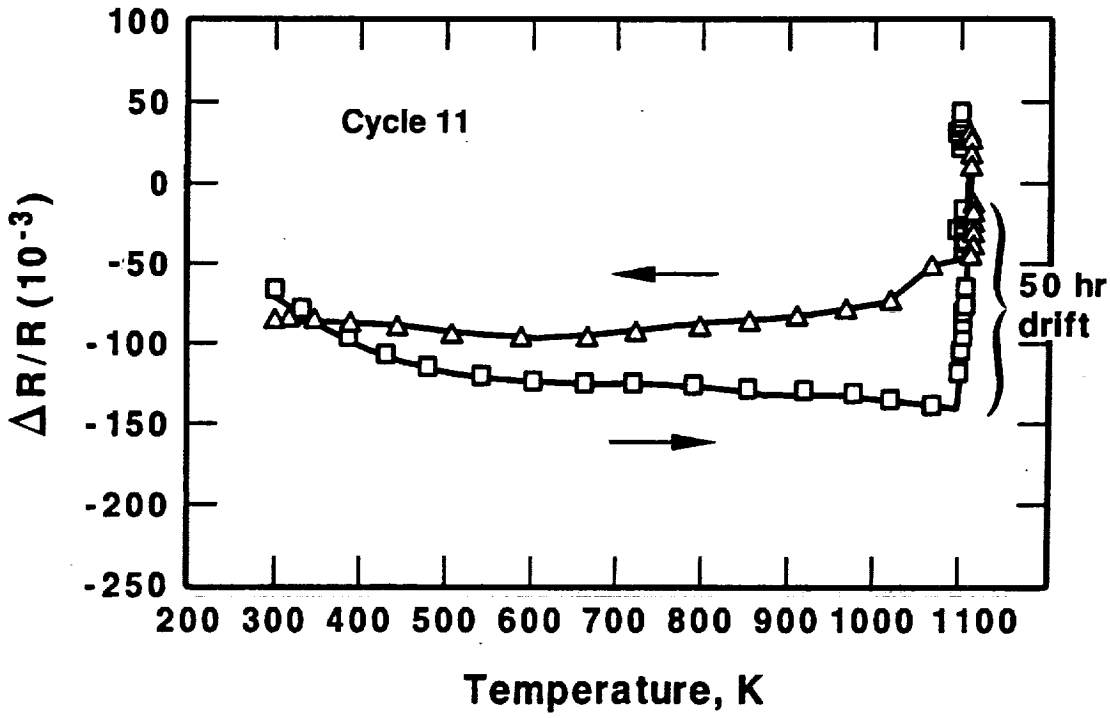

Figure 6.3.8 Effect of strain gage resistance of a 50 hour drift test of Gage 1 on Bar B2 at 1100 K

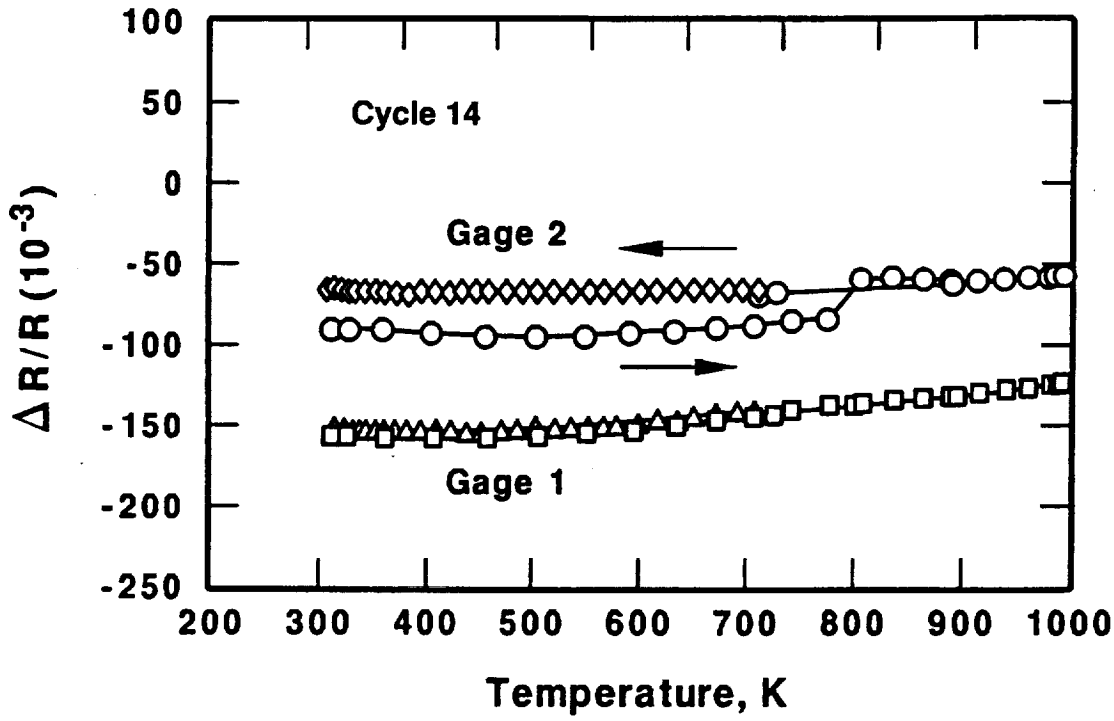

Figure 6.3.9 Effect on strain gage resistance of heating to 1000 K and a 16 hour drift test at 700 K during cooling of Bar B2

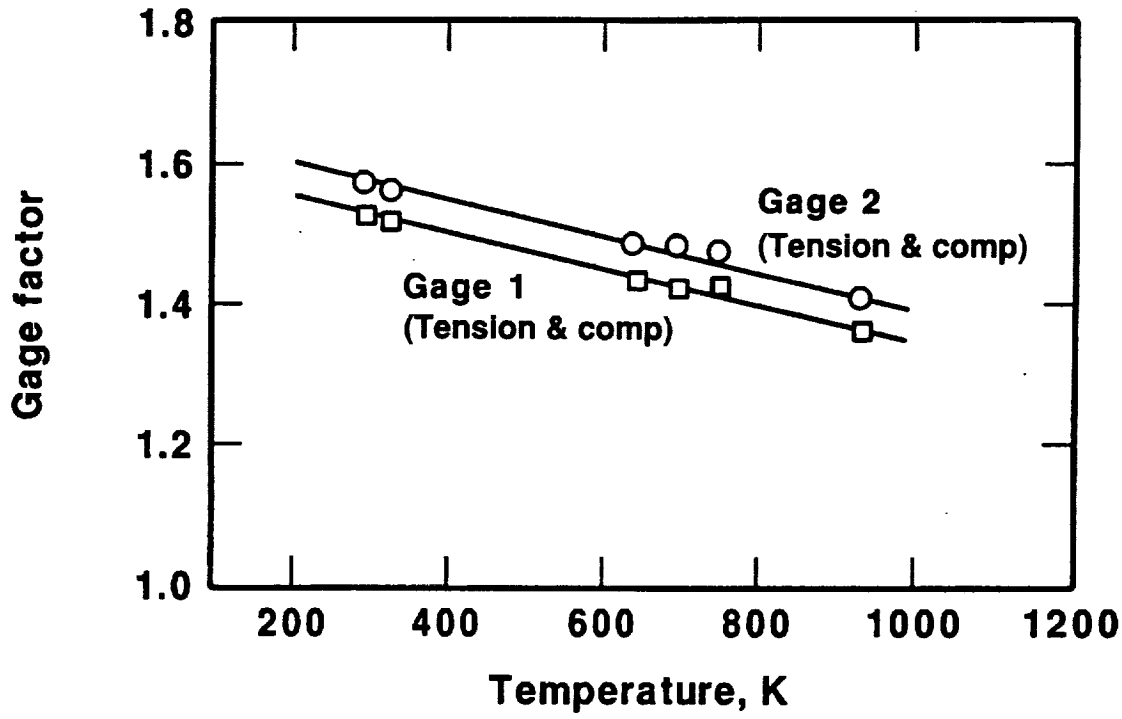

Figure 6.3.10 Gage factor vs temperature on Bar B2 after cycle 4, ±500 microstrain

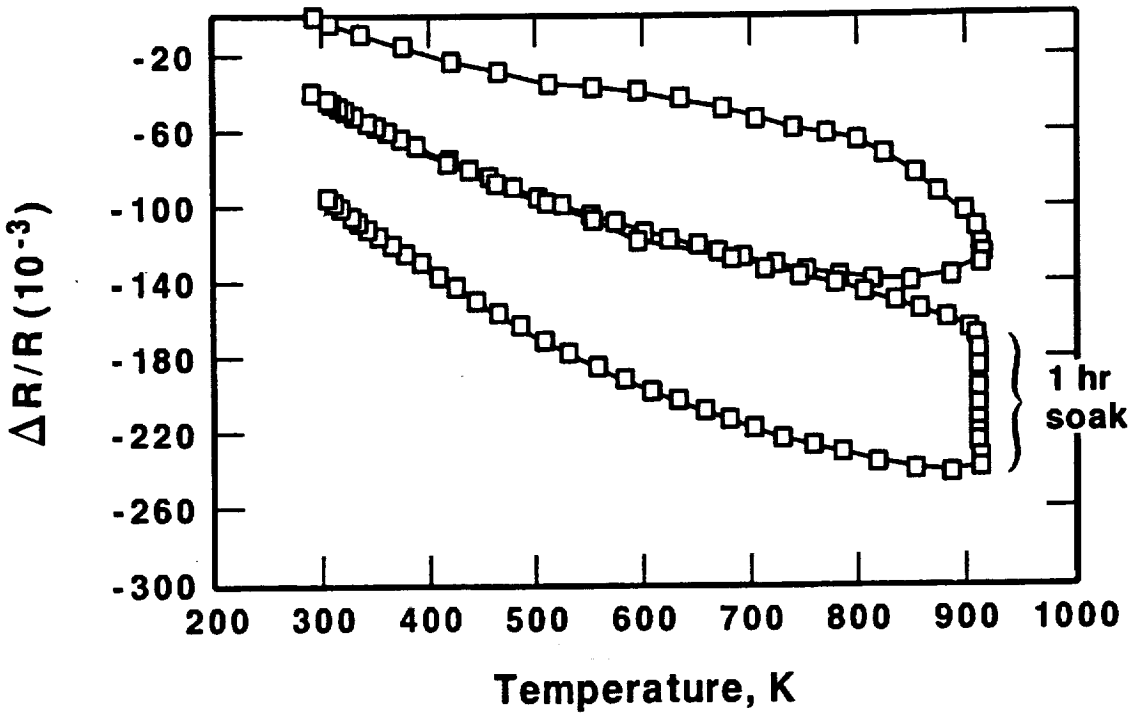

Figure 6.3.11 Change in strain gage resistance, first and second cycle, Gage 1, Bar B5

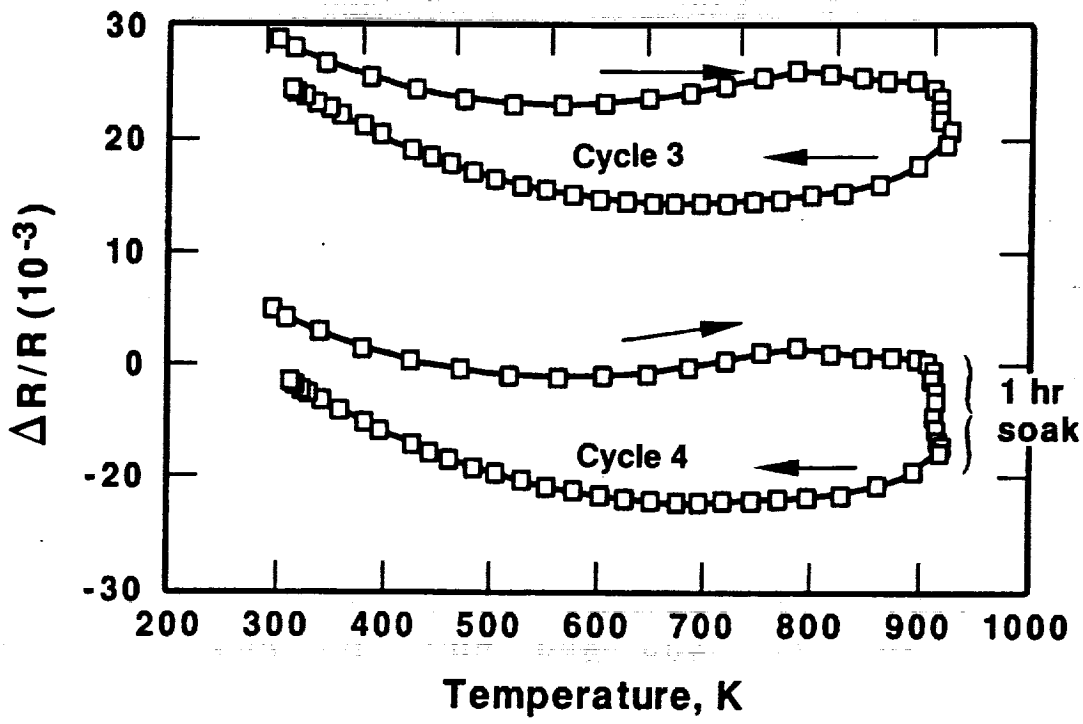

Figure 6.3.12 Change in strain gage resistance, third and fourth cycle, Gage 1, Bar B5

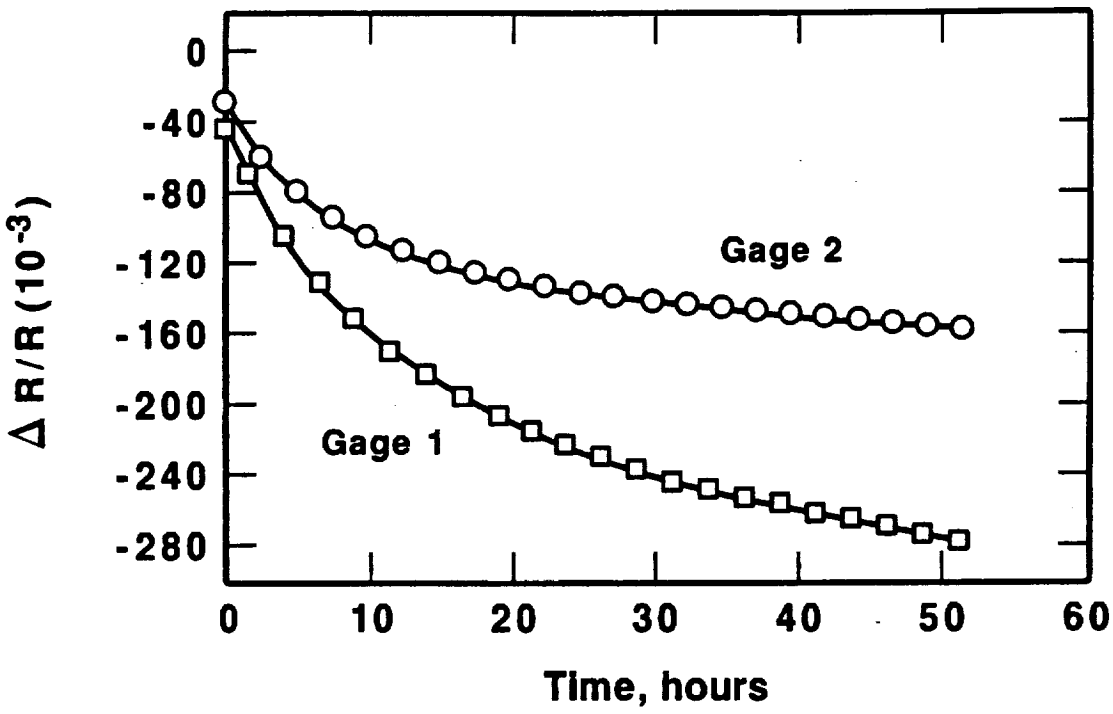

Figure 6.3.13 Decreases in strain gage resistance of gages on Bar B5 during 50 hour drift test at 920 K

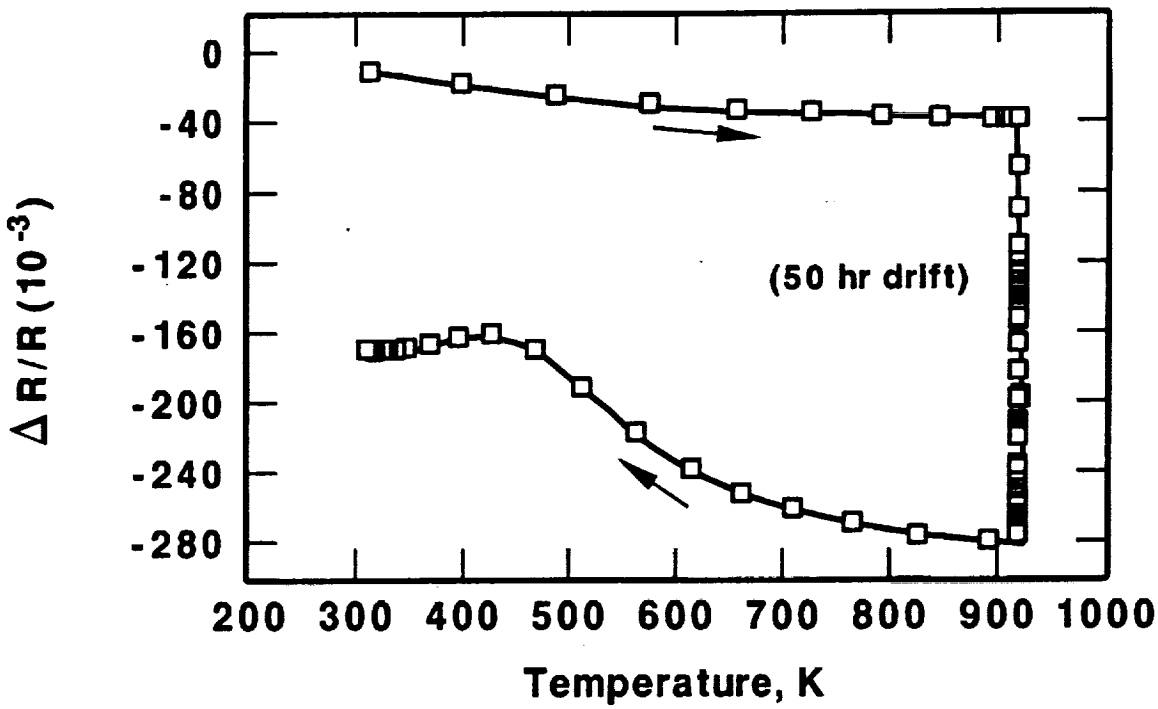

Figure 6.3.14 Changes in strain gage resistance during the fifth cycle with a 50 hour drift test at 920 K, Gage 1, Bar B5

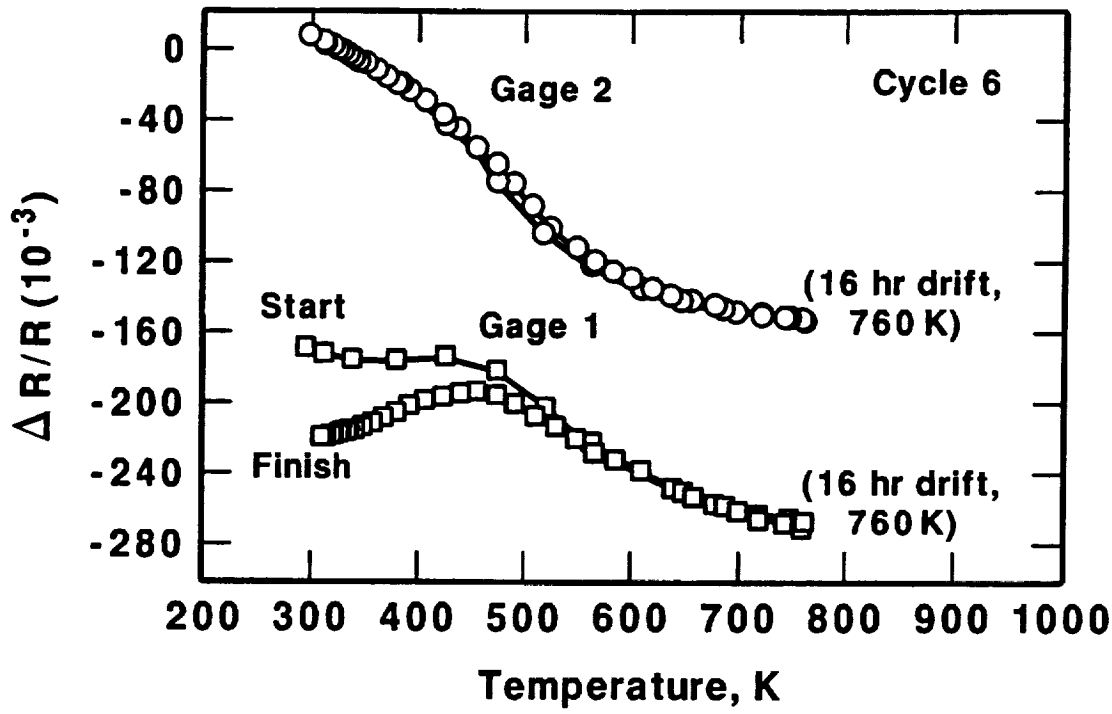

Figure 6.3.15 Changes in strain gage resistances with temperature and during 16 hour drift test at 760 K, Bar B5

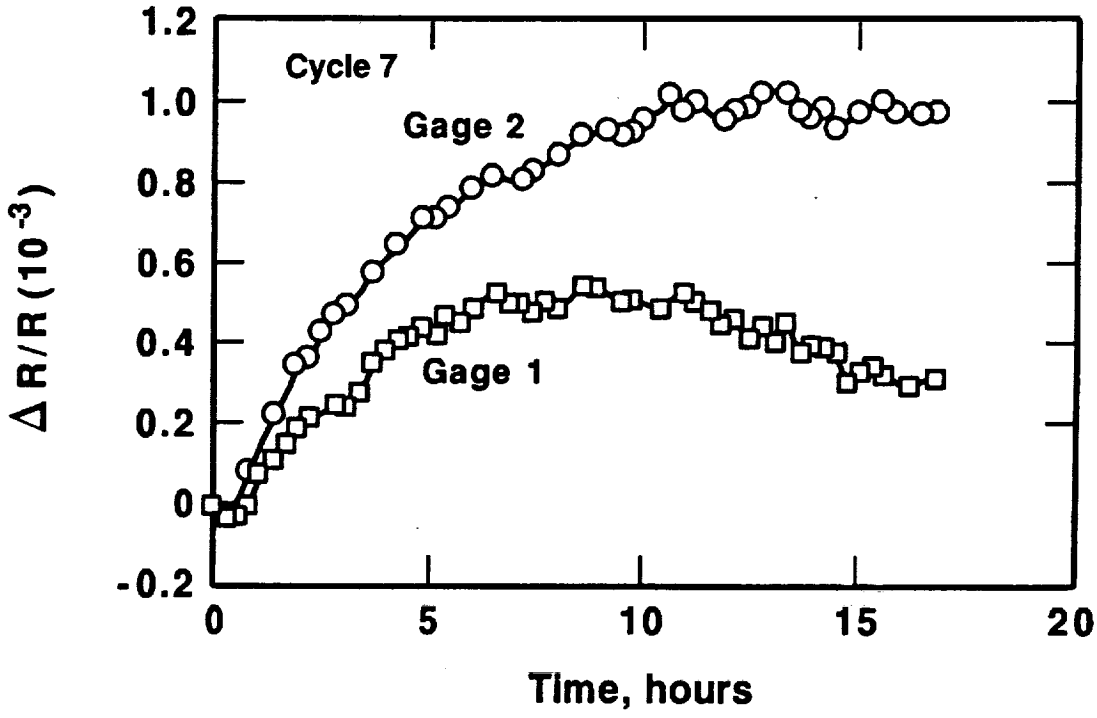

Figure 6.3.16 Changes in strain gage resistance during 17 hour drift test at 700 K, Bar B5

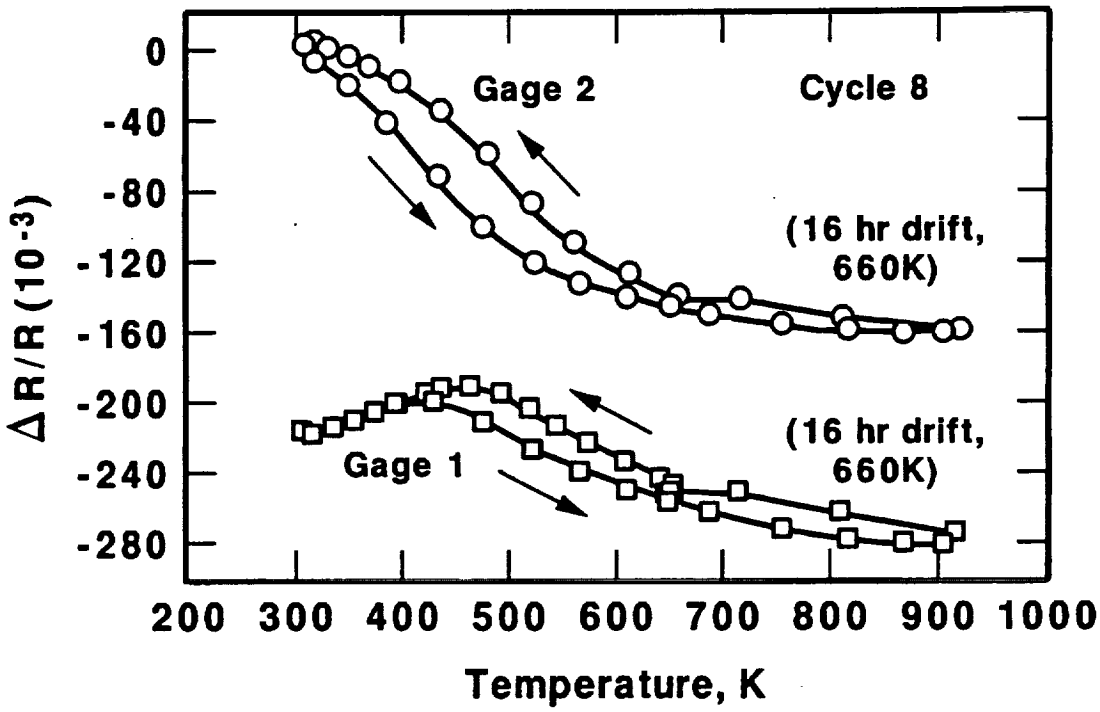

Figure 6.3.17 Changes in strain gage resistance with temperature to 920 K and during 16 hour drift test at 660 K, Bar B5

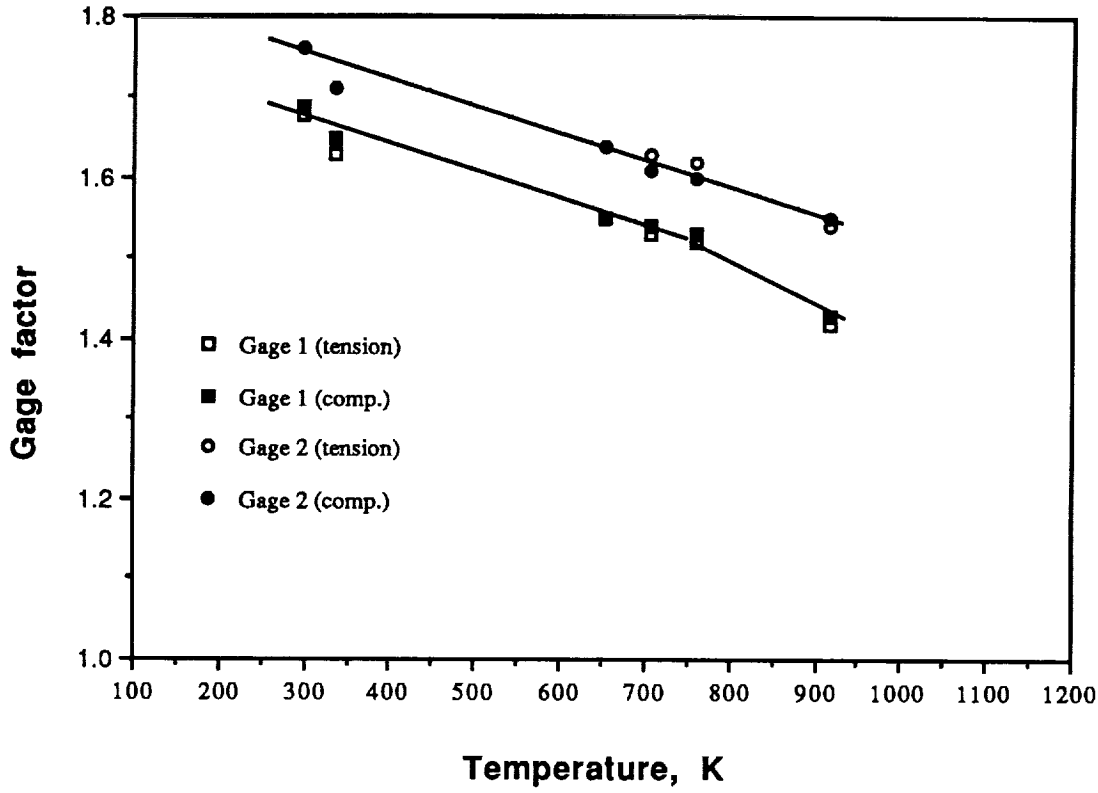

Figure 6.3.18 Gage factors vs temperature. Bar B5 ±500 microstrain, after cycle 4

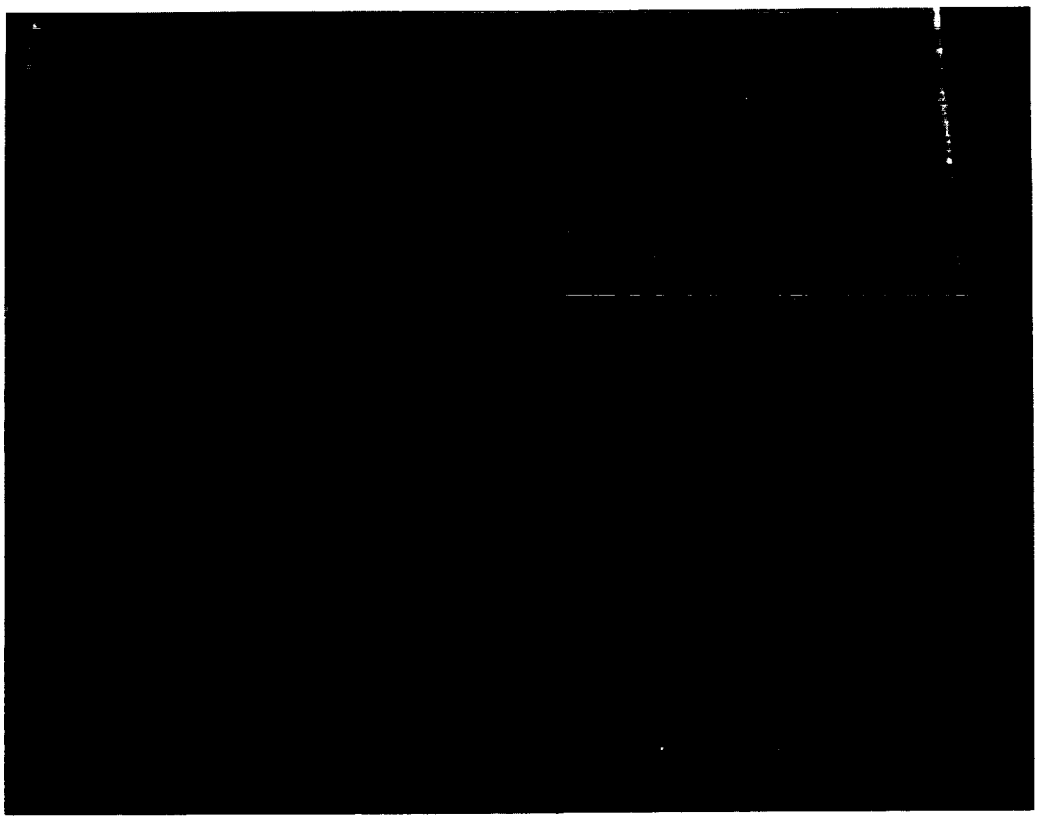

Figure 6.3.19 Gages on Bar B2 after testing

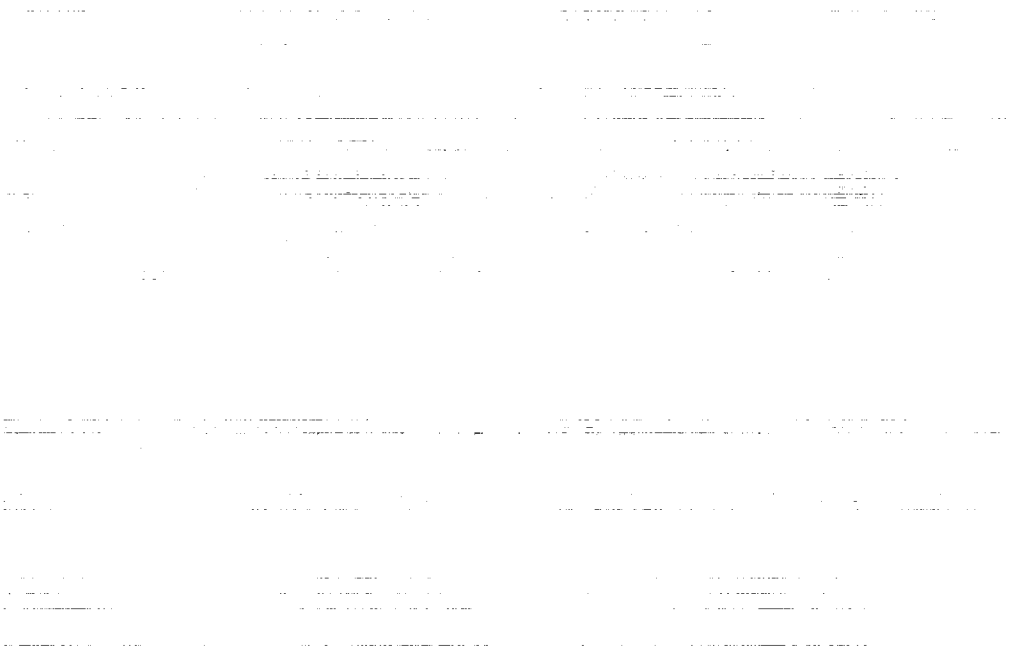

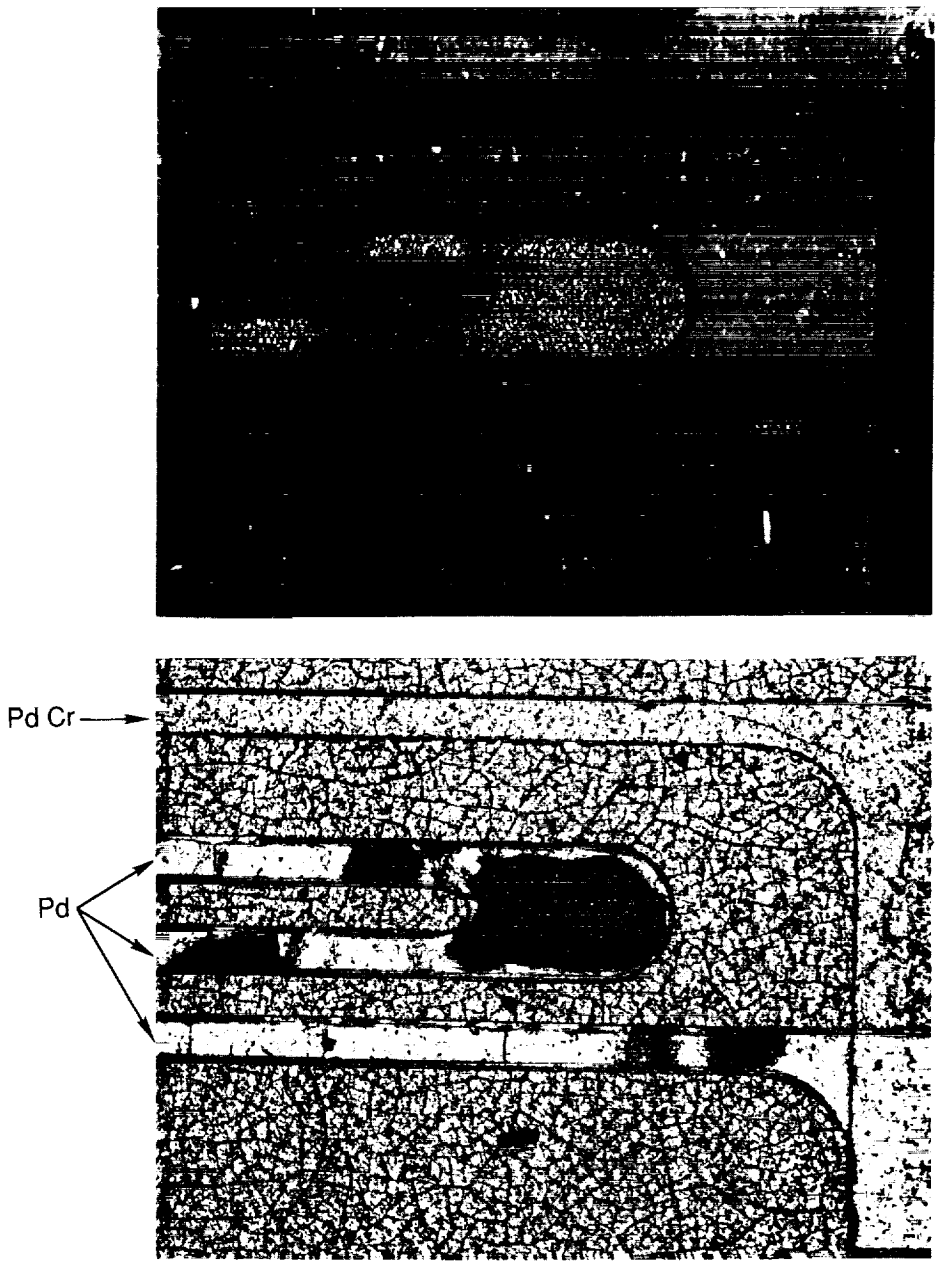

Figure 6.3.20 Grid lines on Bar B2 after testing showing lighting effects

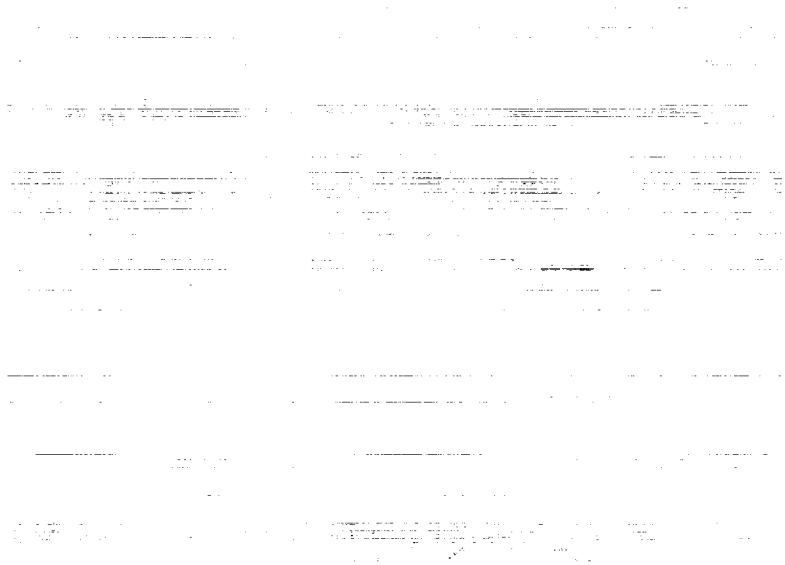

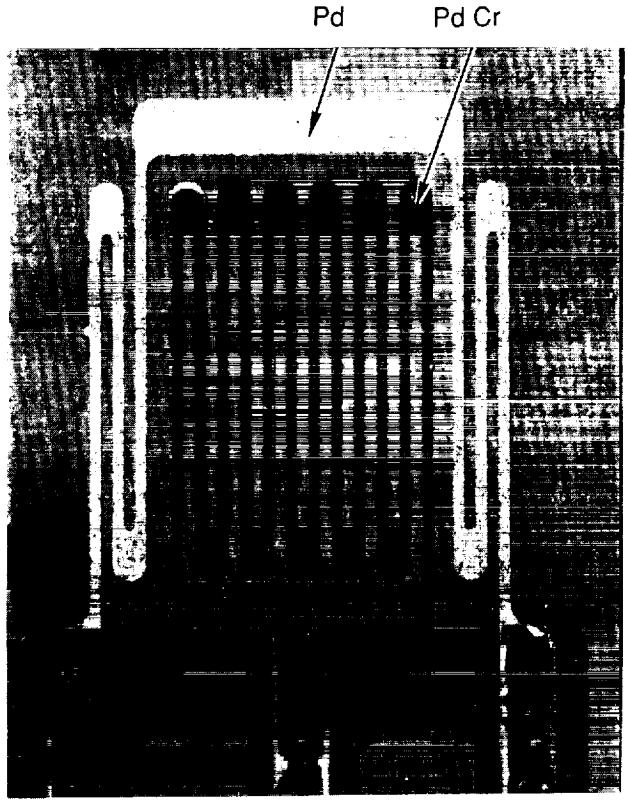

Figure 6.3.21 Gage on Bend Bar B5 after testing. Overcoat spalled from Pd (lighter grid)

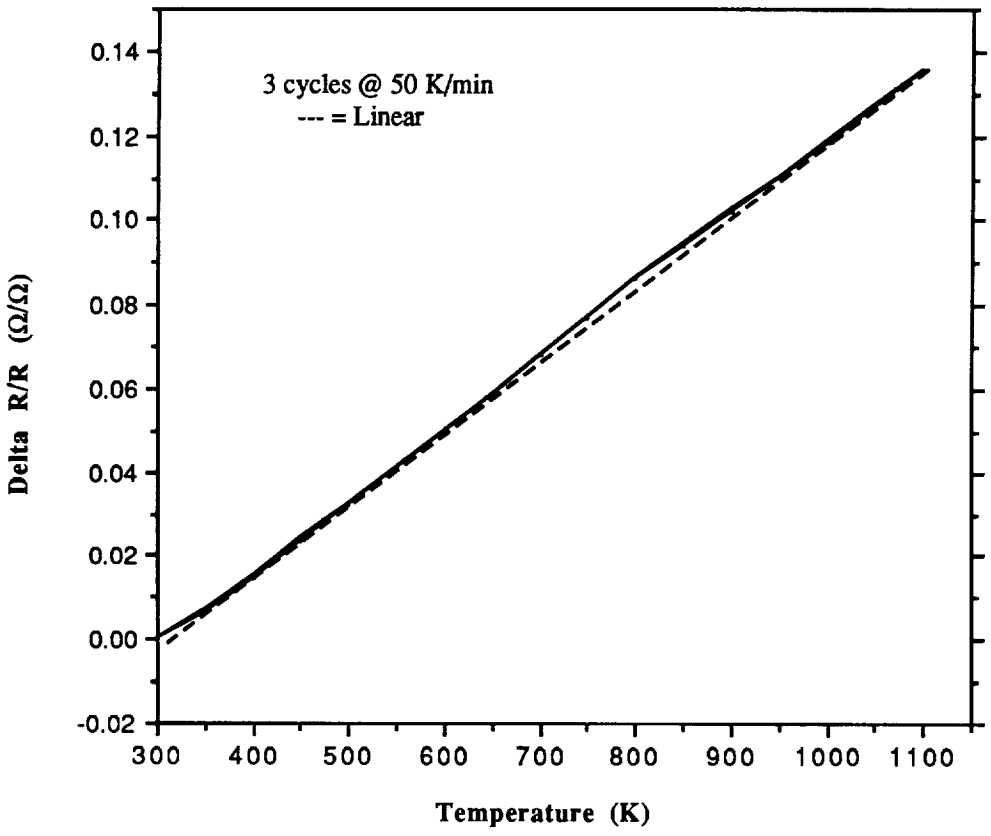

Figure 7.1.1 Change in resistance vs. temperature Sputtered Pd-13Cr

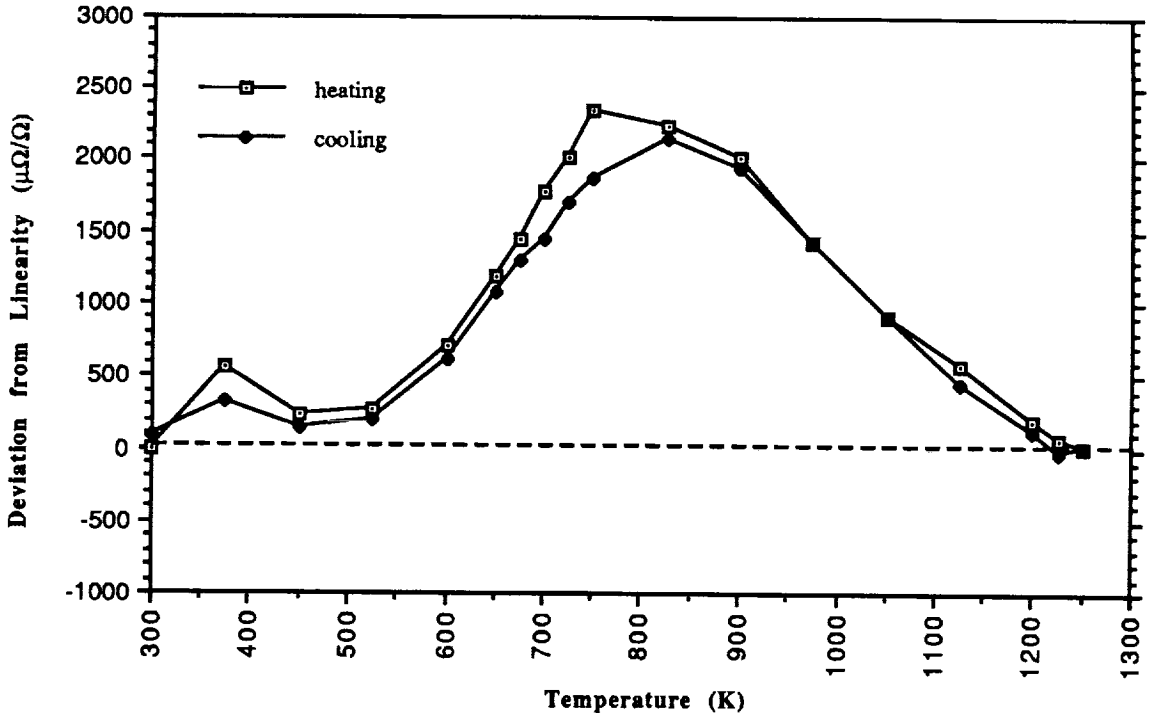

Figure 7.1.2 Deviation from linearity for drop-cast Pd-13Cr

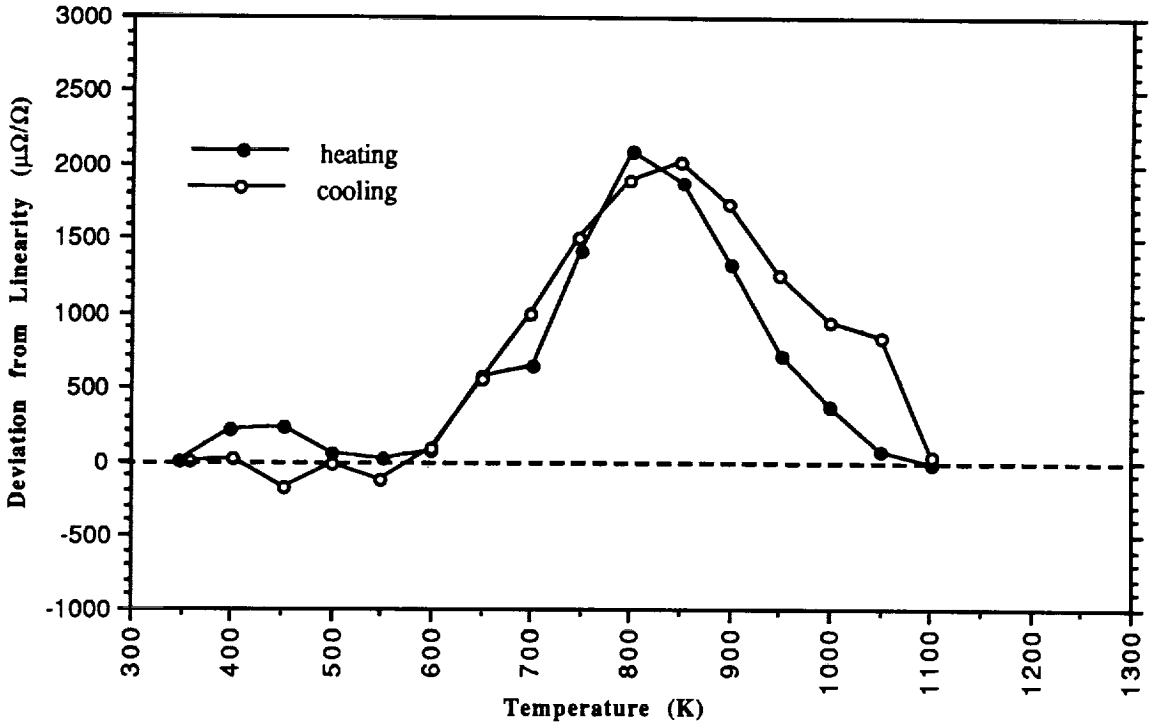

Figure 7.1.3 Deviation from Linearity for Sputtered Pd-13Cr

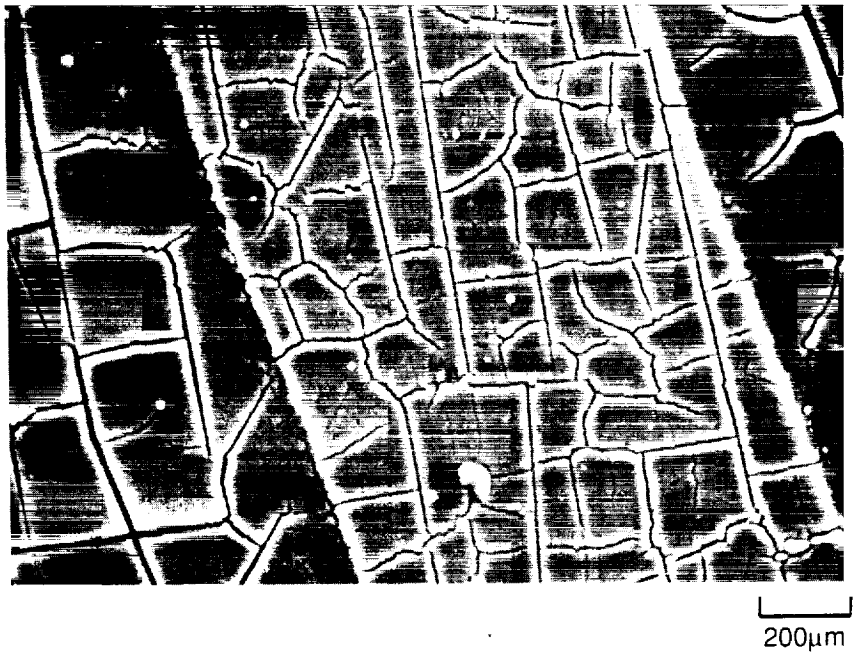

Figure 7.1.4 SEM micrograph of alumina overcoat after 30 min at 1140 K in argon

APPENDIX A

ADDITIONAL INFORMATION

TABLE A1
OVERALL GUIDELINES

The following performance and environmental guidelines, provided in Exhibit B of the Statement of Work, define the limits of the gage system study.

Access:	Individual blades or vanes will be removed from assemblies for gage installation.
Gage Geometry:	3 mm x 3 mm size for small airfoils of span <5 cm. 6 mm x 6 mm size OK for larger airfoils of span >10 cm. 0.2 mm thickness maximum for film or foil gages.
Leadfilm Route:	Shall not pass around leading or trailing edge of airfoil. Route leadfilms to underside of platform.
Leadfilm Width:	3 mm or less.
Temperature:	1250 K on hottest part of surface, 1000 K at root. Gas temperatures to 1600 K with fluctuations ±100 K.
Strain Range:	Below yield strength of blades and vanes (about 2000 microstrain at 1250 K and 3000 microstrain at 1000 K).
Accuracy:	±200 microstrain residual uncertainty after correction for determinable variation in gage factor, apparent strain, and zero indication versus temperature.
Pressure:	25 atm. (2.5 megapascal) (375 psi).
Flow:	Mach 0.3 typical approaching turbine inlet guide vanes. Mach 1.0 typical over airfoil surface. Maximum dynamic pressure estimated from the above is approximately 10 atm. (1 megapascal) (150 psi).
Gas Composition:	Products of combustion of jet engine fuel and air, plus dilution air.
Blade and Vane Material:	Nickel and cobalt based superalloys.
Sensor Life:	10 to 50 hours, with up to 20 thermal cycles.
Strain Gage System Components:	Insulating substrate, strain element including temperature compensating element, lead film or sensor lead wire and its connection to strain element and to trunk leads, and overcoats.
Attachment:	Cementing to blade or vane not encouraged. Sputter deposition, flame spray, plasma spray acceptable.

TABLE A2
QUANTITIES TO BE MEASURED, WITH TYPICAL EXPECTED VALUES AND ACCURACY GOALS

	Typical Expected Value	Maximum Acceptable Uncertainty
MEASURED QUANTITIES		
Gage Initial Resistance at room temp.	60 ohms	0.2 ohms
Date of Test Data (month, day, year)		
Time of Test Data, HR:MIN	14:23	:01
Temperature	930 K	1%
Bridge Excitation (+ Mode)	5.000 volts	0.012 volts
Bridge Output (+ Mode)	20 mV	0.02 mV
Bridge Excitation (- Mode)	-5.000 volts	0.012 volts
Bridge Output (- Mode)	-20 mV	0.02 mV
Ohmmeter Voltage EV (+ Mode)	.50 volts	0.01 volts
Ohmmeter Voltage EV (- Mode)	-.50 volts	0.01 volts
Ohmmeter Voltage EI (+ Mode)	.50 uv	0.01 μv
Ohmmeter Voltage Ei (- Mode)	-.50 uv	0.01 μv
Deflection of Test Bar	3.00 mm	30 μm
Strain (Reference Gage)	1000 μstrain	10 μstrain
CALCULATED RESISTANCE TO GROUND		
At 300 K	10^{+7} ohms	$9x10^{+6}$ ohms
At 1250 K	10^{+6} ohms	$.5x10^{+6}$ ohms
With Insulation Leakage	10^{+5} ohms	10^{+4} ohms
	10^{+4} ohms	10^{+2} ohms
	10^{+3} ohms	1 ohms
	10^{+2} ohms	10^{-2} ohms

TEST AND CALCULATION PROCEDURES

Gage Factor Testing Procedure

All testing will be in air at one atmosphere pressure. The gage factor testing procedure is as follows: For each strain level and temperature, the bar is deflected (strained) twice in each direction (tension and compression) in a 0 + 0 - 0 + 0 - 0 sequence. For each strain gage, an average gage factor is calculated for each direction, strain level, and temperature based on four measurements (from the deflection sequence). The standard deviation is also calculated for the four measurements.

Information to be recorded at each test point and calculations to be performed at each test point are described in the section "Determining Gage Factor at Room Temperature" and "Determining Gage Factor at Elevated Temperature."

Apparent Strain and Drift Testing Procedure

All testing will be in air at one atmosphere pressure. The change in gage resistance with temperature will be measured during heat-up from room temperature to test temperature and cool-down from test temperature to near room temperature. Heat-up time and cool-down time will be about one hour. In addition the drift in resistance in 50 hours at test temperature will be measured and drift in resistance in 16 hours at each of three lower temperatures will be measured.

Information to be recorded at each test point and calculations to be performed at each test point are described in the section "Determining Apparent Strain and No Load Drift at Temperature."

Adjusting Temperature Compensation

To adjust the temperature compensation refer to Fig. B2 and use the following procedure. A & B are 10-turn potentiometers.

1. First measure the strain element resistance R with a low-current ohmmeter (.01 amp or less). Select C (ohms) and set A (ohms) and B (ohms) so that A+F=B=C=R within about 5%.

2. At room temperature adjust B further for bridge balance, i.e., output voltage e corresponding to less than 50 microstrain indicated.

3. At high temperature observe that there is a large bridge unbalance voltage e. Remove this unbalance, while still at high temperature, as follows:

   Adjust A and B in the same direction by equal amounts until the unbalance is again less than 50 microstrain indicated. The direction will be such that A increases the unbalance and B decreases it.

4. Repeat 2 and 3 until no further adjustment is needed. No iteration will be needed if the four bridge arms were initially nearly equal at room temperature (step 1).

An example of initial and final settings of A and B is given below. The quantities f and r are the changes in resistance due to temperature in the composition arm and strain element arm of the bridge, respectively.

The example is for C=R=100 ohms, E=1 volt. EC and ER are the voltages across the bridge arms containing resistor C and R (gage) respectively. (e=EC-ER)

	B ohms	A+F ohms	f ohms	r ohms	EC volts	ER volts	e volts	Change in e Due to Temp	Approx. Apparent Strain (με) for G=2
Before Adjustments									
Room Temp	100	100	0	0	.5	.5	0	0	0
High Temp	100	100	19	20	.5	.5021	.0021	.0021	4200
After Adjustments									
Room	95	95	0	0	.5128	.5128	0	0	0
High Temp	95	95	19	20	.5128	.5128	0	0	0

Measuring Temperature

Gage temperature will be measured using ungrounded Type K thermocouples cemented to the substrate, with thin cement for good thermal contact with the substrate but electrical isolation from the substrate.

The temperature must be recorded to the nearest tenth of a Kelvin unit (±0.1 K), even though the uncertainty due to calibration bias may be several units. This requirement arises because the tcr of the compensated gage may be about 30×10^{-6}/K, effective gage factor about 1.5, and it is desired to construct a lookup table for apparent strain change due to temperature change with resolution of about 2 με. The temperature resolution requirement is then about (2)(1.5)/(30) = 0.1 K.

Measuring Time

Time of day will be recorded at each test point to the nearest minute. Year, month, day will be recorded for each run. Note that if the temperature is constant within 1 K in 5 minutes, then an uncertainty in time of 1 minute translates to an uncertainty in temperature of 0.2 K, which in turn implies an acceptably small uncertainty of about 4 microstrain from this source.

The Bridge Equation

The bridge equation for a dual-element self-compensating strain gage bridge has been examined both in the present NASA program and in a concurrent NASA program, NASA/P&W Contract NAS3-25410. Common nomenclature has been adopted for the two programs. The analysis is presented in the Appendix B . The result is:

$$e' = K\,[U^*x + L^* + V^* + c'] \qquad (12)$$

Where e' is the ratio of bridge output voltage e to bridge excitation voltage E, K is bridge sensitivity factor, U* is gage factor, x is strain, L* and V* are functions of temperature and c' is the fractional change in calibration arm resistance C when the shunt calibration is actuated. (c' = 0 except when the shunt calibration procedure is being used.)

The quantities L* and V* need further comment. L* is the apparent residual fractional change (dimensionless) in gage arm resistance due to temperature after compensation. V* is the error term due to thermocouple emf's in the bridge. Both are functions of temperature. The quantity V* is unique in that its algebraic sign is independent of polarity of bridge excitation voltage. Therefore V* may be measured (and eliminated in calculations) by measuring bridge output with positive excitation (e+) and again with negative excitation (e-). KV* is half the difference between e+ and e-.

Procedures for various measurement subroutines are presented in Section 5.5; all are based on Eqn. (12).

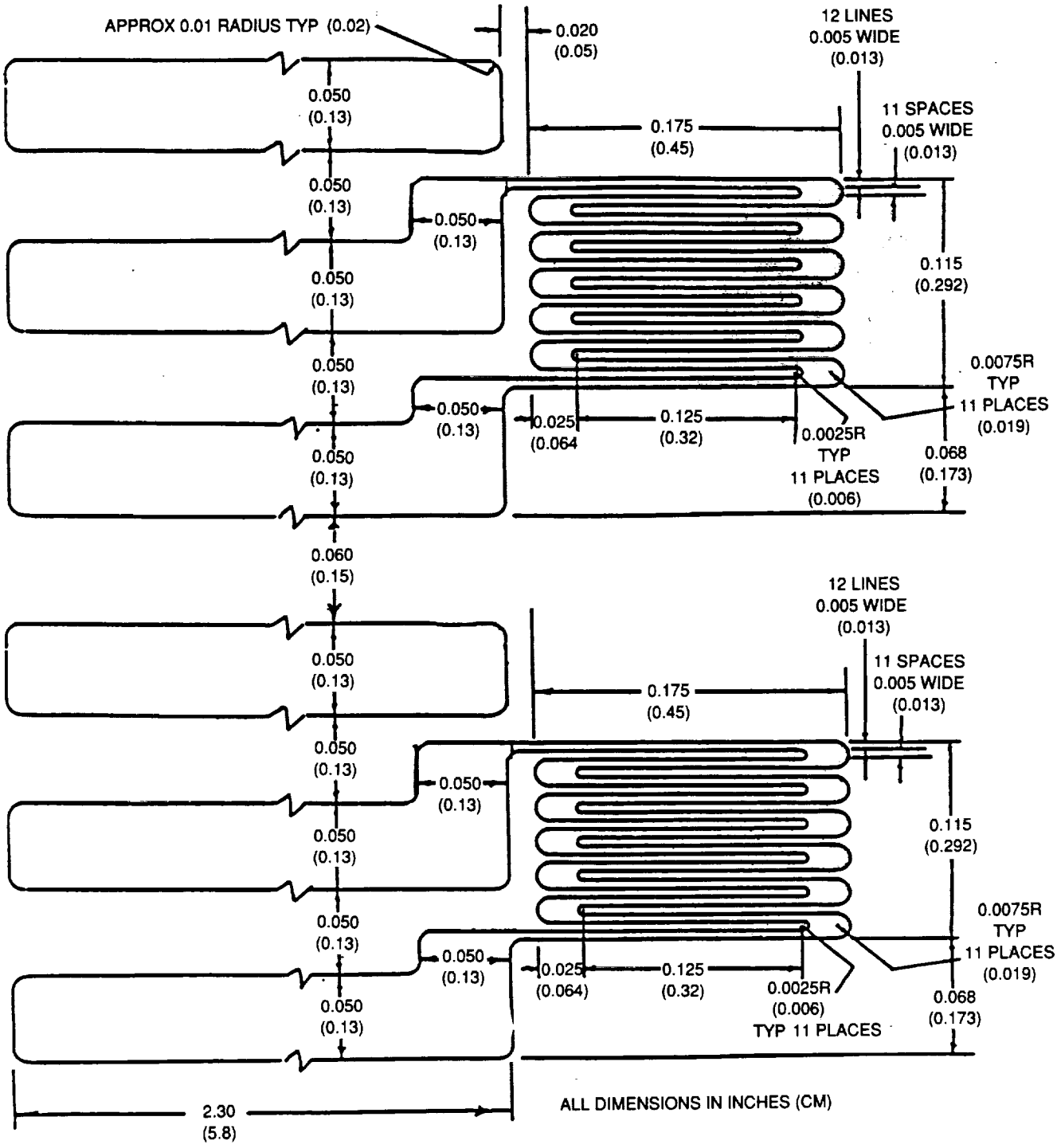

Figure A.1 Mask for two strain gages

91-9-45-4

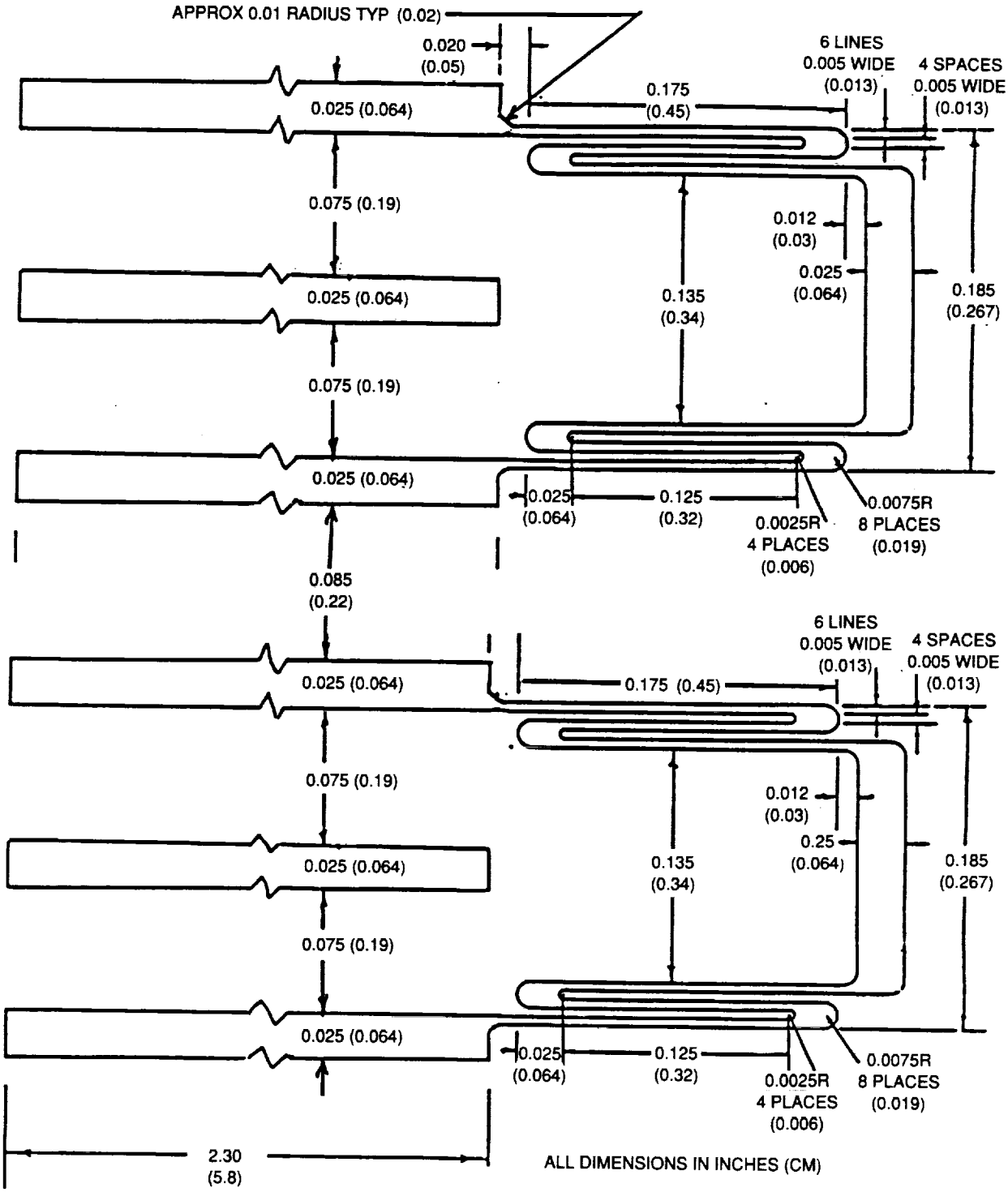

Figure A.2 Mask for two compensation elements

91-9-45-3

TABLE A3
PROPERTIES OF MAR M200 + HF

PWA Designation	PWA 1422
Common Designation	MAR-M-200 + Hf
Approximate Composition	59Ni, 12W, 10Co, 9Cr, 5Al, 2Hf, 2Ti, 1Cb
Max. Rec. Service Temp.	1310 K
Max. Heat Treat Temp.	1477 K
Modulus of Elasticity (E)	
1250 K	80000 MPa
TCE at 1250 K	15.5×10^{-6} K^{-1}
Approximate Elastic Strain Limit	
1250 K	5000×10^{-6}
300 K	6000×10^{-6}
Remarks	Requires corrosion protection such as NiCoCrAlY coating. Properties given are for longitudinal axis of directionally solidified material.

TABLE A4
PROPERTIES OF SOME MATERIALS USED IN STRAIN GAGE SYSTEMS

Material	Composition Wt %	TC EMF Rel. to Pt (μV/K)	M.P. (K)	Temp. Coef. of Lin.Exp. (ppm/K)	Temp. Coef. of Resistance (ppm/K)	Resistivity (ohm-cm) (x10-6)	Product (Res x TCR) (ohm-cm K-1) (x10-6)	Gage Factor	Ratio TCR/GF (x10-6)	Lead Wire Resistance for 1 meter .25 mm wire
Palladium	Pd	-15	1827	12	3800	10.8	.041	6.6	576	2.2
Nickel	Ni	-12	1808	13	4800	10.0	.048	2.0	2400	2.0
Alumel	Ni-2Al-3Mn-1Si	-9	1673		1900	29.0	.055	2.0	950	5.8
Platinum	Pt	0	2046	10	3000	10.6	.032	4.8	625	2.1
Gold	Au	+8	1336	14	3400	2.4	.008	2.0	1700	.48
Aluminum	Al	+9	933	24	4000	2.7	.011			
Pd-13Cr	Pd-13Cr	+19*			170	100.0	.017	1.8	94	20.0
Pt-10Rh	Pt-10Rh	+10	2100		1700	18.0	.031	2.0	850	3.6
Pt-10Ni	Pt-10Ni	+15	1920		1400	30.0	.042	2.0	700	6.0
Copper	Cu	+18	1356	16	3900	1.7	.007	2.0	1950	.34
Nichrome	Ni-20Cr	+23	1673	14	100	108.0	.011	2.0	50	21.6
Chromel P	Ni-10Cr	+32	1700		320	70.0	.022	2.0	160	14.0
Ni-30Cr	Ni-30Cr				100	150.0	.015	2.0	50	30.0
Rhodium	Rh	+13	2239	8						

*NASA Pd-13Cr cast ribbon

APPENDIX B

DERIVATION OF BRIDGE EQUATIONS

Page

A schematic diagram of the Wheatstone Bridge circuit used in this work is presented in Figure B1. Figure B2 shows a simplified version which can be used to derive the specific equations used in this work. The attached nomenclature (Table B1) provides definitions of the terms used in the following equations. Estimated values of the terms can be found in Appendix A, Table A2.

If we assume that the bridge is a simple voltage divider network and refer to Figure B2, the output voltage "e" measured by the bridge can be expressed as

$$e = E\left(\frac{R + r}{R + r + F + f + A}\right) - E\left(\frac{C - c}{C - c + B}\right) + v \qquad (1)$$

If we cross multiply Eqn (1) and introduce the normalized quantities e', r', f', c', m defined in the nomenclature, then:

$$e' = \left(\frac{1 + r'}{1 + r' + m + mf'}\right) - \left(\frac{1 - c'}{1 - c' - m}\right) + v' \qquad (2)$$

Factoring the denominator:

$$e' = \frac{1 + r'}{(1 + m)\,[1 + (r' + mf')/(1 + m)]} - \frac{1 - c'}{(1 + m)\,[1 - c'/(1 + m)]} + v' \qquad (3)$$

To permit a later simplification in the c' term on the right, first multiply numerator and denominator of that term by [1 + c'/(1 + m)]

$$e' = \frac{1 + r'}{(1 + m)\,[1 + (r' + mf')/(1 + m)]} - \frac{1 + c'/(1 + m) - c' - c'^2/(1 + m)}{(1 + m)\,[1 - c^2/(1 + m)^2]} + v' \qquad (4)$$

Eqn. (4) is exact. But c' <.002, so terms of order c'^2 can be neglected without loss of accuracy and (4) becomes:

$$e' = \frac{1 + r'}{(1 + m)\,[1 + (r' + mf')/(1 + m)]} - \frac{1 - c'm/(1 + m)}{(1 + m)} + v' \qquad (5)$$

To simplify notation define a quantity N:

$$N = [1 + (r' + mf')/(1 + m)] \qquad (6)$$

Then, rearranging to a common denominator, (4) becomes:

$$e' = \frac{1 + r' - 1 - r'/(1 + m) - f'm/(1 + m) + c'mN/(1 + m) + v'N(1 + m)}{(1 + m)\,N} \qquad (7)$$

Or:

$$e' = \frac{r'[m/(1 + m)] - f'[m/(1 + m)] + c'N[m/(1 + m)] + v'N[1 + m)^2/m][m/(1 + m)]}{(1 + m)\,N} \qquad (8)$$

Or:
$$e' = \frac{m}{(1+m)^2}\left(\frac{r' - f'}{N} + c' + v'(1+m)^2/m\right) \quad (9)$$

Write r' and f' in terms of gage factors (G,H) and temp. coefs (k,j), i.e.:

$$r' = Gx + kdt, \text{ and } f' = Hx + jdT \quad (10)$$

So:
$$e' = \frac{m}{(1+m)^2}\left(\frac{(G-H)x + (k-j)dT}{N} + c' + v'(1+m)^2/m\right) \quad (11)$$

A troublesome feature of this equation is the factor N in the denominator, which depends on both strain and temperature. In fact, from Eqn (6), (10), $N = 1 + (G + mH)x/(1 + m) + (k + mj)dT/(1 + m)$. If the strain, x, is less than .002, (G + mH)x may be neglected in N in (11). In this case, replace N by $N^* = 1 + (k+ +mj)dT/(1 + m)$. Finally, insert the definitions of K, U*, L* and V* in equation (11). The final result is equations (12) and (13) below. Note particularly that the starred quantities U*, L*, and V* in the final equation are expected to be functions of temperature only. The actual values of U*, L*, and V* are in practice determined by calibration versus strain and temperature. Note that resistive shunting to ground which is a function of temperature only is automatically corrected for in the calibration procedure. If temperature gradients are different in the measurement of unknown strains than during calibration, then resistance to ground effects (and other temperature effects) may not be correctly accounted for. It is recommended that resistance to ground be measured at every calibration and test point.

The following two forms of the bridge equation describe the response of the static strain gage bridge to strain and temperature in terms of the nomenclature given in Table B1. U*, L*, and V* are expected to be functions of temperature only; x is strain.

$$e' = K\,[U^*x + L^* + V^* + c'] \quad (12)$$

or

$$x = (1/U^*)\,[e'/K - L^* - V^* - c'] \quad (13)$$

TABLE B1

NOMENCLATURE

Name	Units	Description	Approximate Quantitative Value
A,B,C	ohms	Bridge resistors (Fig. B2) selected at room temp., no strain	60
D	ohms	Shunt calibration resistor (Fig. B2)	60000
c	ohms	Change in resistance of cal. arm due to applying shunt across C (Fig. B2). c = C-CD/(C+D)	.06
c'		Normalized change in cal. arm resistance. c' = c/C = C/(C+D)	.001
E	(volts)	Excitation voltage (Fig. B2)	5
e	(volts)	Output voltage (Fig. B2)	0 to ± .00
e'		Ratio, output voltage e to excitation voltage E (Fig. B2)	0 to ± .00
F	ohms	Resistance of temp.-dependent compensation element at room temp., no strain, including lead wire no. 1 (Fig. B2)	3
f	ohms	Change in comp. arm resistance due to strain and temp. (Fig. B2)	0 to 12
f'		Normalized change in comp. arm due to temp. and strain, defined f' = f/[A+F] = Hx + jdT	0 to .2
G		Gage factor of strain gage (palladium-chromium)	1.7
G2		Gage factor of compensation element (palladium)	4
H		Adjusted gage factor of compensation arm, defined as H=G2F/[A+F]	0.2
j	K-1	Adjusted effective TCR of compensation arm. defined as j = pF/[A+F]	.00017
k	K-1	Effective TCR of gage (including contribution due to dTCE)	.00017
K		Bridge factor (bridge sensitivity). Analytically, K is defined as m/(1+m)2 in Eqn. (11)	.249 to .25
L*		Apparent residual fractional change in gage resistance due to temp., after compensation. Analytically, L* is defined as the term (k-j)dT/N* in Eqn. (12). Also called Δ R/R	0 to ± .25
m		Bridge ratio = B/C = (A+F)/R	.95 to 1.
N		Term defined by Eqn. (6): N = [1+(r'+mf')/(1+m)]	.95 to 1.
N*		Temperature correction factor. From the deviation, N* is expected to be equal to {1+[(k+mj)/(1+m)]dT}	1 + .0003
p	K-1	Effective TCR of composition element (including contribution due to dTCE)	.0039
R	ohms	Resistance in gage arm at room temp., no strain, including lead wire no. 3 (Fig. B2)	60
r	ohms	Change in gage arm resistance due to strain and temperature (Fig. B2)	12
r'		Normalized change in gage arm resistance r'=r/R=Gx+kdT	0.2

TABLE B1 (cont.)

Name	Units	Description	Approximate Quantitative Value
v	volts	Apparent offset voltage in gage arm due to thermocouple effects	.0003
v'		Normalized apparent offset voltage in bridge arm due to thermocouple effects. v'=v/E	0 to .00
dT	K	Change in strain gage temperature from room temperature	0 to 130
U*		Apparent gage factor of bridge, (ohms/ohm)/(cm/cm) measured by applying strain. Analytically, U* is defined as the term (G-H)/N* in Eqn. (12)	1.5
V*		Error term due to thermocouple emf's in the bridge V* = v'/K in Eqn. (12)	0 to ± .00
x		Strain (cm/cm)	0 to ± .00
TCR	K^{-1}	Temperature coefficient of resistance	.000170(PdCr).0038(Pd)
dTCE	K^{-1}	Difference between temperature coefficients of linear expansion of element and substrate	.000003

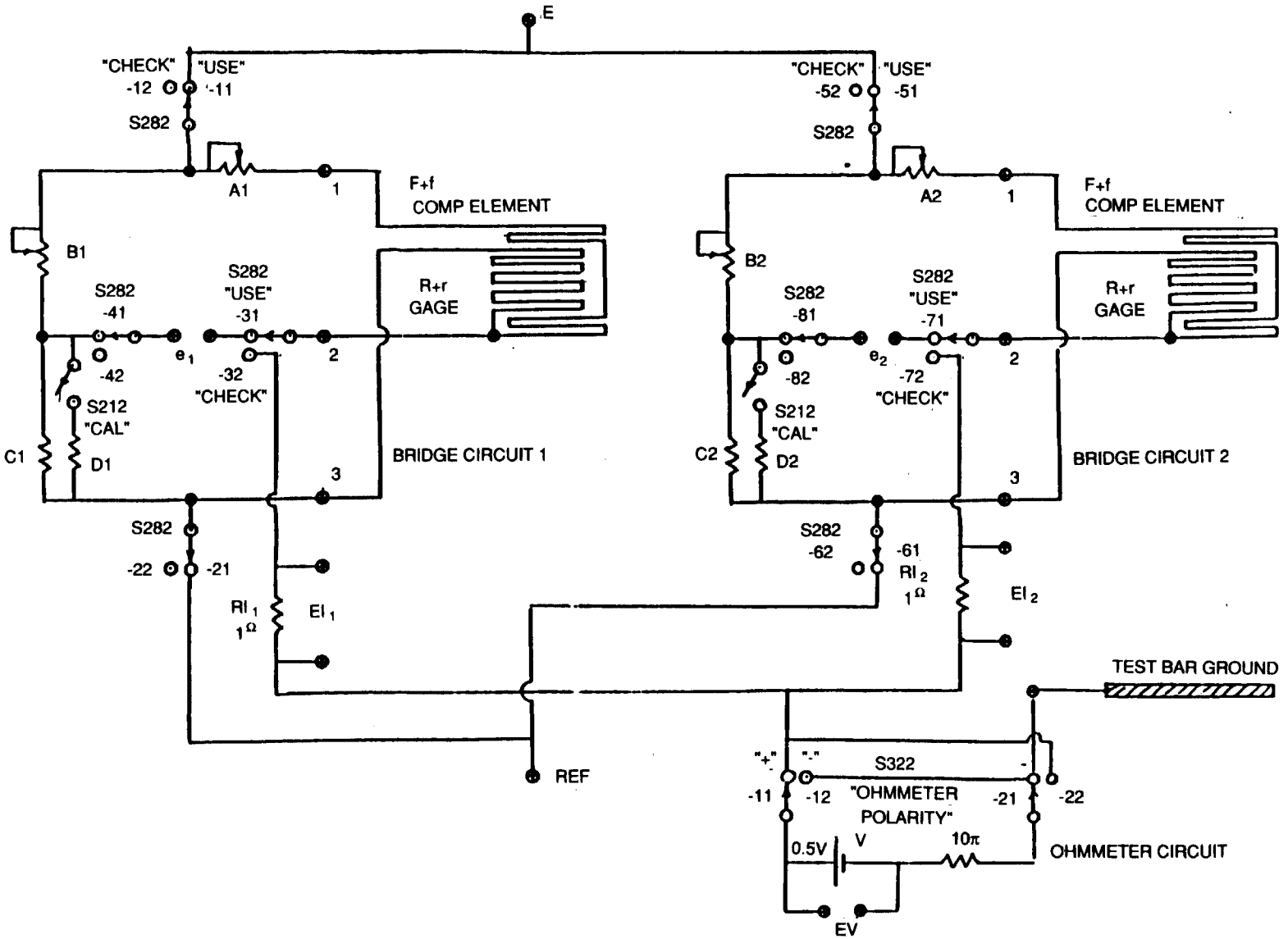

Figure B.1 Bridge circuit schematic diagram

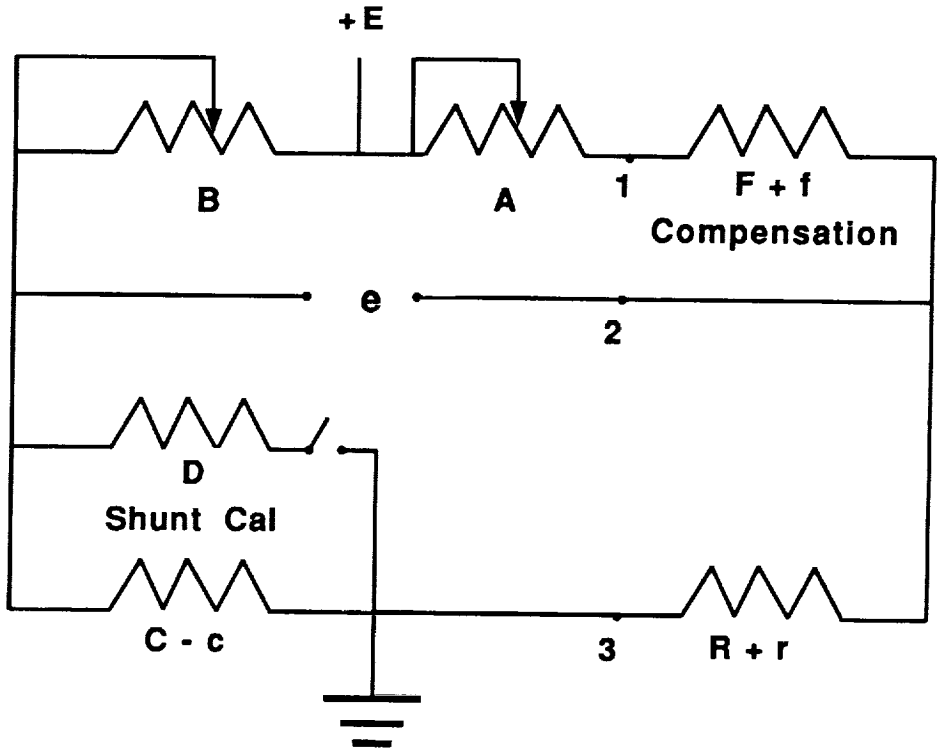

Figure B2 Simplified bridge schematic